UC Davis
UC Davis Previously Published Works

Title

Controlling Molecular Doping in Organic Semiconductors

Permalink

Journal

ISSN

Authors

Jacobs, Ian E
Moulé, Adam J

Publication Date

DOI

Peer reviewed

Controlling Molecular Doping in Organic Semiconductors

Ian E. Jacobs and Adam J. Moulé*

The field of organic electronics thrives on the hope of enabling low-cost, solution-processed electronic devices with mechanical, optoelectronic, and chemical properties not available from inorganic semiconductors. A key to the success of these aspirations is the ability to controllably dope organic semiconductors with high spatial resolution. Here, recent progress in molecular doping of organic semiconductors is summarized, with an emphasis on solution-processed p-type doped polymeric semiconductors. Highlighted topics include how solution-processing techniques can control the distribution, diffusion, and density of dopants within the organic semiconductor, and, in turn, affect the electronic properties of the material. Research in these areas has recently intensified, thanks to advances in chemical synthesis, improved understanding of charged states in organic materials, and a focus on relating fabrication techniques to morphology. Significant disorder in these systems, along with complex interactions between doping and film morphology, is often responsible for charge trapping and low doping efficiency. However, the strong coupling between doping, solubility, and morphology can be harnessed to control crystallinity, create doping gradients, and pattern polymers. These breakthroughs suggest a role for molecular doping not only in device function but also in fabrication—applications beyond those directly analogous to inorganic doping.

1. Introduction

Semiconductors are a ubiquitous component of all modern electronics. They are the basic materials which make up light emitting diode (LED) lighting, photovoltaics, transistors for computing and memory, communications devices, and sensors. Semiconductors are materials with a band gap, meaning that there is an energy gap between states occupied by electrons (valence band) and those that can be filled with the addition of more electrons (conduction band). This gap gives a semiconductor all of the electronic and optical properties that make it unique from a metal. If the band gap becomes too large (3–4 eV) then the material is considered an insulator because the barrier to charge transport is too high.[1,2] Recently, a vast amount of basic and applied research has focused on organic semiconductors (OSCs), which have several features that offer improved performance over inorganic semiconductors. These advantages include mechanical flexibility, light weight, and low-temperature processing. The ease of synthesis additionally allows for chemical tailoring of the OSC to adjust the band gap, charge mobility, solubility, miscibility, volatility, toxicity, and biocompatibility.[3–6]

Pure semiconductors are known as intrinsic semiconductors. However, in most applications the semiconductor is doped to improve either the hole or electron conductivity or to shift the Fermi energy of the material. For inorganic semiconductors, doping involves substitution of an atom or addition of an interstitial atom within the crystalline matrix. These impurity atoms either add electrons to donor states near the conduction band edge (n-type doping), which creates free electrons, or provide empty acceptor states near the valence band edge (p-type doping), which creates free holes. This same terminology is used by analogy in OSCs, but referring to bands in OSCs is inappropriate because the electronic states of organic molecules are much more tightly bound than for crystalline inorganic semiconductors. Instead, electron donor molecules add electrons to the lowest unoccupied molecular orbital (LUMO) or electron acceptor molecules remove electrons from the highest occupied molecular orbital (HOMO) of the OSC. Section 2 contains a detailed discussion of the mechanism for doping OSCs.

In inorganic semiconductors, dopants exclusively take the form of atomic substitutional or interstitial defects, while OSCs can be doped by both atoms and molecules. For the most part, atomic dopants in OSCs present difficulties because their small size allows them to diffuse. Dopant diffusion can have strongly negative effects on both device performance and lifetime.[3,7,8]

A large variety of molecular and ionic species, including acids and bases, can also serve as dopants in OSCs. The molecular nature of these species allows for better control of diffusion, e.g., by covalent anchoring or by controlling the molecule's size or shape. For example, the polymer polyethylenedioxythiophene (PEDOT) is often doped with polystyrene sulphonic acid (PSS), which is a strong Brønsted acid.[9,10] Lewis acids and bases have also been used effectively as molecular dopants.[11–16] These types of acid/base dopants for OSCs have been discussed in detail in past review articles and books.[3–6,10,17,18]

Dr. I. E. Jacobs
Department of Materials Science
University of California, Davis
1 Shields Avenue, Davis, CA 95616, USA

Prof. A. J. Moulé
Department of Chemical Engineering
University of California, Davis
1 Shields Avenue, Davis, CA 95616, USA
E-mail: amoule@ucdavis.edu

The ORCID identification number(s) for the author(s) of this article can be found under https://doi.org/10.1002/adma.201703063.

**ADVANCED
SCIENCE NEWS**
www.advancedsciencenews.com

**ADVANCED
MATERIALS**
www.advmat.de

Here, we will be focusing specifically the use of neutral molecular dopants, where a high electron affinity (EA) molecule acts as an electron acceptor for p-type doping, or a low ionization energy (IE) molecule acts as an electron donor for n-type doping. OSC doping with neutral molecular dopants can be likened to atomic doping of inorganic semiconductors because the interaction between OSC and dopant is purely electronic and does not involve any secondary chemical reactions. To demonstrate the similarities between atomic doping of inorganic semiconductors and molecular doping of OSCs, we highlight an early work which examined the change in the Fermi energy of the small-molecule hole conductor zinc phthalocyanine (ZnPc) with the electron acceptor 2,3,5,6-tetrafluorotetracyanoquinodimethane (F4TCNQ) using ultraviolet photoelectron spectroscopy (UPS) and X-ray photoelectron spectroscopy (XPS).[19] **Figure 1** shows the Fermi energy and HOMO/LUMO levels of ZnPc evaporated onto an indium tin oxide (ITO) substrate, both with and without doping by F4TCNQ. The OSC's bulk IE (labeled in Figure 1 as ionization potential or IP) is seen to be unaffected by doping. Doping shifts the Fermi energy toward the HOMO level, as expected for p-type doping in standard semiconductor theory.[1,2] Doping also reduces the depletion region width, as expected, since the increase in mobile charge density results in more effective charge screening. Finally, an interface dipole is present in both samples due to charge transfer between the substrate and OSC molecules adjacent to the interface.[20] In short, the qualitative effects of molecular
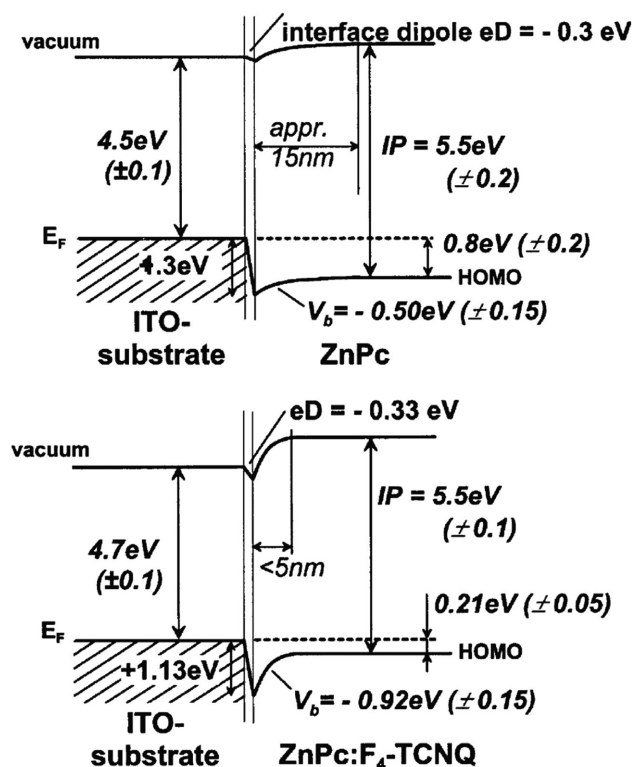
Ian Jacobs holds a B.E. in chemical engineering from The Cooper Union and recently received his Ph.D. in materials science and engineering from the University of California, Davis under the supervision of Prof. Adam Moulé. His graduate research focused on the use of molecular dopants to control semiconducting polymer solubility and methods for controlling doping in OSCs, with applications to nanoscale patterning.

Adam Moulé is an associate Professor of Chemical Engineering at the University of California, Davis. He earned his B.S. in chemistry from the University of Oregon in 1998 and his Ph.D. in physical chemistry from the University of California, Berkeley in 2003. His research focuses on understanding the relationship between complex processing and the resulting physical and electronic structures for organic electronic materials.

doping are generally consistent with standard semiconductor theory.

In contrast, molecularly doped OSCs do not follow standard semiconductor theory when considering the relationship between the density of doped sites and the change in conductivity (σ) or hole mobility (μ_h) as a function of doping ratio. **Figure 2** shows that the conductivity of the semiconducting polymer poly(3-hexylthiophene) (P3HT) initially *decreases* with the addition of F4TCNQ until reaching a threshold doping ratio of about 2×10^{-6}.[21] Above this threshold, conductivity increases initially sublinearly, eventually becoming superlinear at high doping levels (>3%).[22] This behavior is inconsistent with the linear or sublinear increase in conductivity typically observed in inorganic materials, where mobility decreases with doping due to ionized impurity scattering.

Several factors likely contribute to these deviations: (1) OSCs have a higher level of disorder, resulting in hopping instead of band transport;[25] (2) OSCs are prone to trap site formation due to disorder and/or impurities; and (3) the ionized dopants interact strongly with charge carriers due to the low dielectric constant of the OSC.[23,24] This combination of properties implies that doping should broaden the density of states (DOS) and create Coulombic traps.[24] A model by Arkhipov et al.,[23,24] which accounts for these effects, predicts that trapping by ionized dopants should reduce charge carrier mobility and conductivity at low doping levels (see Figure 2, inset). At high doping ratios (>10^{-2}), the potential wells of the Coulombic trap sites

Figure 1. Energy level scheme as obtained from UPS and XPS for the contact between ITO and ZnPc. The upper panel shows the energetic structure for the undoped case and the lower panel for ZnPc p-doped with F4TCNQ. Reproduced with permission.[19] Copyright 2001, Elsevier.

**ADVANCED
SCIENCE NEWS**
_____
www.advancedsciencenews.com
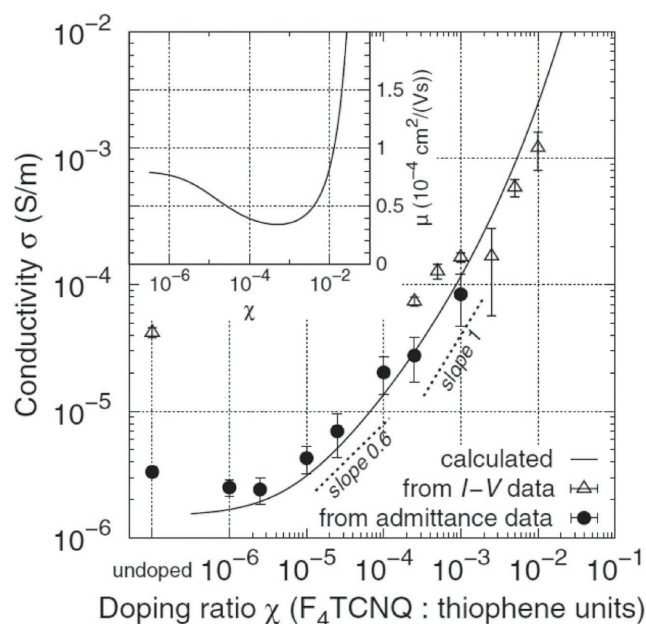
**ADVANCED
MATERIALS**
www.advmat.de

Figure 2. Conductivities as determined by admittance measurements of layers in metal–insulator–semiconductor geometry (solid symbols) and I–V measurements of hole-only devices (open symbols). The line is the predicted conductivity based on the mobility model by Arkhipov et al.[23,24] and the hole densities, which were calculated by Pingel and Neher.[21] The inset shows the calculated mobility values as a function of doping ratio. Reproduced with permission.[21] Copyright 2013, Americal Physical Society.

begin to overlap,[23] strongly increasing carrier mobility and leading to a superlinear increase in conductivity. These predictions are consistent with the experimental data in Figure 2.[21,26]

However, we note that the Arkhipov model assumes a single-phase system, while experimental data have shown that F4TCNQ anions are confined to amorphous domains at low doping levels. It is expected that polarons in doped P3HT should migrate to crystalline domains due to their lower band gap. Therefore, it is not completely clear that charge trapping by dopant anions is *necessarily* the cause of the observed conductivity decrease. For example, the morphology of P3HT films has been shown to be negatively affected by doping, even at low concentrations, leading to reduced conductivity.[27] Likewise, other models have been proposed which similarly predict a superlinear increase in conductivity.[28] These complexities illustrate the difficulty in developing and experimentally verifying quantitative descriptions of doped OSC behavior.

Several good review articles on the theory of molecular doping in OSCs[29–31] and the use of molecular dopants in devices[17,32,33] have recently been published. In this article, we will focus on methods for controlling dopant–OSC interactions, with a primary focus on p-type doping of polymeric OSCs with neutral molecular dopants. In these systems, strong interactions between the OSC and dopant, along with high levels of energetic and morphological disorder, result in a high level of complexity. There is, in particular, a strong coupling between doping interactions and OSC morphology, and vice versa. These effects are often problematic, leading to charge trapping and low doping efficiency. However, in some cases, this

complexity can be harnessed in beneficial ways, for example to increase crystalline order,[34,35] or to enable novel patterning or layering methods.[36,37] These breakthroughs suggest a role for molecular doping in fabrication of OSC devices for which there is no direct correlation in doped inorganic semiconductors.

The first half of this review will highlight how processing conditions can strongly affect structure–property relationships in doped OSCs. We will discuss recent advances in the synthesis of p-type molecular dopants, improved understanding of doping mechanisms, and techniques for sequential processing that allow for better control of doped film morphology. The effects of dilute trap sites and impurities, which act as dopants, will also be discussed. Finally we will introduce methods for controlling defect density using dopants and chemical treatments.

In the second half of this review, we will explore methods for spatially controlling doping in OSC films, which are prerequisites for the use of dopants in novel device structures. In addition, the use of dopants to directly pattern OSC films using the doping-induced solubility control (DISC) technique will be reviewed. These methods are all dependent on controlling the diffusion rate of dopants through OSCs, so we will also discuss quantitative methods for studying dopant diffusion. Finally, we will highlight promising avenues for future work.

2. Theory of Molecular Doping

There exists a large and complex literature surrounding the p- and n-type doping of OSCs. This is because a number of different chemical mechanisms and molecular species can result in the formation of free charges in the OSC. In general, the doping mechanism for a given dopant and OSC system cannot be reliably predicted. We refer to several recent and comprehensive review articles and books that list and categorize different dopant structures and doping mechanisms in OSCs and related devices.[3,4,6,10,17,30,32,38–42] Neutral molecular dopants are understood to interact with OSCs by two mechanisms: ion pair (IP) formation and charge-transfer complex (CTC) formation.[29]

2.1. Ion Pair Formation

In principle, a p-type molecular dopant is a molecule with a LUMO deep enough to extract an electron from the OSC HOMO. Likewise, an n-type molecular dopant is a molecule with a HOMO shallow enough to donate an electron to the OSC LUMO. This simple and commonly held model for molecular doping is depicted in **Figure 3**, using pentacene as an example OSC.[43] In this figure, each dopant is completely ionized and generates one free charge carrier in the OSC, forming an IP.

In some systems, including most polythiophenes doped by tetracyanoquinodimethane (TCNQ) derivatives, this model seems to be a reasonable description of doping.[29] However in other cases, including many small-molecule OSCs or oligomers, this figure does not even qualitatively explain the observed behavior or predict the free charge density.[29,44] This model is incomplete because it does not consider the electronic interaction between the dopant ion and the OSC. As a result,
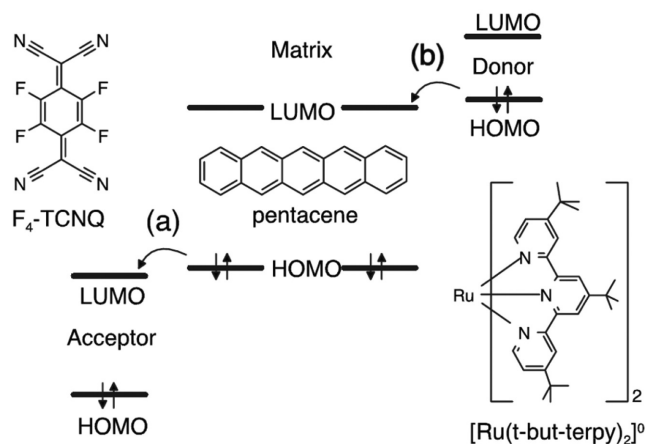
**ADVANCED
SCIENCE NEWS**

www.advancedsciencenews.com

**ADVANCED
MATERIALS**

www.advmat.de

Figure 3. Simplified model of the organic doping process exemplified by the organic semiconductor pentacene doped with F4-TCNQ (p-doping) or [Ru(t-but-terpy)$_2$]^0 (n-doping). Free charge carriers are generated by an electron transfer between dopant and matrix molecule. To facilitate electron transfer, a) the LUMO of the p-dopant has to be lower than the HOMO of the matrix molecule (for p-doping), b) or the HOMO of the n-dopant has to exceed the LUMO of the matrix molecule (for n-doping). Reproduced with permission.[43] Copyright 2008, American Physical Society.

1. It is possible to form locally bound CTCs between dopants and OSC molecules, characterized by hybrid (inter)molecular orbitals and less than integer charge transfer;
2. OSC and dopant energy levels do not clearly predict whether charge transfer will occur;
3. Even in the case of IP formation, it has been demonstrated that only a fraction of the doped sites dissociate to free charge carriers in the bulk of the OSC.

More sophisticated descriptions of IPs exist, but have not been widely discussed in the context of OSC doping. For example, it is often stated that IP formation should only occur if $EA_{dopant} > IE_{OSC}$ and n-type doping should only occur if $IE_{dopant} < EA_{OSC}$. This is not precisely correct. In the field of organic charge-transfer salts, which were studied extensively in the 1960–1980s, it was realized that the Madelung energy (electrostatic energy) of the ionized state acts to stabilize the IP.[45,46] Because EA and IE are referenced to vacuum, the value IE – EA represents the free energy for electron transfer between two well-separated molecules. However, in a doped OSC (or a charge-transfer salt), the electron and the hole are in close proximity. Therefore, the energy of an ion pair can be written as[47]

$$E(\delta) = (IE - EA)\delta - k\frac{e^2}{r}\delta^2 \qquad (1)$$

where δ is the degree of charge transfer, k is Coulomb's constant, e is the electric charge, and r is the separation between the electron and the hole. The value of δ that minimizes $E(\delta)$ determines the amount of charge transferred in the interaction. In charge-transfer salts, the $1/r$ dependence can give rise to a pressure-dependent neutral–ionic phase transition.[47] Likewise in the Arkhipov model, which similarly accounts for the interaction between charge carriers and dopant ions, this distance dependence causes factors such as doping efficiency,

carrier mobility, and conductivity to be strongly doping level dependent. These effects will be discussed in the following sections.

2.2. Charge-Transfer Complexes

If the degree of charge transfer is <1, dopants and OSCs form CTCs rather than ion pairs. CTCs were first observed in electrically conductive materials in the 1950s[48] and characterized in detail in the 1970s in charge-transfer salts of donor molecules like tetrathiafulvalene (TTF) paired with acceptors such as TCNQ.[31,45,49] CTCs can form between two organic molecules even if $EA_{dopant} \ll IE_{OSC}$ (p-type) or $IE_{dopant} \gg EA_{OSC}$ (n-type). These interactions likely occur to some degree at nearly all interfaces. For example, the donor/acceptor mixtures used for organic photovoltaic (OPV) devices have been shown to form weak CTCs at the interfaces and are believed to be integral to the performance of OPVs.[50–53] CTCs have also been observed at OSC–inorganic interfaces.[54] In the last decade, it has become apparent that CTCs are also commonly formed between molecular dopants and OSCs.[55]

A CTC forms as a result of hybridization of an occupied frontier molecular orbital from a donor and an unoccupied frontier orbital from an acceptor. In this sense, a CTC is analogous to a coordinate covalent bond formed by the linear combination of molecular orbitals. CTC formation results in the creation of new local HOMO and LUMO states, analogous to bonding and antibonding states. Because the molecular orbitals themselves are interacting, the degree of hybridization and the resulting energetic splitting of these orbitals are highly dependent on the energetic and spatial overlap of the individual orbitals, as well as the OSC HOMO and dopant LUMO energetic mismatch.[29] The magnitude of these charge-transfer (CT) splittings have been experimentally determined to be >1 eV in blends of 2,7-dioctyl[1]benzothieno[3,2-b][1]benzothiophene (C8-BTBT) and F(n)TCNQs using UV–vis spectroscopy,[56] and 0.9 eV in quaterthiophene (4T) and F4TCNQ using UPS and XPS.[44] These large splittings can be rationalized by considering the bond-like character of a CTC: when the OSC HOMO and the dopant LUMO hybridize, both electrons from the OSC HOMO are transferred to the lower energy hybrid orbital. This stabilizes the CTC HOMO at the energetic expense of the CTC LUMO.

In the OSC/dopant CTC, there is fractional charge transfer between the OSC and dopant; the charge is shared between the OSC and dopant. In contrast, in an IP, there is integer (or nearly integer) charge transfer from the OSC to the dopant. Conceptually, we can think of IPs as the limiting case of CTC formation, in which the degree of charge transfer goes to one. Going back to our analogy to atomic bonding, we can think a CTC as analogous to a polar covalent bond, and an IP as analogous to an ionic bond.

An important consequence of CTC formation is that the lower energy CTC state (that is, the "bonding" or local HOMO state) contains *both* of the HOMO level electrons from the donor, while the higher energy CTC state (the "antibonding" or local LUMO state) remains empty. This concept is inconsistent with the model depicted in Figure 3, in which it is assumed that a single electron hops from the donor to the acceptor.[57]

Detailed UPS studies have verified that upon doping with strong p-type molecular dopants like F4TCNQ, the ionization energy of small-molecule OSCs like C8-BTBT is increased.[44,56–58] This result is not expected for p-type dopants that simply ionize the OSC. According to the standard model of polaron states in OSCs[3,18,59] the IE should decrease upon doping due to the formation of singly occupied polaron states within the OSC band gap. Instead, the IE is increased far beyond either parent molecule, indicating that a new hybrid state is formed.[57]

2.3. Characterizing Doping Mechanisms

Further evidence for the existence of CTCs comes from characterization of their optical absorption bands.[56] Before going on to a discussion of the electronic consequences of IP versus CTC formation, we will briefly discuss spectroscopic methods for distinguishing between these cases. Detection and quantification of both mechanisms is simple using UV–vis–NIR spectroscopy, since both IPs and CTCs show strong absorption features, along with bleaching of the ground state absorbances of the neutral OSC and dopant. The new absorbing species are either the radical ions of the OSC and dopant, or the OSC-dopant CTC.

The easiest method to determine the ionized spectrum of a dopant molecule is to ionize the dopant in solution with an oxidizing or reducing agent, forming a radical anion for p-type dopants or a radical cation for n-type dopants. Iodide, provided by KI, is often used to reduce p-type dopants. The ionized spectrum of the OSC is often more difficult to determine because many OSCs are insoluble or poorly soluble (once doped) and may also undergo spectroscopic changes upon aggregation or crystallization. OSC films can be charged in field-effect geometry, in which the OSC forms one side of a parallel-plate capacitor along with transparent electrode (like ITO) covered by a dielectric.[60] A potential applied to the substrate yields a capacitive injection of charge into the OSC, allowing the ionized absorbance to be recorded.

Figure 4a shows UV–vis–NIR spectra of neutral films of P3HT (black line) and F4TCNQ (light dashed line), the F4TCNQ radical anion (dark dashed line), and several P3HT:F4TCNQ films. Blends of P3HT and F4TCNQ all show the same two peaks. These are labeled here as ICT for integer charge transfer, but could be more clearly defined as F4TCNQ anion absorbance features. Labels P1 and P2 indicate the first and second polaron absorbances for P3HT+.[61] These spectra can be reproduced by a linear combination of the neutral and ionized OSC and dopant spectra,[62] indicating that no other species (such as CTCs) are formed. Figure 4c shows absorbance spectra of P3HT with a series of TCNQ dopants with EA ranging from 4.23 eV (TCNQ) to 5.24 eV (F4TCNQ). The position of the anion absorbance does not change, indicating that each dopant molecule is either fully ionized or completely neutral. The decrease in ionized OSC and dopant absorptions,
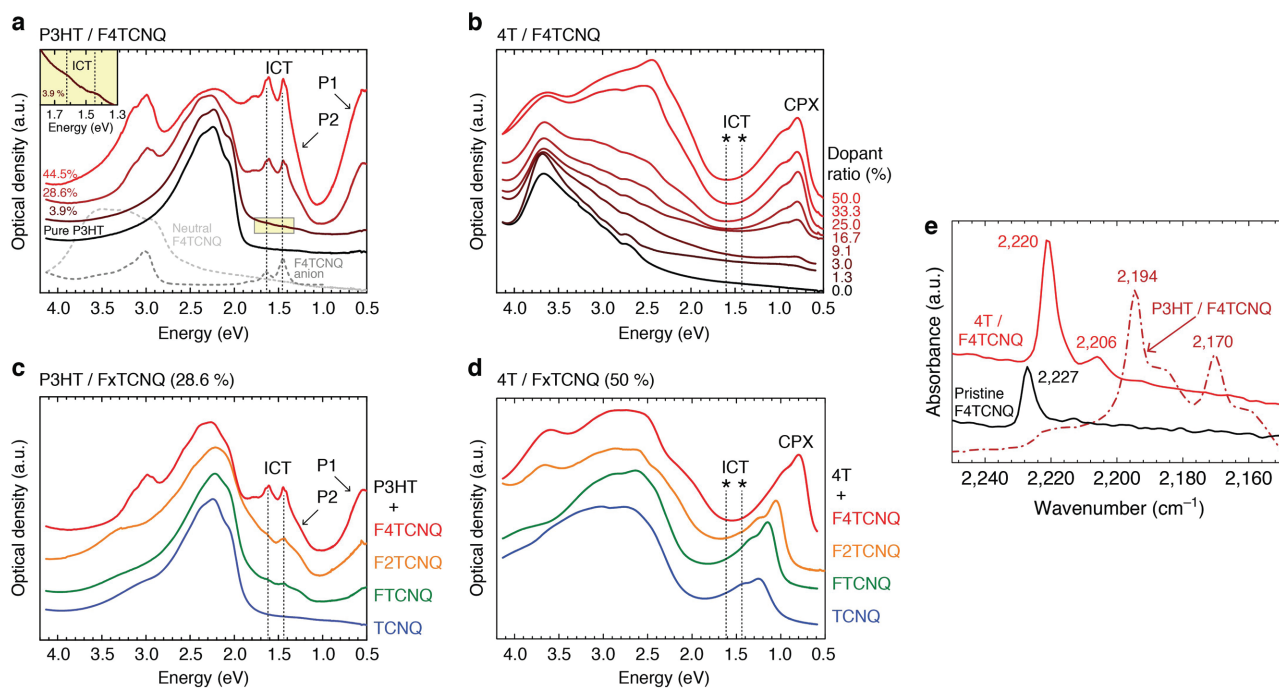

Figure 4. UV/Vis/NIR spectra of a) P3HT blended with F4TCNQ at an increasing ratio with the inset showing the zoomed region around the ICT features in the film of 3.9% dopant ratio (one F4TCNQ per 25 quaterthiophene segments), b) 4T blended with F4TCNQ at increasing ratio, c) P3HT blended with the full range of differently strong dopants (TCNQ to F4TCNQ) at a dopant ratio of 28.6%, and d) of 4T blends with the full range of differently strong dopants (TCNQ to F4TCNQ) in 1:1 ratio (50%); P1 and P2 indicate the optical transitions of the positive polaron in P3HT[18,60–63]; asterisks indicate the expected transition energies related to dopant anions (ICT) that are absent in the 4T case. e) FTIR spectra in the characteristic cyano-stretching region for 4T films in 1:1 blends (50% dopant ratio) with the acceptor F4TCNQ; pristine 4T does not exhibit any vibrational bands in the region displayed. The spectrum for an F4TCNQ-doped P3HT film (28.6% dopant ratio, that is, one dopant per 2.5 quaterthiophene segments of the polymer backbone) is shown as reference. Reproduced with permission.[44] Copyright 2015, Nature Publishing Group.

**ADVANCED
SCIENCE NEWS**
www.advancedsciencenews.com

**ADVANCED
MATERIALS**
www.advmat.de

as the dopant EA is reduced, is consistent with an equilibrium between the neutral and ionized states, as described by Torrance.[45] We conclude that P3HT doped by F(n)TCNQ always dopes by IP formation.

In contrast, Figure 4b shows absorbance spectra of quaterthiophene (4T), an oligomer that is structurally similar to P3HT, mixed with increasing amounts of F4TCNQ. No F4TCNQ radical anion absorption is observed in mixtures with 4T; instead, a new absorption feature at 0.7 eV is evident (marked as CPX, another acronym for charge-transfer complex).[29,44] Figure 4d shows absorbance spectra of 4T with the same four TCNQ dopants as depicted in Figure 4c. Unlike P3HT, the 4T spectra show significant shifts in absorption maxima upon doping. This observation is consistent with CTC formation. The CT band of the doped films (labeled CPX) redshifts with increasing dopant EA, but does not precisely follow the IE − EA energy difference. In mixtures of the donor C8-BTBT and F(n)TCNQ's, Salzmann and co-workers showed that the optical absorption bands of the complex were always observed at energies greater than the IE − EA energy difference, indicating that molecular hybridization must be occurring.[56] Spectral shifts of this type are not possible for an IP, which have fixed anion and cation absorbances.

The degree of charge transfer can also be directly measured using Fourier transform infrared spectroscopy (FTIR).

Figure 4e shows a shift in the C≡N vibrational stretch in F4TCNQ upon ionization. In samples of neutral F4TCNQ, the C≡N stretch occurs at 2227 cm^{-1}. If F4TCNQ is fully ionized to F4TCNQ$^{•-}$, the C≡N stretch redshifts 33 cm^{-1} to 2194 cm^{-1}, and other modes become symmetry allowed.[64] Critically, this shift has been reported to be linear with the degree of charge transfer.[44,64,65] The spectrum of P3HT/F4TCNQ in Figure 4e shows a shift to 2194 cm^{-1} indicating complete ionization, consistent with IP formation.[44]

Alternatively, if a CTC state is formed, there is less than a full charge transferred to the F4TCNQ and the C≡N stretch shifts proportionally to the degree of charge transfer.[65] In the 4T/F4TCNQ sample, the peak shifts only 7 cm^{-1} to 2220 cm^{-1}, indicating a charge transfer of 0.21 electrons ($\Delta \nu / \nu$ = 7 cm^{-1}/33 cm^{-1}).[44] We expect that vibrational shifts could be used to characterize charge transfer in other dopants or in different functional groups if spectrally isolated absorption features exist.

2.4. A Unified Mechanism of Doping in OSCs

Salzmann et al. recently proposed a unified mechanistic model for doping in OSCs.[29] **Figure 5** is a graphical depiction of this
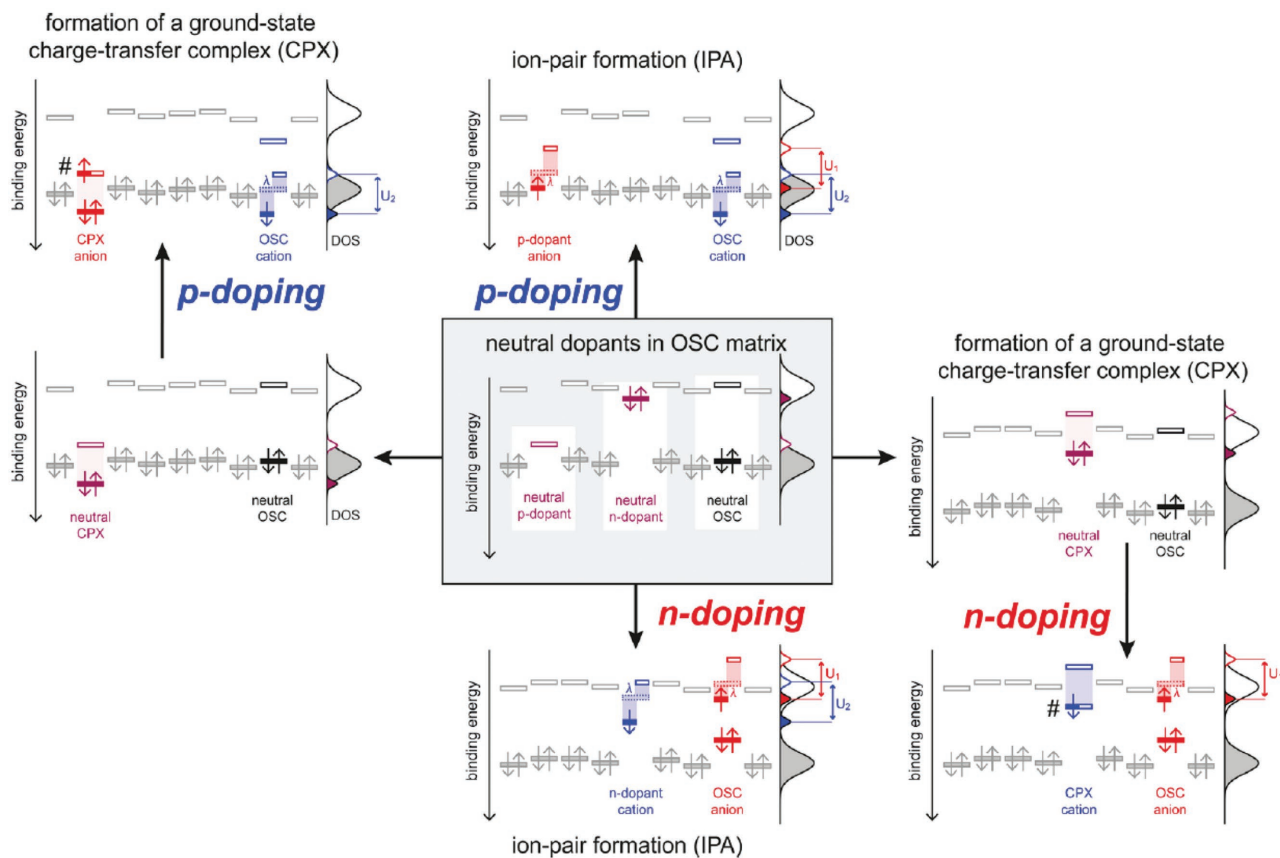

Figure 5. Comprehensive picture of energy levels and the corresponding DOS upon molecular p-/n-doping in the alternative cases of ion pair formation (top and bottom) and the formation of charge-transfer complexes (left and right) with its subsequent ionization; λ is the reorganization energy, and U_1 and U_2 denote the Hubbard U of dopant and OSC, respectively; the levels of the ionized CPX (marked with #) are approximated by those of the neutral species. Reproduced with permission.[29] Copyright 2016, American Chemical Society.

model. The center panel depicts neutral p- and n-type dopants in a generic OSC. The panel to the left of the center shows the formation of a hybridized CTC between the OSC and a p-type dopant, characterized by a new doubly occupied HOMO level with IE greater than the OSC HOMO. The corresponding situation for n-type doping is shown to the right.

Formation of CTCs does not directly create free charge carriers in the OSC. Rather, the CTCs must be thermally ionized by excitation of an electron from a neighboring neutral OSC site to create free charges. This is shown in Figure 5 upper left (p-type) and lower right (n-type), assuming the charge carriers are well separated from the dopant ions. Because the CTC LUMO generally lies significantly higher in energy (at least several kT) than the OSC HOMO, the probability of generating a free charge carrier by this process is quite low. As a result, OSC/dopant systems, which form CTCs, show low doping efficiencies and low conductivity.[29,44,66]

The panels above and below the center depict ion pair formation, assuming completely ionized and separated states; that is, a free hole and an immobile dopant radical anion for p-type doping or a free electron and an immobile dopant radical cation for n-type doping. Doping efficiency in IP forming systems is typically higher, but still only on the order of 10%.[21,66] Factors contributing to this low efficiency are discussed in Section 2.5.

The Salzmann et al. model also incorporates the effects of electron–electron interactions. In the standard model of OSC polaron states,[3,18,59] there are no electron–electron interactions, so polaronic distortion of the OSC implies that $IE_{OSC}^+ < IE_{OSC}$. This is inconsistent with the observation that only a single electron is transferred in IP formation.[67] The revised model accounts for the on-site Coulomb interaction, a term commonly known as the Hubbard (U).[68,69] This interaction splits the occupied and unoccupied HOMO levels of the dopant cation, as shown in Figure 5, while relaxation of bond lengths in the ion (represented by λ in Figure 5)[29] and off-site (Madelung) Coulombic interactions[67,70] shift the positions of these bands. Inclusion of these on-site and off-site Coulombic interactions has allowed for quantitative modeling of UPS and XPS data[67,71] and optical spectra.[72] Critically, this revised model correctly explains why the IE value increases when an electron is removed and the EA decreases when an electron is added to either the dopant or the OSC.[29]

There are a variety of factors that may affect whether a particular donor/acceptor pair forms CTCs rather than IPs. Analysis of doped small-molecule mixtures with planar TCNQ-type dopants shows CTC formation in face-on geometries.[44,56] There are also reports of complete ionization of pentacene using F4TCNQ in herringbone-type structures.[73–75]

A recent theory article attempts to quantify the coupling between F4TCNQ and the host OSC using ab initio methods to account for environmental screening effects, combined with a parameterized model Hamiltonian.[75] Using pentacene/F4TCNQ they showed that full ionization in small molecules is possible, even when $EA_{dopant} < IE_{OSC}$. They conclude that difference between the IP of the semiconductor and EA of the dopant is an important parameter and likely explains why OSCs like 4T or BTBT will form fractional CTCs with F4TCNQ. However, other factors such as the electron–hole (Madelung) interaction, spin statistics and Jahn–Teller like relaxation effects were also

found to be critical determinants of ionization fraction. These factors are strongly dependent on both the material and on the sample morphology.[75]

Comparisons of doping in homopolymers versus push–pull co-polymers show that homopolymers are ionized by p-type dopants like F4TCNQ, while co-polymers form localized CTCs.[66,76] Simulations show that the donor groups on the co-polymer lose considerable charge density to the dopant, while the acceptor part of the polymer remains essentially unchanged by the presence of the high EA dopant.[76] One explanation for this result could be that the CTC forms in a molecularly doped co-polymer because there is an energetic penalty to delocalizing a cation across a push–pull polymer. An IP forms in a doped homopolymer because the cation delocalizes. The comparison of P3HT and 4T doped with F4TCNQ validates this conclusion: P3HT/F4TCNQ forms an IP while 4T/F4TCNQ forms CTCs.[44,62,77] Alternatively, the preference for CTC formation in co-polymers might suggest that the donor group of the co-polymer is effectively electronically isolated in a face-to-face interaction with the planar dopant and is similar to the co-crystal of small-molecule OSC + dopant.

These generalizations can be applied for planar dopants where the flat shape of the molecule makes face-to-face molecular orientation preferential. 3D dopants like $C_{60}F_{36}$ or $Mo(tfd)_3$ (see **Figure 6** for structures) may be more likely to form IPs because their geometry prevents formation of intermolecule hybrid orbitals.[78] Their larger size also likely increases the mean electron–hole distance, reducing the Coulombic binding. On the other hand, these 3D dopants are larger and cause more structural reordering of the OSC, which may limit the maximum doping density or affect polaron delocalization.

It is still an open question as to why some OSCs ionize and others form CTCs when mixed with molecular dopants.[29,30,72] Future work will need to focus on understanding how local electronic structure and delocalization affect the type of charged state that forms.

2.5. Doping Efficiency

It is widely understood that molecular dopants generate free charge carriers in OSCs with less than 100% efficiency.[17] There are a variety of reasons for this observation including dopant aggregation,[79] CTC state formation,[29] Coulombic binding of IPs,[21,24,26,80,81] and local trapping of the free charge at structural defects.[82] Methods for measuring doping efficiency are discussed in Section 4.2.

One recent study by Tietze et al. looked at both p- and n-type doping efficiency in pentacene.[78] The authors were able to show that doping at very low concentrations primarily results in trap filling (see Section 5). At higher concentrations the so-called saturation regime is reached, in which the Fermi energy is higher than the acceptor energy (E_A) for p-type dopants or lower than donor energy (E_D) for n-type dopants. In this regime, each new dopant efficiently produces new free charges. With still higher dopant concentration, additional dopants compete for charges with the OSC HOMO and LUMO states because the Fermi level is between the HOMO level and the E_A for p-type dopants or between the E_D and LUMO level for n-type
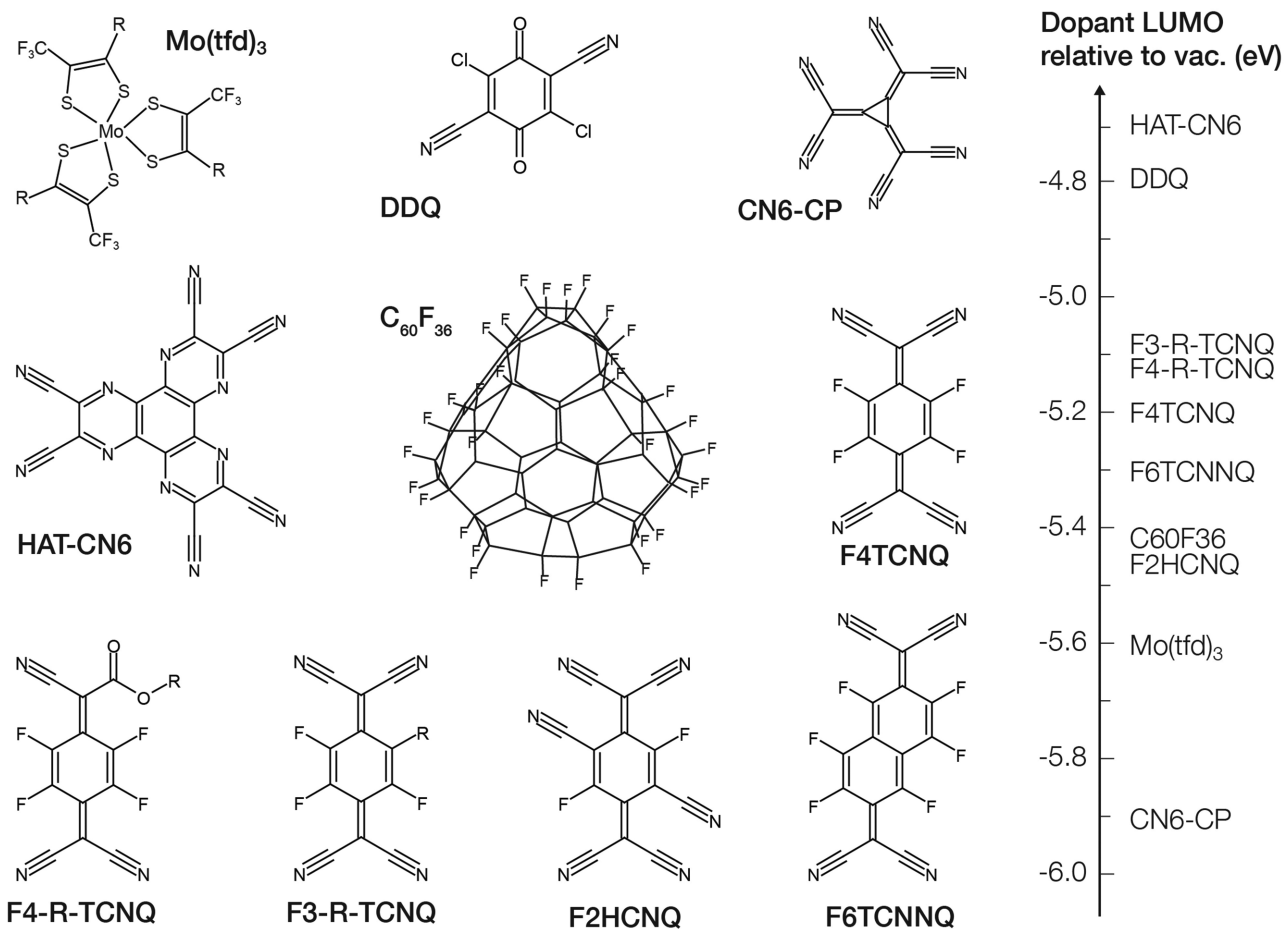
**ADVANCED
SCIENCE NEWS**

www.advancedsciencenews.com

**ADVANCED
MATERIALS**

www.advmat.de

Figure 6. Molecular structures of several p-type molecular dopants with high electron affinities (EAs). Note that Mo(tfd)$_3$ and F4-R-TCNQ feature tailorable side groups that can be used to change the solubility, miscibility, or processability of the dopant. LUMO values that correlate to the EA are listed. These LUMO values are tabulated from several articles and come from various measurements, so considerable uncertainty in the absolute doping strength is likely.

dopants. This third highly doped regime is termed the dopant reserve. This description of dopant efficiency is appealing as it is consistent with inorganic semiconductor theory but may not account for disorder effects in OSCs[23] or account for interaction between charges in a low dielectric medium.[83] In fact, many studies have shown that the presence of the dopant itself causes the formation of traps in the OSC which pin the Fermi level to the band edge and prevent metallic transport.[42,67,84,85] The model and data presented by Tietze et al. are an ideal representation that is valid in highly crystalline small-molecule samples (like pentacene) but may need considerable adjustment in semicrystalline or disordered samples.

OSC and dopant energy levels also do not always provide a reliable prediction for doping efficiency. For example, both poly[2,5-bis(3-tetradecylthiophen-2-yl)thieno[3,2-b]thiophene] (PBTTT) and *N*-(4-(2-butyl)-phenyl)diphenylamine (F8-PFB) have HOMO levels of −5.1 eV, yet doping with F4TCNQ can yield 10^8 higher conductivity in PBTTT than F8-PFB.[34,86] Likewise, dopant EAs are not always good predictors of doping efficiency. Li et al. studied F4TCNQ derivatives, F4MCTCNQ and F4OCTCNQ, in which one of the nitrile groups was replaced with a methyl- or octyl-ester solubilizing groups.[87] Although

these ester-substituted dopants had slightly lower EAs than F4TCNQ, they were more effective at quenching fluorescence and yielded higher conductivity in P3HT films. These observations suggest that miscibility and molecular packing of the dopant may play a major role in determining doping efficiency.

Finally, doping efficiency is also affected by the OSC morphology. Gao et al. studied doping of P3HT h-aggregate and j-aggregate nanofibers with F4TCNQ, using optical and Raman spectroscopy and electron spin resonance (ESR).[88] They observed >10× higher doping efficiencies in j-aggregate nanofibers, which were interpreted as resulting from increased hole delocalization due to the more planar backbone of j-aggregate nanofibers. Here, the more ordered sample showed higher doping efficiency. Another recent study by Müller et al. looked at the effect of casting solvent on doping efficiency in mixed-solution cast P3HT:F4TCNQ films, observing stronger π–π stacking and higher doping efficiency in films cast from chloroform as opposed to chlorobenzene (CB).[89] These results were surprising because chloroform-cast P3HT films typically show lower crystallinity than chlorobenzene-cast films.[90] Here the presence of the dopant caused the chloroform-cast sample to form with more order. These examples show that OSC

morphology and doping efficiency are strongly affected by electrostatic interactions between the dopant, solvent, and OSC in solution. Clearly, these interactions are complex and difficult to predict. There is no theory or clear empirical trend at this point that relates the size, solubility, or other chemical properties of the molecular dopant to the doping efficiency or the degree of disorder that is induced in the OSC.

2.6. Summary

Molecular dopants can either form IPs or CTCs within the OSC. The formation of IPs or CTCs in both polymers and small-molecule OSCs seems to depend more on the identity of the OSC than the dopant. Both IPs and CTCs have been observed in polymers and small-molecule OSCs. The difference between the resulting states can be determined using UV–vis–NIR spectroscopy and comparison to absorbance of OSC and dopant anion and cation spectra.

A recent model by Salzmann et al. explains the energetic differences between IP and CTC states. CTC states must be thermally ionized to create free charge carriers in the OSC, resulting in low doping efficiency.[29] Due to the strong local interactions between charges in low dielectric materials, there is evidence that even in IPs, charges are often Coulombically bound, particularly at low doping levels, resulting in doping efficiencies considerably below unity.

Future research needs to focus on relating local changes in structure, charge-transfer interactions, and disorder in the OSC to the presence of the dopant. A related topic is to understand how the dopant shape, size, and orientation affect disorder and charge delocalization in the OSC. Addressing these challenges requires improving chemical imaging and energetic mapping techniques, increasing control of the dopant location in OSCs, and advancing modeling of delocalized electronic states.

3. Dopant Molecules

Our discussion of dopant molecules will focus narrowly on nonreactive p-type molecular dopants, although we briefly review molecular n-type dopants. To clarify terminology, molecular dopants are defined as neutral small molecules with high EAs (p-type) or low IEs (n-type) that accept or donate electrons from OSCs, respectively. This classification excludes discussion of salts that leave charged or neutral counter ions, reactive molecules, ionomers, and atomic species, except for historical context or when necessary to clarify doping mechanisms. Thus, the only interaction between OSCs and the dopants discussed here is electron transfer, which is reversible and does not involve changes to the bonding structure.

3.1. Atomic Dopants

Initial studies of OSCs with molecular dopants were centered on diatomic halogens Cl_2, Br_2, and I_2 as p-type dopants[91,92] and alkali metals as n-type dopants.[93] Halogens were attractive because they are volatile and can be added to the sample

as a gas that diffuses into the OSC. Iodine reacts to form I^- or I_3^- leaving a hole on the OSC. This reaction is reversible. With heating the iodine is removed from the film, and the OSC recovers its original electronic properties.[3] In fact, the low barrier to sublimation made the use of I_2 for doping problematic because even at room temperature it rapidly diffuses through and out of the films. In addition to contaminating other OSC layers within a device, iodine vapor leaving the film can contaminate other samples in a glovebox.[94] Lighter halogens are even more problematic, since Cl_2 and Br_2 are both more reactive and more volatile. In general, atomic ions render devices unstable due to dopant diffusion.[95]

O_2 is another diatomic species that can dope OSCs, which has been studied extensively in the context of OSC stability.[96–98] However, this process is complex because exposure to light can induce excitons on the OSC (or polarons in mixtures of donor/acceptor OSCs) that can react with the O_2 to form O_2^-, which in turn can react with the OSC.[96–122] In addition, there is evidence that photoinduced O_2^- creates traps in small-molecule OSCs.[103,104] In general, encapsulation is required for organic optoelectronic devices because O_2 can react in various ways with OSCs and usually these reactions are not desired.

3.2. n-Type Dopants

Early n-type dopants were also atomic dopants, namely alkali metals.[93] These materials are unstable when exposed to air or water and are therefore unsuitable for commercial applications. Many n-type molecular dopants have also been explored including tetrathiafulvalene derivatives such as BEDT-TTF,[123] organic dyes such as acridine orange base[124] and Pyronin B,[125,126] and organometallics such as [Ru(terpy)$_2$]^0,[127] $W_2(hpp)_4$,[128] and $Cr_2(hpp)_4$.[128] In particular, these last two compounds are good n-type dopants for C_{60}, yielding conductivities as high as 4 S cm^{-1}.[128]

An early approach by Gregg and Cormier was to use a zwitterionic OSC host molecule (a perylenediimide derivative) as an n-type dopant, in which the positive counterion was located at the end of a long alkyl side group.[129] The aim here was to immobilize the dopant counterion and to minimize structural disturbance to the doped OSC crystal. They observed a remarkable ten orders of magnitude increase in conductivity at 1 mol% doping level, as well as a quadratic dependence of the conductivity on doping level, indicating an increase in charge carrier mobility with doping level consistent with the Arkhipov model.[23] Surprisingly, this approach of using structural derivatives of the host OSC as dopants has not gained traction, despite its apparent success.[83,129]

Metal sandwich compounds such as cobaltacene[130] and decamethylcobaltacene[131,132] have also been applied as n-type dopants, but are unstable in air. A recent innovation to address air instability was the use of metal sandwich dimers that cleave upon doping. The dimers can be solution processed and only generate the air-unstable dopant after the cleavage reaction, which combines the benefits of longer storage life for the dopants, easy solution processing, and efficient n-type doping.[125,133–136] This is a promising approach for stabilizing extremely low IE dopants and may also be of interest in the

context of strong p-type dopants, which become increasingly difficult to stabilize as EAs increase.[137]

3.3. p-Type Dopants

The discovery of quinone structures with unsatisfied aromatic rings has led to a number of dopant structures with increased EA and lower volatilities. The prototypical compound of this class is TCNQ.[138–141] TCNQ was studied in detail because of its ability to form charge-transfer salts with electron donor small molecules.[31,45,46,138,139,141] The resulting organic salts showed conductivity increases of up to 10^{10} and revolutionized the organic electronics field.[45] However, TCNQ does not have a high enough EA (–4.3 eV relative to vacuum)[56] to effectively dope most OSCs. In particular, the recent synthesis trend has been toward small molecules and polymers with alternating electron donor and acceptor groups along the backbone of the OSC, which reduces the band gap and often increases the charge mobility for both holes and electrons.[142–148] These donor–acceptor co-polymers have proven difficult to dope efficiently, even with dopants which have an EA deeper than the polymer IE.[66,76,86]

Other recent OSCs have naturally high IEs, making them difficult to p-type dope.[149,150] Following this idea, an ideal p-type molecular dopant would be able to accept an electron from the HOMO of any conjugated small molecule or polymer. With IE in the range of 5.9 eV for polyfluorene polymers and even higher for fullerenes, it is synthetically challenging to develop dopant molecules that have an EA approaching 6.0 eV. The most common synthetic strategy used thus far are to develop an electron-poor core consisting of delocalized π-bonds or a metal center, then decorate the outside of the molecule with electron-withdrawing groups such as ester, fluorine, –CF$_3$, or nitrile groups that further deplete the core of the molecule and drive up the EA.

Figure 6 shows the molecular structure and approximate EA for a number of high EA molecular dopant structures. The EA was not directly measured using the same measurement technique for all of the molecules. Instead a combination of UPS, Kelvin probe measurements, and cyclic voltammetry (CV) measurements were used. We attempt to compare these measurements across the various articles and used the UPS measurements of –5.24 eV for F4TCNQ and –5.6 eV for Mo(tfd)$_3$ measured by the Kahn and co-workers as a reference to all other measurements.[151,152] There is likely an error of up to ±0.1 eV on the LUMO value of each value listed, which accounts for differences in techniques used by various groups.

Most of the depicted dopants were originally developed for small-molecule vacuum-deposited devices and were later adapted for use in solution-processed materials. The dopant structures can be classified into two categories:

1. Planar structures—including F4TCNQ and structural analogs, F6TCNNQ, 2,3-dichloro-5,6-dicyanobenzoquinone (DDQ), HATCN6, and CN6-CP.
2. 3D structures—including C$_{60}$F$_{36}$ or C$_{60}$F$_{48}$ (not shown), Mo(tfd)$_3$, and structural analogs.

The most studied dopant listed here is F4TCNQ, which has been used as a strong molecular dopant for decades,[151,153] mainly due to the wealth of knowledge surrounding its parent compound TCNQ.[45] Exchange of a fluorines for the 2,3,5,6-hydrogens in TCNQ increases the EA by ≈0.9 eV. This shift does not increase linearly with the number of fluorines substituted.[56] Nitrile groups are more strongly electron withdrawing than fluorine, so F2HCNQ has an EA that is ≈0.25 eV higher than F4TCNQ.[154] F6TCNNQ also has a slightly higher EA than F4TCNQ.[155]

F4TCNQ sublimates at 80 °C in vacuum and has been shown to contaminate the vacuum chamber in which it was deposited.[156] Subsequent samples prepared in the same vacuum chamber can be partially doped from F4TCNQ that sublimates from the walls of the chamber.[157] By comparison, F6TCNNQ is a larger molecule with a higher sublimation temperature that does not cause inadvertent contamination of samples.[155] The diffusion of dopants will be discussed in detail in Section 9.

Finally, structural modifications of F4TCNQ have been made with the goal of reducing the unwanted diffusion of the dopant. One strategy is to replace a fluorine with a bulkier side group.[158] A similar synthetic strategy is to replace a nitrile with a tailorable ester.[159] The ester substituted F4-R-TCNQ has been shown to increase the solubility of the dopant[159] and also to significantly decrease the diffusion rate of the dopant in an OSC layer.[160]

DDQ is one of a series of benzoquinones used as strong electron acceptors.[161] Its EA is not as high as F4TCNQ, but it is highly soluble, more easily solution processable, and can be used as a p-type dopant for trap filling or CTC formation.[162,163] HATCN6 is a larger planar structure that is poorly solution processable and has been used to study the effect of electron acceptors on the work function of metal surfaces.[164] Both DDQ and HATCN6 are interesting synthetic starting points for development of higher EA molecular dopants.

CN6-CP was originally synthesized in the 1970s[165,166] and was recently identified as a promising molecular dopant by Karpov et al.[137] With an EA of –5.87 eV, this is the strongest p-type dopant yet reported in the OSC literature.[137,165,166] The authors report that CN6-CP can be sublimated at 200 °C. Interestingly, although the neutral molecule was reported to be essentially insoluble and reactive toward many solvents, it is apparently both stable and soluble when blended with conductive polymers such as PDPP(6-DO)$_2$TT in CH$_2$Cl$_2$. PDPP(6-DO)$_2$TT is a high mobility donor–acceptor polymer which has previously proven difficult to dope to high concentrations.[167] However, upon doping with CN6-CP, conductivities of 30–70 Ω^{-1} cm^{-1} were achieved upon doping at a 1:1 molar ratio.[137]

3D dopant structures are bulkier than the planar structures, and thus promising for reducing diffusion rates.[87] C$_{60}$F$_{36}$[168] and C$_{60}$F$_{48}$[169] (not shown) are two examples of substituted C$_{60}$ molecules that are decorated with electron-withdrawing fluorine to increase the EA. Both molecules are completely insoluble and can only be processed using vacuum deposition. Their EAs are higher than that of F4TCNQ and they have been shown to be more stable against thermal diffusion.[87,157] However, their bulkiness means that they displace more volume within an OSC layer, limiting achievable doping levels and likely

**ADVANCED
SCIENCE NEWS**

www.advancedsciencenews.com

**ADVANCED
MATERIALS**

www.advmat.de

causing more significant morphological disruption. Their size also precludes intercalation into crystalline domains, except perhaps in materials such as PBTTT with loosely packed side chains.[170,171]

Finally, Mo(tfd)$_3$ is an organometallic dopant with three side rings arranged in a pinwheel-like pattern. This dopant has been well studied in vacuum-deposited samples and demonstrates a high EA of −5.6 eV and good bair stability.[152,172] Recently, one −CF$_3$ group on each side ring was replaced with an ester to make the dopant solution processable.[173] Given the desire to create organic electronic devices using solution-processing methods, we predict that more work into tailoring the solution processability of molecular dopants like Mo(tfd-R)$_3$, F3-R-TCNQ, and F4-R-TCNQ will be performed in the near future.

Alkyl silanes[174–179] are large gas-phase molecules that show excellent doping properties in films of P3HT and PBTTT and better thermal stability than halogens. For example, the conductivity of the polymers P3HT and PBTTT can be increased by 10^6–10^7 with exposure to hydrolyzed fluoroalkyl trichlorosilane (FTS), reaching conductivities over 10^3 Ω^{-1} cm^{-1} in PBTTT. The conductivity decreased by only 0.5% per hour in vacuum which shows reduced volatility compared to halogens. This has been argued to result from cross-linking between silane molecules.[174] These films also show high Seebeck coefficients and thermoelectric power factors[178,179] that make them promising candidates for use in polymer thermoelectrics.[39] Currently, there are no data available about diffusion of alkyl silanes after doping.

3.4. Summary

A molecular dopant is defined as a neutral small molecule that can either donate or accept an electron from an OSC without undergoing any covalent-bond-breaking reaction. The only chemical interaction between a molecular dopant and an OSC is electron transfer, which is reversible. Effective design of p-type molecular dopants places an emphasis on maximizing the EA so that it is higher than the IE of most OSCs to make charge transfer favorable.

Most p-type molecular dopants have an electron-poor core with electron-withdrawing groups decorated on the extremities of the molecule to further reduce the EA. All of the p-type dopant structures were originally developed for use in vacuum evaporated small-molecule devices and only recently have the organic electronics community sought to use the same structures in solution-processed devices. As a result, many of the dopants are poorly soluble or insoluble. Recently, some of the structures have been altered with the additional design criteria of solubility or miscibility. Future work in the design and synthesis of molecular dopants needs to focus on increasing the dopant strength, reaction yields, solubility/miscibility, and development of air/stable dopants.

4. Fabrication and Morphology

The effects of doping on film morphology—and conversely film morphology on doping—is complex and often difficult to

characterize. Doping can strongly affect and be affected by the OSC crystal structure,[21,44,56] degree of crystallinity,[28,34,35,88] miscibility of the dopant with crystalline and amorphous phases,[21,27,28] differences in the electronic properties of amorphous and crystalline phases,[27,28,35,88,180] changes in trap density induced by dopants,[21,24,42,84,85,181,182] and changes to the morphology as a function of doping density.[22,27,77] At this point, it is difficult to identify even general empirical rules for doping efficiency, as discussed in Section 2.

In identifying the difficulty of predicting the interaction between dopants and OSCs, we point out that modeling this system at the molecular scale requires both electronic (usually, density functional theory (DFT)) and structural (usually, molecular dynamics) components and that development of multiscale models combining these levels of theory is at the leading edge of theoretical capabilities.[52,183–194] We encourage more research in this area.

In this section, we will focus on the interactions between p-type molecular dopants and semiconducting polymers, the role that the doping method plays in determining the doped film morphology, and the consequences of these morphological differences on charge transport properties.

4.1. Fabrication Methods

Most molecular dopants were first synthesized for and tested using vacuum deposition methods. In this case, a doped film is created by co-evaporating the small-molecule OSC and the dopant at the desired mixing ratio in a high vacuum chamber. This method of deposition is satisfying because the exact ratio between OSC and dopant can be measured using a quartz microbalance, and the exact thickness of the mixed layer is easily controllable. Polymer OSCs cannot be vacuum deposited, but can be doped sequentially by thermal evaporation after spin coating.[34,37]

For solution processing there are two fabrication methods: co-deposition from solution and sequential deposition. For co-deposition, the polymer and dopant are mixed together in solution at the desired mixing ratio and then co-deposited onto a substrate using spin or blade coating.[55,195] This method has the advantage that the mixing ratio is known and controlled before deposition. The major disadvantages of this deposition method are (1) many molecular dopants, like $C_{60}F_{36}$, are insoluble or poorly soluble, limiting the total solution concentration and thereby film thickness that can be achieved and (2) many polymers show reduced solubility when ionized, causing them to crash out of solution or to form undesired structures in solution. For example, P3HT and PBTTT will spontaneously crystallize in good solvents if even extremely low concentrations of F4TCNQ are added to the solution.[22,27,37,77,180] The strong interaction between the dopant and polymer in solution makes it nearly impossible to create doped polymer films with morphology that is comparable to undoped films using this method. Interestingly, some systems appear to show the opposite effect, displaying increased solubility upon doping.[137]

Sequential deposition of the OSC and dopants has several processing advantages. For sequential doping, the dopant

**ADVANCED
SCIENCE NEWS**
www.advancedsciencenews.com

**ADVANCED
MATERIALS**
www.advmat.de

molecules could be either evaporated onto a polymer film[34,179] or deposited from an orthogonal solvent that does not dissolve the polymer film.[27,37,196–198] Small nonpolar dopants such as F4TCNQ evaporated onto P3HT rapidly penetrate the film and diffuse through the entire film thickness because the polymer has significant amorphous domains.[34,37,160]

A few studies have attempted to quantify how far dopant molecules will diffuse into a polymer or small-molecule film from evaporation or what controls the mixing. One recent study used XPS and sputtering to determine the concentration profile of F4TCNQ in PBTTT;[34] however, less destructive methods such as X-ray or neutron reflectometry could yield better measurements. In the listed studies, the authors have generally assumed that these sequential methods produce an essentially homogeneous doping profile through the entire film depth. Diffusion measurements, which will be discussed in Section 9, suggest that this is a reasonable assumption for small dopants such as F4TCNQ,[87,160] but not for larger molecules.[87,198] Therefore, some degree of caution should be used when applying sequential doping techniques for new OSC:dopant systems, particularly with bulky 3D dopants.

For large area processing, the idea of sequentially depositing dopant molecules from solution is very attractive.[199] The sequential doping technique was first developed with the observation that phenyl-C61-buteric acid methyl ester (PCBM) molecules could be sequentially added to P3HT films at up to 30 vol% PCBM[200] using marginal solvents like dichloromethane or cooled toluene.[200–202] Neutron scattering and X-ray studies showed that the amorphous domains of the polymer swelled and filled with PCBM, while crystalline P3HT domains remained insoluble.[202]

Using the same technique, F4TCNQ can be added to P3HT using orthogonal solvents for the P3HT such as acetonitrile (AN), acetone, or dichloromethane.[27,37,196,197] The main disadvantage of solution-based sequential deposition of dopants into polymer films is that the doping density depends on the uptake of dopants into the film rather than the solution mixing ratio or the mass of dopant deposited by evaporation. Therefore, additional work is required to characterize the doping concentration.[27]

4.2. Characterizing Film Doping Level

The density of ionized dopants in an OSC film can be quantified against a calibration curve using various techniques, including UV–vis–NIR spectroscopy, fluorescence quenching, or UPS. More sensitive absorption techniques such as photothermal deflection spectroscopy, can detect doping levels as low as ≈10^{-2} mol%.[22,62] These measurements quantify the density of ionized dopants, or the total charge carrier density in the doped OSC.[22,29,41,44,56,60,62] Secondary ion mass spectroscopy (SIMS) can also be used to determine the density of dopant molecules (although the ionization state is not determined) if the dopant has a unique atom or isotope. UV–vis–NIR is the simplest method for characterizing high doping levels (>1%). Fluorescence quenching is very sensitive to low dopant concentrations (<1%), but is often completely quenched above a few mol% doping and requires a calibration curve.[36,87,203]

Additionally, even neutral dopant molecules within the OSC may act as fluorescence quenchers by trapping photoinduced charges, complicating the analysis of doping level. With these caveats, UV–vis—NIR and fluorescence quenching are straightforward and complementary techniques for characterizing film doping level.

In general, these values provide a good estimate of the total dopant density assuming that nearly all dopants are ionized, which is reasonable in many systems.[22,44,62] However, the addition of a large volume fraction of dopants often leads to the formation of a neutral dopant phase, either because the doping sites are all filled[22,27] or because the dopants crystallize or cluster due to lack of miscibility.[79] Therefore, it is necessary to validate the assumption that ionization is efficient when calculating doping levels from spectroscopy, especially at high doping levels. Ionization efficiency can usually be measured, since neutral phases are typically visible in UV–vis–NIR or FTIR spectra[22,44,62,66] and can sometimes be observed by atomic force microscopy (AFM).[159]

Optical spectroscopy does not provide an indication of the free charge carrier density, which is often much lower than the total carrier density.[21,26] Measurements of dopant density and ionized dopant density are not consistent because doping efficiencies are generally <100%, as discussed in Section 2. With an appropriate model,[24,29,78,204] the density of free charge carriers can be determined by observing the doped OSC band bending at a metal interface (shown in Figure 1).[19,21] Simultaneous measurement of the dopant density and the free carrier density is necessary to determine the doping efficiency.

4.3. Langmuir Isotherm Equilibrium Model

An interesting question is what factors determine the doping level in an OSC film prepared using sequential deposition. Jacobs et al. studied this by sequentially doping P3HT from various concentration solutions of F4TCNQ in AN.[27] The film doping level was reported to depend only on the concentration of the sequential doping solution and was independent of exposure time, indicating that a thermodynamic equilibrium was reached between the concentration of F4TCNQ in solution and the concentration of F4TCNQ•− incorporated into the P3HT film. The equilibrium loading of a small molecules into a porous matrix follows a typical Langmuir isotherm model[205] given by

$$\frac{C_d}{C_{d,sat}} = \Theta = \frac{K_{eq}C_s}{1 + K_{eq}C_s} \tag{2}$$

where C_d is the film doping level, $C_{d,\,sat}$ is the saturated film doping level which would be reached if doped with an infinitely concentrated solution (and assuming no phase change of the OSC), Θ is the proportion of occupied doping sites in the film, C_s is the concentration of the dopant in solution, and K_{eq} is the equilibrium constant. Using this model, Jacobs et al. fit the doping level in the P3HT film as a function of the F4TCNQ solution concentration (**Figure 7**), obtaining $C_{d,sat}$ = 4.9 mol% and ΔG = −0.23 eV (K_{eq} = 8000). The $C_{d,sat}$ value was consistent with AFM images of doped films, which
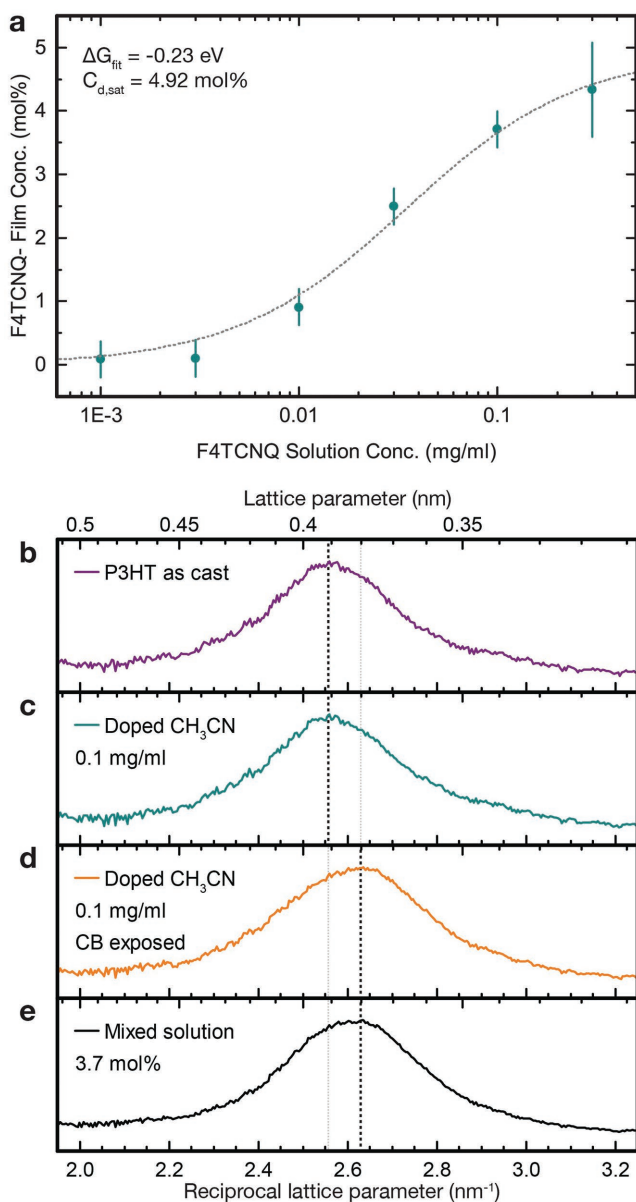
Figure 7. a) Film doping level (given as F4TCNQ film concentration) as a function of doping solution concentration. Data points are experimental data with doping level estimated by IR absorption; the dashed line is a fit to a Langmuir isotherm model.[27] b–e) Radially integrated electron diffraction patterns showing the P3HT π–π stacking peak. Films c–e have similar doping levels, but different preparation methods. b) Undoped P3HT, c) P3HT:F4TCNQ sequentially doped from a 0.1 mg mL^{-1} AN solution, d) P3HT:F4TCNQ sequentially doped from a 0.1 mg mL^{-1} AN solution, wetted with ≈50 µL CB and allowed to dry (≈10 min), and e) P3HT:F4TCNQ doped at 3.7 mol% prepared by the mixed solution method. Reproduced with permission.[27] Copyright 2016, Royal Society of Chemistry.

showed the formation of phase-segregated clusters above 5 mol% doping, while the obtained ΔG was nearly identical to the difference between the HOMO of the P3HT and LUMO of F4TCNQ. The consistency of these observations suggests that the Langmuir isotherm model accurately describes the doping reaction equilibrium. In addition, the ΔG suggests

that incorporation of the dopant into the film is mainly driven by ionization.[27]

A spectroscopic study of F4TCNQ doping in P3HT solution-mixed samples confirms that both ionized and neutral F4TCNQ are present in the film and that the ratio of neutral to ionized F4TCNQ increases with increasing mol% F4TCNQ.[62] Additionally, a recent article by Kroon et al. on F4TCNQ doping of a thiophene with polyethylene oxide (PEO) side chains (p(g$_4$2T-T)) corroborates the concept of an equilibrium between neutral and ionized dopants which changes as a function of the doping level. Kroon et al. published ionization efficiency versus mol% doping data that show identical behavior to the plot in Figure 7a, although they did not fit their data to a Langmuir isotherm model.[163]

This equilibrium model for molecular doping has several important consequences. First, it establishes that the doping density in sequentially doped films is controlled by thermodynamic equilibrium with the accessible doping sites in the polymer. Second, it allows for determination of the total density of accessible doping sites within the polymer film, although when doping from a polar solvent, the site density is limited to the density of amorphous sites Third, the concepts of available doping site density and binding energy per site in the polymer have significant implications for development of dopant diffusion and drift models (as discussed in Section 9). Finally, as will be discussed below, it is not only possible to reliably and predictably dope an OSC film using sequential solution processing, but also to control the placement of the dopants into the amorphous or crystalline phases of the polymer by choice of solvent or postdoping film processing (e.g., annealing or solvent exposure).

4.4. Morphology of Sequentially Doped Films

Several groups have studied the structure of doped films using X-ray diffraction (XRD).[22,34,44,56,77,197,206] For example, Duong et al. used grazing incidence X-ray diffraction (GIXD) to study P3HT:F4TCNQ films fabricated by the mixed solution method and observed no change in the P3HT crystal structure below about 3 mol% doping.[22] However, at higher doping levels, a shift in the unit cell dimensions was observed, which was consistent with intercalation of F4TCNQ molecules between the P3HT chains in the π–π stacking direction.[22] Cochran et al. published a very thorough study using solid-state NMR and XRD, examining the structure and morphology differences in films of solution cast PBTTT and PBTTT mixed with F4TCNQ.[77] In the solution-mixed films, they similarly concluded that F4TCNQ was intercalated into the PBTTT π–π stacking, creating a co-crystal that presumably formed in solution. Müller et al. studied the effect of casting solvent on mixed-solution cast P3HT:F4TCNQ and observed a much stronger π–π stacking peak in films cast from chloroform as opposed to chlorobenzene.[89] In addition, optical spectroscopy and conductivity measurements indicated the chloroform-cast films showed higher doping efficiency. This suggests that interactions between the polymer and dopant in solution or during spin-coating strongly affect the morphology and properties of the resulting films.[89]

**ADVANCED
SCIENCE NEWS**
www.advancedsciencenews.com

**ADVANCED
MATERIALS**
www.advmat.de

Jacobs et al. studied P3HT films sequentially doped by F4TCNQ/AN solutions using electron diffraction.[27] Figure 7b shows P3HT π–π stacking (010) peak of an undoped film along with films prepared by mixed-solution and sequential methods. After sequentially doping with F4TCNQ/AN, conductivity measurements and UV–vis–NIR spectra indicated efficient doping, but no shift in the π–π stacking peak was observed (Figure 7b). This indicates the F4TCNQ is not able to penetrate into crystalline P3HT domains but easily diffuses into amorphous domains, presumably because the AN (which is highly polar) is unable to swell the crystalline domains but is able to infiltrate the less dense amorphous domains.[27]

A greater activation energy, e.g., thermal stress, or a decrease in the activation barrier, e.g., by interaction with solvent molecules, is needed to allow diffusion of F4TCNQ into crystalline P3HT domains. Figure 7c shows the π–π stacking peak of a P3HT film doped from F4TCNQ/AN after exposure to CB. Note that P3HT:F4TCNQ films are insoluble in CB.[27,37] This film does show a reduction of the π–π stacking spacing, indicating that CB exposure allows for incorporation of F4TCNQ molecules into the P3HT crystallites and that this intercalation is thermodynamically favorable.[22,27] Within the amorphous domains of a P3HT film, F4TCNQ can be loaded to ≈5 mol% before the F4TCNQ forms a separate pure phase, visible by UV–vis spectroscopy and AFM.[27] However, it was observed that P3HT films could be doped beyond this limit using a solvent which was able to infiltrate/dissolve the crystalline domains. These higher doping levels are possible using either a two step sequential doping process, first from F4TCNQ in AN followed by F4TCNQ in CB solution,[27] or in a single doping step from F4TCNQ dissolved in a co-solvent mixture of 3:1 dichloromethane:tetrahydrofuran (THF).[197] The polarity of the solvent used in the sequential doping solution controls whether the dopant molecule is included or excluded from the polymer crystallites.

Crystallites in semicrystalline polymers show a lower band gap than amorphous domains. Therefore, in the morphology described above, charge carriers should segregate to crystalline domains, spatially separating them from the dopant anions. This effect has been observed spectroscopically by Gao et al. in P3HT:F4TCNQ.[35,180] The segregation of dopants from conduction pathways is analogous to modulation doping in inorganic semiconductors, which yields improved carrier mobilities by reducing trapping or scattering of charge carriers by ionized dopants.[207] Jacobs et al. showed that sequentially doped P3HT/F4TCNQ films with dopants segregated from crystalline domains allow for conductivities of >1 S cm^{-1} at 4× lower dopant density than in solution-mixed films. At a given doping level, the sequentially doped films are over an order of magnitude more conductive than those prepared by mixed-solution doping.[27]

Films of PBTTT doped with F4TCNQ show an even more dramatic example of the benefits of sequential doping.[34,208] Kang et al. prepared PBTTT/F4TCNQ samples by first depositing the PBTTT from solution and then evaporating the F4TCNQ onto the PBTTT layer.[34] They demonstrated that the F4TCNQ diffuses into the PBTTT film and efficiently dopes the polymer by ion-pair formation, as was seen in the solution-mixed samples prepared by Cochran et al.[77] However, in the sequentially deposited samples, the F4TCNQ does not intercalate between the polymer backbones, but is found in the free space between the polymer side chains. In this configuration, the dopant does not affect the packing of the polymer backbone but does increase the hole density. At molar doping ratio of 0.3–0.35 a conductivity of 250 S cm^{-1} was measured, which is a 100-fold increase over the 2 S cm^{-1} at a molar doping ratio of 0.25 reported by Cochran et al.[34,77] Even higher conductivities of 670 S cm^{-1} were recently reported by Patel et al. in PBTTT films doped by F4TCNQ in the vapor phase.[208]

The dramatic improvement in conductivity in these samples appears to be due to a fundamental change in the nature of charge transport, resulting from the high charge density and higher degree of structural order observed in sequentially doped samples. Kang et al. goes on to show that the room temperature Hall mobility of holes in this sample (1.8 cm^2 V^{-1} s^{-1}) is higher than other reported doped polymers such as PEDOT:PSS (which also showed nonideal Hall effect behavior), AsF$_5$ doped poly(p-phenylene), or AsF$_5$ doped polyacetylene.[34,209,210] They also observed a Pauli-like spin susceptibility and positive magneto-conductance, both of which are characteristic of coherent, band-like charge transport, in contrast with the hopping transport typically observed in OSCs.[42]

Several factors appear to drive the observed improvements in charge transport. Sequentially doped films show increased edge-on film texture relative to mixed-solution films,[197] which is known to correlate with improved charge transport.[60] However, it has also been observed that mixed-solution doping results in the formation of nanoscale aggregates in solution[27] which reduces the density of tie chains between crystalline domains and reduce charge transport.[25] It is also plausible that the spatial separation of charge carriers and dopant ions may reduce charge trapping, increasing the free carrier density. This last theory is supported by ESR measurements by Kang et al.[34] In addition, both Kang et al and Patel et al. observed increases in film crystallinity upon doping, which should contribute to the improved charge transport.[34,208]

In PEDOT:PSS, which is more conductive but also more disordered, no such evidence of coherent transport has been observed, suggesting that the high degree of order maintained during sequential deposition is an important prerequisite to band-like transport.[34] Interestingly, a new model by Kang and Snyder shows that the conductivity and Seebeck coefficient of nearly all OSCs can be explained by a power law relationship with a power law parameter (which they call the transport parameter (s)) of $s = 3$.[211] However, PEDOT:Tos (Tos is tosylate), a close relative of PEDOT:PSS, was instead found to be consistent with $s = 1$, indicating a fundamental difference in the nature of charge transport. PEDOT:PSS and PEDOT:Tos generally show higher conductivities and thermoelectric power factors than other OSCs, so studies aimed at explaining the differences in charge transport between these two material classes are likely to be a fruitful line of research.

Diffraction studies can provide only limited structural information about the crystalline domains in polycrystalline films. The diffraction data indicate an average spacing into which several equivalent crystalline structures can be minimized. Neutron scattering may be useful in further characterizing the structure of both crystalline and amorphous doped films. A recent study by Harrelson et al. discussed the use inelastic

**ADVANCED
SCIENCE NEWS**

www.advancedsciencenews.com

**ADVANCED
MATERIALS**

www.advmat.de

neutron scattering (INS) for this application. INS provides a spectrum analogous to FTIR spectroscopy without being subject to selection rules, so all structures present in the film are observed in the spectrum with equal weighting. This property allows for decomposition of the spectrum into a linear combination of structural fits. Harrelson et al. observed that in undoped P3HT two crystal structures were present, while only one was observed in P3HT:F4TCNQ. In addition, they observed changes in the side chain configuration in doped films.[212]

Scanning probe techniques have also been applied to the characterization of doped film morphology.[206] For example, Duong et al. used conductive AFM, along with XRD, UV–vis spectroscopy, and bulk conductivity measurements to study the morphology of P3HT:F4TCNQ films coated from solutions at different temperatures. They observed lower doping efficiency, lower conductivity, and higher crystallinity in films coated from hotter solutions. Conductive AFM revealed that films cast from hotter solutions showed more uniform topography and conductivity.[206] The authors suggested that these results may indicate segregation of dopants to amorphous domains at higher casting temperatures, but this is at odds with other results which have shown that incorporation of dopants into crystallites reduces, rather than increases conductivity.[27,34,77] Further work is necessary to better understand the role of solution temperature in mixed-solution doping.

As described in Kang et al., ESR can also be useful in characterizing doped film morphology. PBTTT sequentially doped using FTS vapor yielded higher conductivities, up to 10^3 S cm^{-1}.[174,175,177–179] ESR studies of these films also showed a Pauli-like spin susceptibility, similar to PBTTT:F4TCNQ.[177] Interestingly, FTS-doped PBTTT shows more promising thermoelectric performance than PBTTT films doped by F4TCNQ using a mixed-solution process.[178,179] Since the Seebeck coefficient is related to film disorder,[213] it is plausible that this increase in performance is due to the increased order resulting from the vapor phase sequential doping process. It will be interesting to see if the PBTTT:F4TCNQ films described by Kang et al. show similarly improved thermoelectric performance.[34]

Several groups have also investigated an electrochemical form of sequential doping: using ionic liquids to gate organic field effect transistors (OFETs).[42,84,214–217] This method can yield very high conductivities and charge densities; we refer the reader to the review by Kim et al.[42] In a recent study, Tanaka et al. used ESR of OFETs to characterize the morphology of PBTTT films electrochemically gated by ionic liquids.[217] They observed complete bleaching of the PBTTT π–π* absorption, yet measurement of the g-tensor by ESR indicated that the PBTTT chains maintained their as-cast, edge-on morphology. Temperature-dependent ESR also revealed Pauli-like spin susceptibility. These results demonstrate the power of ESR to characterize film texture, and further indicates that it should be possible to maintain good film morphology using sequential doping, even at extremely high doping levels.[217]

4.5. Summary

Together, these studies serve to highlight both the complexity and importance of doped film morphology on charge transport,

and demonstrate the power of sequential doping methods to minimize morphological disruption. Although sequential doping has been successfully applied to several polymer:dopant systems,[27,34,134,178,198] further work is needed to verify if this technique can be used to control the dopant anion location within the OSC matrix. In the near future, we expect to see more studies evaluate the use of sequential doping to control structure and morphology in OSC films.

5. Controlling Defects and Impurities with Dopants

5.1. Defects and Trap Sites in OSCs

The molecular nature of organic semiconductors results in significant structural and energetic disorder, even in crystalline films.[25,213] As these defects are often due to molecular packing and do not necessarily involve changes in covalent bonding,[25,218,219] the defect energy is low, and consequently the defect density is high, typically on the order of 10^{17}–10^{19} cm^{-3},[82,101,103,104,130,181,220–227] but occasionally as low as 10^{15} cm^{-3} in highly purified materials.[103,228,229] These defects produce a tail in the density of states which extend into the band gap of the OSC, and are generally well fit by an exponential function.[218,230–234] An example of these exponential band states in copper phthalocyanine (CuPc) measured by UPS is shown in **Figure 8**a.

The low ionization energy of these tail sites makes them susceptible to doping by impurities leftover from chemical synthesis or introduced during sample preparation and measurement.[235–240] Common environmental impurities in OSCs include water[226,238,241,242] and oxygen.[96–114,116–122] However, even in "impurity-free" samples (to the extent that such a thing is possible) defects formed by self-ionization of conjugated bonds into charged defect pairs have been proposed to exist, on the basis of their chemical reactivity with oxidizing or reducing agents.[223,228,240,243,244] In most OSC samples, positively charged defects are more delocalized than negatively charged defects, causing materials to behave as if they were slightly p-type doped.[132,223,228,235,238,239,243,245,246] OSCs based on napthalenediimide or perylenediimide groups typically show the opposite behavior, behaving as if they were slightly n-type doped.[33,83,223]

The intrinsic p-type behavior of most OSCs is generally a result of defects or the interaction of the OSC with its environment, rather than an intrinsic property of the material. Until the mid-2000s, most OSCs were thought to be inherently better hole conductors than electron conductors. However, work by Chua et al. demonstrated that OFETs composed of a wide range of OSCs prepared using a cross-linked divinyltetramethylsiloxane-bis(benzocyclobutene) dielectric unexpectedly displayed ambipolar behavior.[238] This effect was found to be highly dependent on the dielectric layer used in the OFETs, with bare SiO$_2$ dielectrics yielding almost no n-type conduction. FTIR spectroscopy of OFETs revealed the source of the problem to be p-type doping of the OSC by silanol groups at the surface of the silicon substrate.[238] In addition to demonstrating that many OSCs display intrinsically balanced electron
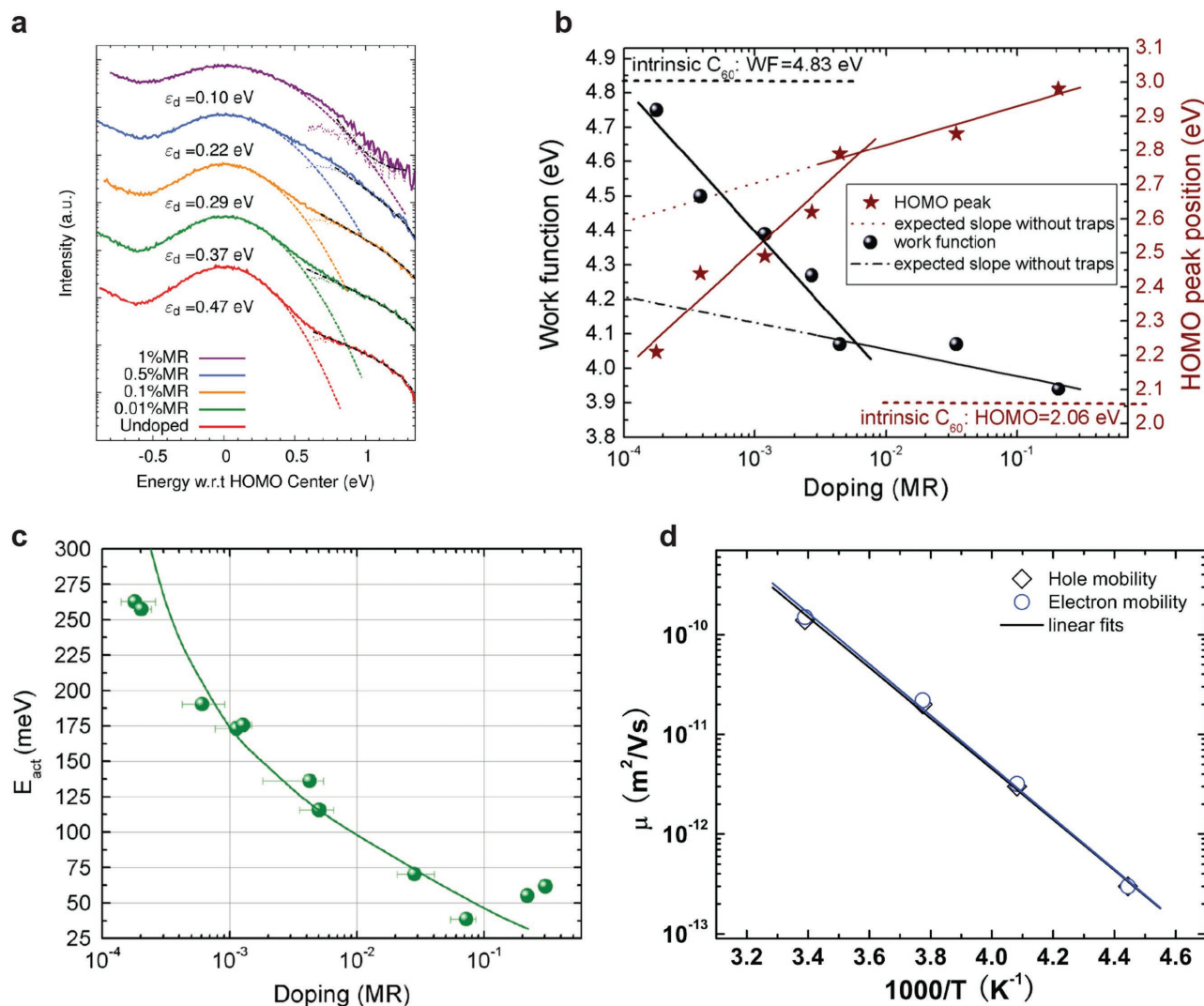
ADVANCED
SCIENCE NEWS
www.advancedsciencenews.com

ADVANCED
MATERIALS
www.advmat.de

Figure 8. a) CuPc HOMO band measured by UPS p-type doped with varying concentrations of Mo(tfd)$_3$. Colored dotted lines indicate Gaussian fits to the HOMO band; black dashed lines indicate exponential fits to tail states extending into the band gap. The decay rate of the exponential fits is shown, and decreases with increasing doping level. Also note the broadening of the Gaussian fits with increased doping. Reproduced with permission.[181] Copyright 2016, American Chemical Society. b) Plot of work function and HOMO peak position with respect to the Fermi level as a function of doping level in C$_{60}$ n-type doped by [RuCp*(mes)]$_2$ obtained by UPS.[82] c) Conduction activation energy in the same system as in part (b), obtained by variable temperature I–V measurements. The solid line indicates the activation energy obtained from Monte Carlo simulations with a trap density of 1.9×10^{18} cm^{-1}. Reproduced with permission.[82] Copyright 2012, American Physical Society. d) Arrhenius plot of electron mobilities in decamethylcobaltacene-doped MEH–PPV and hole mobilities in undoped MEH–PPV at various doping levels, revealing balanced hole and electron transport after LUMO trap filling. Reproduced with permission.[132] Copyright 2010, American Physical Society.

and hole transport, this work illustrates how seemingly insignificant interactions can dominate the observed properties of OSCs.

Doping by impurities can also lead to somewhat counterintuitive effects. Liu et al. studied the effects of material purity on perylene diimide/pthalocyanine bilayer solar cells.[247] In impure samples, the OPV devices showed a power conversion efficiency (PCE) of 0.4%; however, after purification of the materials, the PCE dropped 200-fold to 0.02%. This surprising result was understood to be due to unintentional doping of the film layers by impurities. In the impure (doped) device, the electric field is concentrated at the heterojunction, providing a

strong field to split excitons and reduce recombination. Purification reduces the conductivity of the layer, resulting in a more uniform field over the device and consequently reducing the field at the interface.[247] Thus, defect sites are not always undesirable, although intentional doping of pure materials is more controllable and yields superior results.[223] Again, we stress that despite their low concentration, defects and impurities play a major role in determining seemingly intrinsic material properties. In the following subsections, we will discuss methods for controlling defect sites with intentional doping, as well as approaches for controlling intrinsic doping in OSCs.

**ADVANCED
SCIENCE NEWS**

www.advancedsciencenews.com

**ADVANCED
MATERIALS**

www.advmat.de

5.2. Trap Filling with Dopants

Defect states deep within the band gap are highly localized and therefore have high hopping-transport activation energies; these states are often referred to as trap sites.[211,245] These trap sites can be filled by doping, typically at very low doping levels, which has the effect of "smoothing out" the energetic landscape for charge transport.[82,181,182,227,248] Olthof et al. studied trap filling in C_{60} and observed nonlinear shifts in work function (Figure 8b), conductivity, and charge carrier mobility at doping levels below 10^{-2} mole ratio (MR). These shifts are indicative of trap filling and result in an order-of-magnitude decrease in hopping activation energy (Figure 8c), consistent with Monte Carlo simulations with a trap density of 1.9×10^{18} cm^{-1} (solid line in Figure 8c).[82]

In a separate work, the same group also investigated the effects of ultralow n-type doping on OFETs made from purified and unpurified C_{60}.[249] They observed that in unpurified samples, doping at 1 ppt decreased the OFET threshold voltage from 18 to 5 V, while OFETs made using purified C_{60} showed threshold voltages of near 5 V independent of doping level. The reduction in threshold voltage in the unpurified samples is consistent with trap filling by the dopants, while in purified samples the trap density was lower, and thus not strongly affected by doping.[249]

Trap filling at ultralow doping levels has also been observed in polymers. Zhang et al. studied the effect of doping with decamethylcobaltacene, a strong n-type dopant,[131] on charge carrier mobility in poly[2-methoxy-5-(2-ethylhexyloxy)-1,4-phenylenevinylene] (MEH-PPV) using space charge limited current measurements.[132] As shown in Figure 8d, they observed that the hole mobilities in undoped (i.e., intrinsically p-type doped) MEH-PPV were nearly identical to the electron mobilities in n-type doped MEH-PPV. In addition, the temperature dependence of the carrier mobility was the same, indicating that the degree of disorder in the HOMO and LUMO bands was similar. As with the work by Chua et al. discussed above,[238] this strongly suggests that most observations of preferential p- or n-type conduction in OSCs are likely due to unintentional doping.[132]

There have been many other device studies that explore the effects of trap sites and trap filling by doping in OFETs,[28,42,84,135,175,177,214–216,250–254] OPVs,[248,255–261] and organic light emitting diodes (OLEDs),[32] which we will not discuss in detail here. Many of these articles are covered in an excellent review on doped organic transistors by Lüssem et al.[17] and a past review on doped transport layers by Walzer et al.[32]

5.3. Complexities in Low Doping Level Studies

As discussed in Section 4, effects of doping in OSCs are often complex, depending on the interplay between trap-filling, doping-induced structural disorder, and Coulombic interaction between charge carriers and dopant ions. In ultralow doping studies, the complexities described above are further compounded by the difficulty in characterizing interactions which occur between species at concentrations too low to be easily detected using microscopy, spectroscopy, or diffraction methods.

It was not until recently that direct spectroscopic evidence of trap filling was obtained, due to the relatively low density of these states. Figure 8a shows UPS spectra demonstrating trap filling in CuPc by the dopant Mo(tfd)$_3$ taken from Lin et al.[181] As the doping level increases, the exponential tail states become positively charged by the dopants and are therefore no longer visible to UPS, which is only sensitive to states occupied by electrons; that is, the dopants fill the trap sites. This is visible as a shortening of the decay rate (η_d, shown below each curve) of the exponential DOS tail and results in a reduction in the hopping activation energy as previously discussed.[181]

As described theoretically by Arkhipov et al., doping also leads to broadening of the HOMO DOS, visible in Figure 8a, and creates new tail states in the band gap due to Coulombic interaction between charge carriers and dopant anions.[24] Theoretically, this results in a decrease in charge carrier mobility at low doping levels, followed by a strong increase in mobility at higher doping levels as the Coulomb potentials of nearby dopant ions begin to overlap.[23] Behavior consistent with this model has been observed experimentally in P3HT:F4TCNQ (see Figure 2), using a combination of impedance measurements from metal–insulator–semiconductor devices and current–voltage measurements of films doped at the ppm–ppt level.[21,26] However, it turns out this effect alone was not sufficient to explain the DOS broadening depicted in Figure 8a.[181] GIXD revealed that doping also results in increased crystalline disorder, even at low doping levels, and simulations showed that this structural disorder accounts for the extra DOS broadening observed.[181]

A recent study by Shang et al. further demonstrates just how difficult sorting out the effects of ultralow doping on device performance can be.[182] In P3HT:PCBM OPV devices, it was found that doping with F4TCNQ at ultralow levels (10^{-5}–10^{-6} wt%) increased open-circuit voltage (V_{OC}) and fill factor (FF), yielding an $\approx$0.35% increase in PCE in both annealed and unannealed cells. Although the hole mobility increased upon doping in annealed cells, it decreased in unannealed cells, indicating that an increase in hole mobility could not explain the improved FF. Instead, transient photocurrent and charge extraction experiments showed that the improvement in the unannealed cells was due to trap filling by dopants. In the annealed cells, no trap filling was observed. The improvement in the FF was attributed to a shift in the P3HT/PCBM CT-state energy resulting from a beneficial effect of doping on the film morphology. In both samples, doping at 10^{-4} wt% strongly decreased device performance as a result of doping-induced Coulombic traps.[182]

In poly[2,6-(4,4-bis-(2-ethylhexyl)-4H-cyclopenta[2,1-b;3,4-b′]-dithiophene)-alt-4,7(2,1,3-benzothiadiazole)]:[6,6]-phenyl-C71-butyric acid methyl ester (PCPDTBT:PC70BM) solar cells, doping with F4TCNQ at 1:250 molar ratio has also been reported to increase PCE from 6.4% to 7.9% as a result of increased short-circuit current density (J_{sc}).[262] Doping at moderately high levels (up to 4 mol%) was previously observed to increase the rate of ultrafast CT exciton splitting, and resulted in a shift of the CT photoluminescence (PL) band, consistent with a reduced trapping at the donor–acceptor interface by CT excitons.[248] However, Shang et al. confirmed that while doping increased PCE, it also continually increased the trap

ADVANCED
SCIENCE NEWS
www.advancedsciencenews.com

**ADVANCED
MATERIALS**
www.advmat.de

density at ultralow doping levels between 10^{-6} and 10^{-4} wt%, which should lower J_{sc} by increasing recombination. Instead, it was found that doping led to an unintentional increase in film thickness, presumably by increasing the solution viscosity, which increased the external quantum efficiency at long absorbance wavelengths.[182] These results serve to illustrate the care needed in analyzing ultralow device studies—in all three systems studied, PCE increased upon doping, but these improvements were all attributed to different mechanisms.

Since trap sites in OSCs can take the form of morphological defects such as packing defects, heterogeneities in chemical structure, or impurities, it is not always clear that effects observed at low doping levels are purely due to charge transfer. Recent work by Nikolka et al. demonstrated that OFETs made from indacenodithiophene-*co*-benzothiadiazole (IDTBT) displayed poor device performance and showed a significant threshold voltage shift upon bias stress, which could be attributed to hole trapping.[242] Consistent with the trap filling studies discussed previously, OFETs made from IDTBT films with 2 wt% TCNQ or F4TCNQ additives resulted in nearly ideal, hysteresis-free device performance and very little threshold voltage shift upon bias stress.

However, although TCNQ and F4TCNQ may be capable of doping deep trap sites in IDTBT, it was also found that many residual solvents (e.g., toluene or chlorobenzene) which do not display any doping behavior resulted in similarly improved device performance. Variable angle spectroscopic ellipsometry (VASE) and device aging experiments under different environmental conditions pointed to water incorporated into the film in nanometer-sized voids as the likely cause of hole trapping. This was confirmed by DFT simulations of IDTBT–H_2O complexes which showed a significant reduction in backbone planarity,[242] which was previously shown to be the major factor in the nearly disorder-free transport displayed by IDTBT.[213]

The authors speculate that additives may act to reduce the deleterious effects of water by either displacing water from the edges of the voids or by interacting with water more strongly than the polymer, reducing the concentration of polymer–H_2O complexes.[242] This result suggests that many past studies on trap filling in OSCs where significantly more than 1 mol% doping was required may need to be re-examined in light of the effects of H_2O impurities.[248,251]

5.4. Compensation Doping

In many situations, such as when high photoluminescence or electroluminescence efficiencies are required (as in OLEDs), quantitatively undoped films are desired to minimize exciton quenching.[203] In this case, the goal is opposite to those described above; rather than using dopants to fill tail states, we aim to empty the tail states and decrease the free carrier density as much as possible. In inorganic semiconductors, doping occurs by substitution or addition of interstitial defects to the semiconductor lattice. It is not possible to remove these dopant atoms from the lattice, but the effective doping level in the material can be reduced by addition of dopants of the opposite polarity, i.e., adding n-type dopants to a p-type material. This process is called compensation doping.

When a semiconductor is compensated, the n-type (p-type) dopants trap the free holes (electrons) in the material, decreasing the free carrier density. When the numbers of n- and p-type dopants are equal, the material behaves as an intrinsic semiconductor, but note that the total charge density in the material never decreases; all that is changing is whether the charges are localized or delocalized. The ionized p- and n-type impurities left behind act as scattering centers and broaden the DOS.[21,24,181] In inorganics, where doping is efficient and intentional doping levels are ppm–ppt, this effect minimally affects performance, and as a result compensation doping is widely used in industry.[1,2] In organic materials, where intentional doping levels are typically on the order of percent due to low doping efficiency,[21,22,62] it is likely that compensation may result in significant performance degradation. However, for films doped by intrinsic defects at concentrations of a ppt or less, compensation doping is a useful method for reducing the effective doping level.

Compensation doping can also be used to measure the density of intrinsic defects and to understand the role that intrinsic defects play on the optoelectronic properties of the OSC. For example, Liang et al. used cobaltacene as an n-type dopant to compensate intrinsic charges in P3HT. Remarkably, as shown in **Figure 9**, they observed a ninefold increase in PL intensity at cobaltacene loadings of 1.2×10^{18} cm^{-3}.[130] This corresponds to an increase in PL quantum efficiency (PLQE) from 3% to 26%. Typical reported PLQEs for P3HT are near 3%, suggesting that most P3HT samples are dominated by impurities.[263] Likewise, PL lifetime doubled to nearly 1 ns, and showed mono-exponential kinetics rather than the typically observed biexponential decay.[264,265] They also observed a drastic decrease in film conductivity, shown in Figure 9. These results confirm that nominally intrinsic P3HT films show doping levels on the order of 1.2×10^{18} cm^{-3}, and that free charge carriers, not compensated charges, are strong quenchers of PL in P3HT.[130]

Compensation has also been used in the context of chemical sensing of amines. Since amines are strong donors, they can
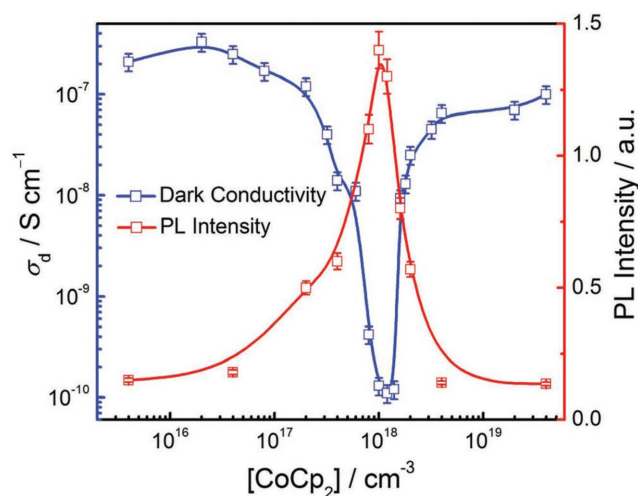

Figure 9. Low-field conductivity (left axis) and photoluminescence intensity (right axis) of P3HT films as a function of cobaltacene ($CoCp_2$) concentration. Reproduced with permission.[130] Copyright 2012, Wiley.

ADVANCED
SCIENCE NEWS
www.advancedsciencenews.com

ADVANCED
MATERIALS
www.advmat.de

compensate p-type doped films, resulting in reduced film conductivity. Huang et al. studied the chemical sensing properties of nanofibers composed of a ring-shaped arylene–ethynylene tetracyclic π-conjugated donor called DTC doped with FTS.[176] They were able to observe a strong reduction in conductivity within seconds upon exposure of aniline vapor at 80 ppb. These films showed good chemical selectivity for amines and no response to common solvents or water vapor.[176] Similar effects were observed in polyaniline nanofibers, where strong reversible changes in conductivity upon exposure to ammonia vapor were demonstrated.[266] Chemical sensing was covered in the following reviews.[267,268]

5.5. Passivation of Charged Defects and Impurities

Ideally, it is preferable to completely remove charged defect sites from the OSC rather than compensating them and leaving localized charges behind. In small molecules, defects and impurities can often be removed by repeated sublimation of the material.[103,229,249] This process removes impurity molecules that are significantly more or less volatile than the OSC. In polymers this route is unavailable; however, impurity density and polydispersity can often be reduced by washing with marginal solvents[269] or by dissolving the polymer in a good solvent and reprecipitating it by addition of a poor solvent.[270] Clearly, these methods are unable to remove defects in covalent bonding on the polymer backbone.[228] However, several studies, discussed below, have demonstrated that it is possible to chemically passivate defect sites in polymers, yielding significant improvements in material properties.

Gregg and co-workers studied the effects of strong nucleophiles and electrophiles on the optoelectronic properties of P3HT.[223,228,243,271] In their initial study, they observed that treatment of P3HT with dimethylsulfate (Me$_2$SO$_4$), an electrophile, nearly doubled the exciton diffusion length from 7 to 13 nm and increased the air stability of the material.[228,243] Since Me$_2$SO$_4$ is not electrophilic enough to react with unperturbed P3HT, the effects were attributed to methylation of negatively charged defects on the polymer backbone, converting anionic sp^2 carbons to neutral sp^3 carbons. This treatment increases conductivity by a factor of 5 and shifts the Fermi level toward the polymer HOMO,[228] suggesting that it behaves as a weak p-doping reaction, effectively similar to the ultralow doping studies described previously.

Treatment of P3HT with lithium aluminum hydride (LAH), a nucleophile, similarly doubles the exciton diffusion length from 7 to 14 nm and increases the air stability of the P3HT.[228] The increased air stability is surprising since the work function of LAH-treated P3HT is reduced, which would generally be expected to make P3HT more reactive toward oxygen. These results suggest that the air instability of OSCs such as P3HT is mediated by charged defect sites on the backbone, which are passivated by LAH.[228] As with the reaction with Me$_2$SO$_4$, LAH is proposed to hydrogenate positively charged defects on the polymer backbone, dedoping the material through a chemical reaction. The authors observed a 1000-fold reduction in p-type defect density in LAH-treated P3HT, along with a 10-fold increase in hole mobility.[228]

An additional study looked at the effects of sequential treatment with LAH and Me$_2$SO$_4$ to remove both positively and negatively charged defects.[271] This treatment doubled the photoluminescence intensity but showed lower air stability and hole mobility than LAH treatment alone. Both LAH and Me$_2$SO$_4$ are believed to convert conjugated sp^2 carbons to unconjugated sp^3 carbons, which may result in a more flexible polymer that can more easily find low-energy configurations.[223,228,243,271] These nonconjugated sites may themselves act as electronic traps, but the low concentration of these sites makes the structures difficult to determine.

A similar passivation effect was recently observed by treating P3HT films with 1-propylamine (PA).[244] This led to a decrease in conductivity of at least two orders of magnitude and a PL increase of 1.4 relative to untreated films. The reduction in conductivity appears consistent with the compensation doping report by Liang et al., described above.[271] Interestingly, treatment with diethylamine (DEA), which has a similar pK_a value and is an equally strong electron donor, had no effect. This suggests that 1-propylamine is not acting as an n-type dopant to compensate intrinsic p-type defects, but instead must be passivating defects in P3HT by a chemical mechanism available only to primary amines. Diethylamine does, however, increase the PLQE in PBTTT films. Comparison of chemical passivation of defects in P3HT and PBTTT by amines indicates that the chemical nature of defect sites is highly material specific and poorly understood at this point.[244]

5.6. Summary

Dilute defects and impurities are a pervasive feature in OSCs (particularly polymers) and strongly dictate the optoelectronic properties of these materials. Recently, there has been an effort toward characterizing the energetic distribution of trap sites and the effects of dopants on the DOS. This work is important to improving our understanding of both the fundamental physics of OSCs, and how engineer their optoelectronic properties. Impurity studies are complicated by the difficulty in detecting dilute defects, identifying the chemical or structural origin of the defects, and determining how dopant molecules interact with these sites.

The research tools used to investigate defects and traps leave an unfortunate level of ambiguity in the assignment of the origin of defects. We stress the need for further multidisciplinary studies on defect and trap sites and the development of new experimental techniques that can unambiguously characterize dilute defects and impurities in OSCs. Furthermore, we emphasize the need for care in sample preparation and data interpretation in ultralow doping studies. Finally, we encourage all groups to include more detail in the experimental sections of their future papers to help make comparative studies easier to perform.

6. Dedoping

As in inorganic semiconductor process engineering, we anticipate many situations in which it may be preferential to begin

**ADVANCED
SCIENCE NEWS**

www.advancedsciencenews.com

**ADVANCED
MATERIALS**

www.advmat.de

from a (perhaps unintentionally) doped OSC film and selectively remove dopants. An example of a situation in which removing intentional dopants might be useful is in DISC patterning,[36,37] which will be discussed in Section 8. Unlike compensation, which never decreases the total charge density in the material, dedoping processes neutralize or remove both free carriers and counterions. This could entail either removal of the neutral dopant molecule[3,87,272] or removal of the ionized dopant along with a soluble counterion.[37,244]

Dedoping is possible in molecularly doped OSCs because charge-transfer reactions are inherently reversible equilibrium processes, as described in Section 4 and Figure 7. Therefore, factors that affect this equilibrium—for example heat, solvent quality, the presence soluble competitive donor molecules, and chemical reactions which affect molecular energy levels—can induce dedoping. This processing pathway is unavailable to inorganic semiconductors, but is important to OSCs because their low doping efficiencies limit the usefulness of compensation doping. Therefore, the development of methods to remove dopants from OSC films in a controllable and quantitative way is extremely important.

6.1. Thermal Dedoping

The most common dedoping approach in the literature is heating, which results in sublimation of neutral dopant molecules out of the film. Dopants with high vapor pressure, such as I_2, sublimate out of films at room temperature and can be almost completely removed by heating at elevated temperatures.[3,37,273] There is evidence that at low concentrations oxygen doping may be reversible.[106] Thermal dedoping is commonly observed in films doped by F4TCNQ,[34,87,273] but does not result in complete recovery of film fluorescence.[87] We are not aware of any studies which have attempted to determine the origin of this irreversibility, but speculate that ion pairs consisting of deep trap sites doped by F4TCNQ should have a higher activation energy toward neutralization. Therefore, we would expect thermal dedoping of trap sites to proceed more slowly than dedoping of bulk sites.

In many situations, thermal dedoping of F4TCNQ is undesired and reduces device performance or lifetime.[87,274–277] Issues derived from the high volatility of F4TCNQ led to the synthesis of less volatile dopants like F2HCNQ,[278] F6TCNNQ,[155] and Mo(tfd)$_3$[152] as p-type dopants. Fluorinated fullerenes such as $C_{60}F_{36}$[87,157,168,279] and $C_{60}F_{48}$[280] have also shown superior thermal stability, although these compounds are not solution processable.

6.2. Solution-State Dedoping

As described in Section 4.3, any variable that shifts the doping reaction equilibrium toward the neutral states of the polymer/OSC will dedope the OSC. A simple way of shifting the reaction equilibrium is to expose the doped film to a solvent which is a poor solvent for the OSC but a good solvent for the dopant. **Figure 10**b shows a UV–vis spectrum of a P3HT:F4TCNQ film (black line) before and during exposure to AN (blue line), a poor

solvent for P3HT. Neutral F4TCNQ can be observed in solution, visible as the sharp peak near 390 nm in the AN-exposed spectrum. Dedoping proceeds until a new equilibrium is established,[27] resulting in only partial dedoping. In principle, one would expect that several successive wash steps should remove a large fraction of the dopant.

The doping reaction equilibrium can be shifted more strongly by the presence of soluble electron donor (acceptor) molecules, which can compete with the OSC for positive (negative) charges. If this competitive donor is a stronger donor than the OSC, then it is possible to dissolve both the charged donor and dopant molecules into a polar solvent, removing them from the OSC.[244] This process is effectively compensation doping followed by dissolution of the compensated ions. In this case the residual dopant density in the film is controlled by the doping reaction equilibrium, which is controlled by the relative donor strengths of the OSC and the competitive donor molecule. Single-step competitive dedoping of P3HT:F4TCNQ films using triethylamine as a competitive donor and acetone as the solvent results in ≈50% recovery of as-cast fluorescence intensity (Figure 10c, orange line), corresponding to a residual film doping level on the order of 1 ppt.[244]

6.3. Reactive Dedoping

A further modification of the competitive dedoping approach is to incorporate a donor molecule that reacts with the charged dopant. Recently, two such reactions were characterized by Jacobs et al. (Figure 10a).[244] Both primary and secondary amines react in a 2:1 ratio with F4TCNQ to yield ion pairs with LUMO levels well above the P3HT HOMO. These reactions "deactivate" the F4TCNQ, preventing it from re-doping the polymer. Figure 10b shows UV–vis spectra of a P3HT:F4TCNQ undergoing reactive dedoping with DEA by the mechanism shown in Figure 10a. The doped film (black line) is immersed in a cuvette containing AN, resulting in partial dedoping due to equilibration of F4TCNQ between the film and the solvent. The addition of 1 ppt DEA results in the formation of product **1**, indicated by the appearance of the absorption peak at ≈3.6 eV. Simultaneously, a strong reduction in film doping level is observed by the recovery of the P3HT π–π^* absorption and the reduction of F4TCNQ$^{•-}$ bands at 1.45 and 1.6 eV and the broad P3HT polaron band centered near 1.5 eV. Increasing concentrations of DEA result in faster dedoping.[244]

Measurement of film fluorescence intensity after dedoping is a simple method to study residual dopant density because mobile charge carriers are extremely efficient fluorescence quenchers.[130,203] Figure 10c shows film fluorescence intensity after reactive dedoping normalized to the as-cast fluorescence (before the films underwent sequential doping).[244] Both of the reactions shown in Figure 10a result in full recovery of the as-cast fluorescence intensity in a single step. As discussed in Section 5.5, dedoping with PA yields greater fluorescence intensity than as-cast dry film because PA also reacts with intrinsic defect sites in the polymer. Treatment of undoped P3HT with PA yields an identical increase in fluorescence intensity. UV–vis spectroscopy indicates that the dedoping reaction products are essentially insoluble in P3HT but highly soluble in
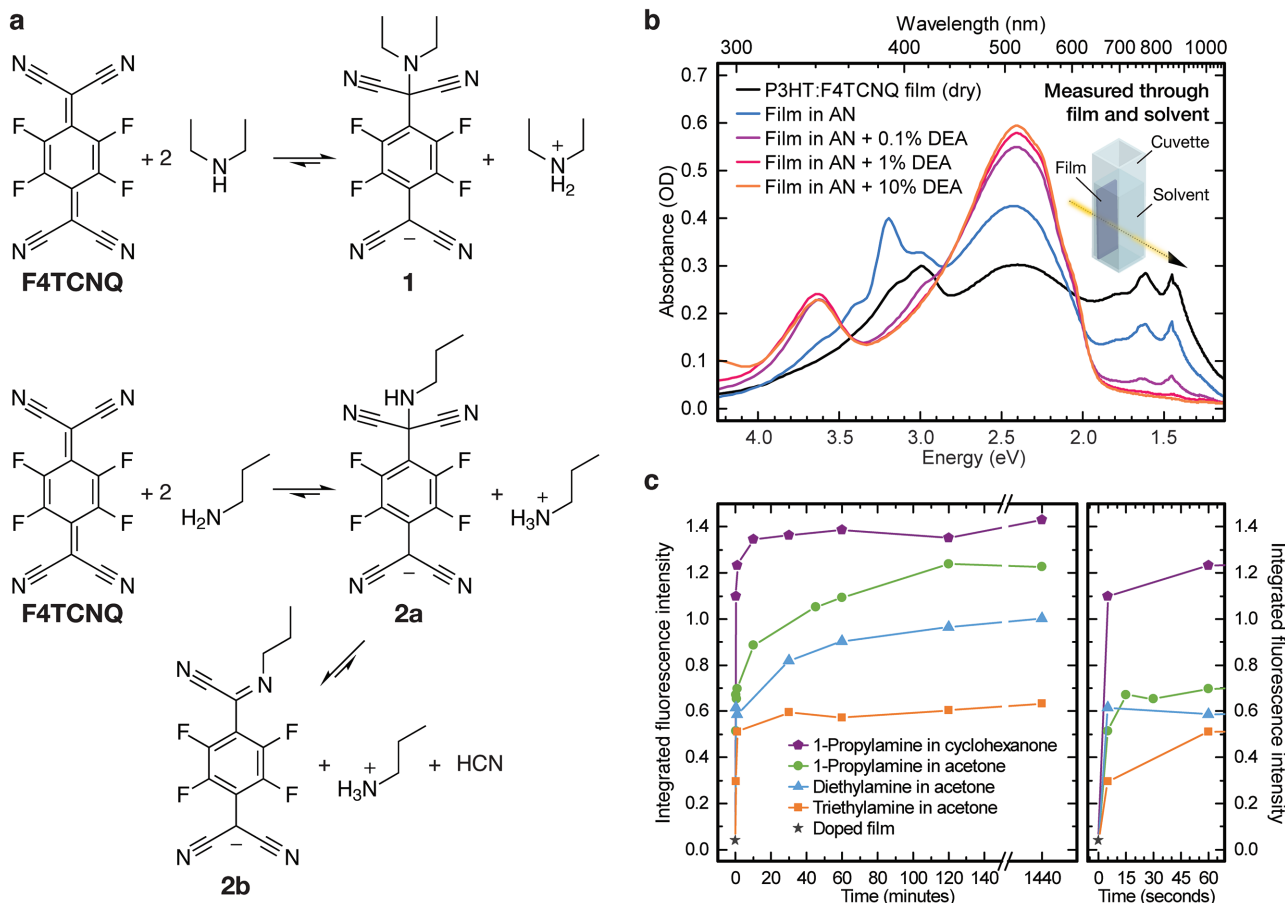
Figure 10. a) Chemical dedoping reactions for F4TCNQ. These reaction products all have LUMO levels well above the P3HT HOMO, indicating that they are no longer able to function as dopants. b) In situ UV–vis measurements of a P3HT:F4TCNQ film (black line) undergoing chemical dedoping in an AN containing increasing amounts of DEA (see the diagram for measurement geometry). Spectra were taken 7 min after addition of DEA. c) Integrated film fluorescence intensity after exposure to amine solutions (10% amine v/v). Fluorescence intensity is normalized to as-cast film fluorescence before sequential doping,[27] so an intensity of 1.0 indicates complete dedoping. Intensities greater than 1 in PA-treated films are due to reaction with intrinsic defect sites within the as-cast polymer. Reproduced with permission.[244] Copyright 2017, American Chemical Society.

polar solvents such as acetone, acetonitrile, and cyclohexanone, consistent with these being dedoping processes, as opposed to compensation processes.[244]

This dedoping approach is successful because the doping equilibrium is effectively controlled by the chemical reaction equilibrium and because the reaction product is insoluble in the OSC. Both of these conditions should hold in other systems. By nature, dopants are either strong electrophiles (p-type) or strong nucleophiles (n-type), so there should in general be a range of strongly exothermic reactions in which these materials can participate. For example, there is a significant literature describing reactions of TCNQs with nucleophiles such as amines.[281–283] In addition, the ionized molecules resulting from these reactions will generally be insoluble in OSCs due to their low dielectric constants.

We expect that dedoping reactions of the type shown in Figure 10 are widespread in all molecular dopants.[244,272] In fact, as dopant strength increases, dedoping reactions become so exothermic that they become problematic. For example, the recently published dopant CN6-CP shows an extremely high EA of −5.9 eV, which unfortunately makes it reactive toward

most solvent molecules.[137] This reactivity makes dedoping strong dopants trivial, but may limit their processability in common solvents or in gloveboxes in which typical solvents are used.[94] Strategies in which the neutral dopant undergoes a reaction to form dopant molecules in situ look to be a promising solution to this issue, but thus far have been primarily applied to n-type dopants.[125,133–136] The synthesis of extremely strong acceptors (p-type) or donors (n-type) that are air stable and solution processable remains a major research challenge.

6.4. Photochemical Dedoping

Photoactivated dedoping reactions allow for direct fabrication of doping gradients and could enable simple fabrication of OFETs and integrated circuits. To our knowledge, the first optical dedoping effects were observed in polythiophenes doped by FTS vapor, which has been shown to yield extremely high conductivities in P3HT (50 S cm^{-1}) and PBTTT (>10^3 S cm^{-1}).[174,175,177–179] In these films, exposure to

polar solvents such as acetone or water resulted in a strong decrease in conductivity and recovery of the π–π* absorption band. Removal of the polar solvent vapor by vacuum resulted in recovery of the doped state, indicating that the FTS remains in the film and is temporarily deactivated by the presence of the polar solvent. Interestingly, the rate of conductivity decrease during polar solvent exposure was reported to increase linearly with light intensity, which the authors assigned to a nonthermal mechanism.[174] The origin of this effect is still not understood, but a photochemical reaction between FTS and the polar solvent molecules is possible.

A photochemical dedoping reaction which does allow for fabrication of doping gradients was recently described in works by Jacobs et al. and Fuzell et al.[36,37,272] P3HT:F4TCNQ films, which are insoluble when doped,[37] regain solubility when immersed in THF and simultaneously exposed to 405 nm light.[37] Other wavelengths of light showed no effect on the solubility, indicating that the effect was not due to heating. Fuzell et al. characterized the photochemical reaction mechanism (**Figure 11**a).[272] It was observed that both F4TCNQ and F4TCNQ•− absorb strongly near 405 nm, and that while solutions of F4TCNQ•− in CH_3CN are stable under 405 nm illumination, neutral F4TCNQ solutions are not.[272] The addition of a dilute quantity of THF (<1 ppt) strongly increased the reaction rate in the presence of light, but no reaction occurred in the dark. Multidimensional NMR was used to identify the structure of the photoproduct, shown in Figure 11a (lower left structure). Since the photoproduct lacks the quinone structure that makes TCNQs strong acceptors, it can no longer function as a dopant. Interestingly, the F4TCNQ–THF product itself is not stable, and slowly converts back to neutral F4TCNQ on a timescale of hours to days.[272]

As with the amine-based dedoping reactions described in Section 6.3,[244] this photochemical reaction is used to push the doping reaction equilibrium toward the undoped state.[272] Figure 11a shows the reaction scheme for optically dedoping a thin film. In the presence of an OSC such as P3HT, F4TCNQ exists in equilibrium between the anionic and neutral species (see Figures 7 and 10b). In thin films, this equilibrium strongly favors the anionic state, but if this film is exposed to a solvent which is simultaneously a good solvent for the dopant and a nonsolvent for the polymer (such as AN or acetone), then a significant fraction of the F4TCNQ•− is converted to F4TCNQ. If the film is then exposed to 405 nm light during exposure to the solvent, the F4TCNQ reacts to form the photoproduct, which dissolves into the solvent. As the neutral F4TCNQ is consumed, the equilibrium converts F4TCNQ•− in the film to F4TCNQ, dedoping it.[272]

F4TCNQ displays varying degrees of photoreactivity in a wide variety of solvents. We can rationalize this photoreactivity by considering the electronic structure of the excited state, F4TCNQ*. The LUMO level of F4TCNQ lies at −5.24 eV with respect to vacuum, and its π–π* absorption is ≈3.2 eV, giving a HOMO of about −8.4 eV. Therefore F4TCNQ* can accept an electron at −8.4 eV, making it an exceedingly powerful electrophile. In effect, photoexcitation increases the acceptor strength of a p-type dopant by approximately the material's HOMO–LUMO gap energy. Very few solvents are stable against such strong electrophiles, so photochemical reactions
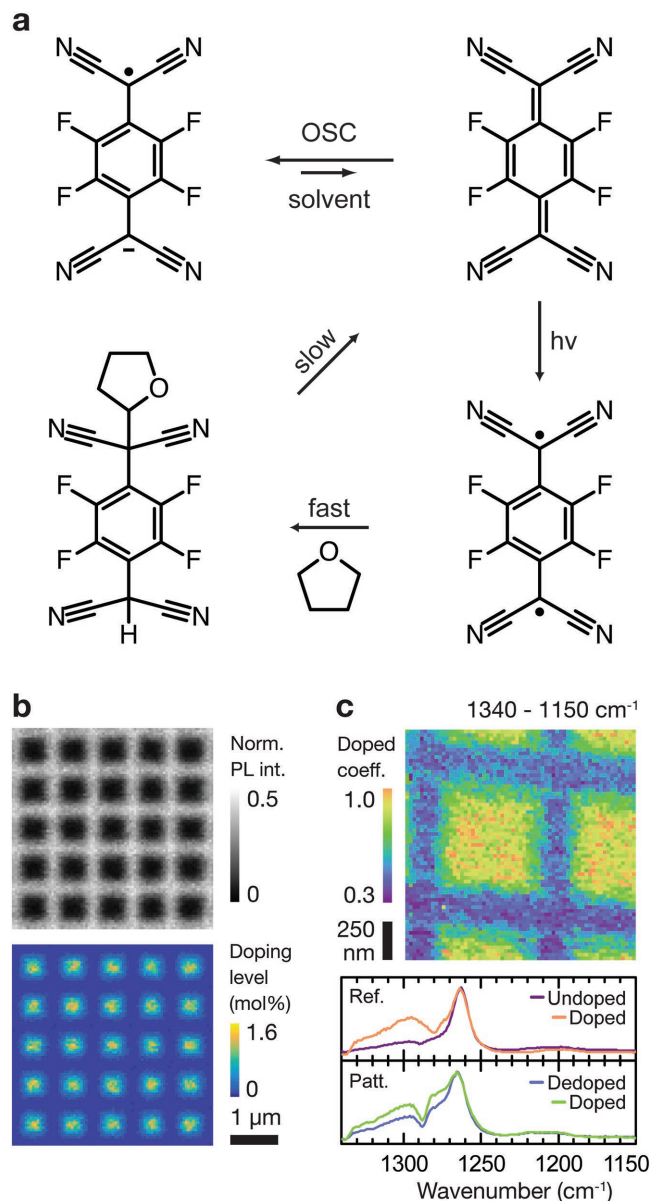

Figure 11. a) Reaction scheme for the optical dedoping reaction between F4TCNQ and THF.[272] b) Laser scanning confocal microscope (LSCM) fluorescence image (top) of a 2D doping gradient formed in a P3HT:F4TCNQ film by exposure to 405 nm in CH_3CN, and estimated doping level map (bottom) obtained from a fluorescence calibration curve.[36] c) High-resolution doping-level map obtained using hyperspectral photoinduced force microscopy (PiFM) infrared imaging. This map was generated by fitting a linear combination of doped and undoped reference spectra (plots below, orange and purple lines) to the raw PiFM image. Green and blue lines show spectra of the doped and dedoped regions. Reproduced with permission.[36] Copyright 2017, Wiley.

similar to the one described by Fuzell et al. almost certainly occur in all p-type dopants, in the presence of a wide variety of solvents. An analogous argument can be made for n-type materials.

The photochemical stability of dopant molecules is an important consideration when handling solutions of molecular

**ADVANCED
SCIENCE NEWS**
www.advancedsciencenews.com

**ADVANCED
MATERIALS**
www.advmat.de

dopants. It is important to store dopant solutions in the dark, or in vials that are opaque at wavelengths the dopant molecule absorbs. The application of this reaction to fabrication of nanoscale lateral doping gradients (Figure 11b–c) is described in the following section.[36]

6.5. Summary

We posit that dedoping is simple and feasible in most doped OSCs, despite the fact that it is impossible in inorganic semiconductors. Dedoping is a relatively new idea that adds a significant new capability to the fabrication tool kit for OSCs. Volatile molecular dopants can be directly removed by heating. Molecular p-type dopants can be chemically deactivated by reaction with stronger nucleophiles than the OSC and removed using a selective solvent. This idea has been demonstrated for F4TCNQ but has not yet been applied to other p-type dopants. In principle, n-type dopants can also be deactivated by reaction with electrophiles (as occurs unintentionally by reaction with O_2), but this idea has not yet been applied in a controlled way. Finally, photochemical dedoping of F4TCNQ has been demonstrated to proceed rapidly with a variety of solvents upon excitation with 405 nm light. Controlled and selective photochemical reactions with all molecular dopants are likely feasible but again this approach has not been demonstrated for other dopants. Sections 7.2 and 8 will discuss the application of these dedoping reactions in OSC fabrication.

7. Doping Gradients

Most electronic devices composed of inorganic semiconductors are fabricated by creating sharp doping gradients within a single material, such as p–n homojunctions. Difficulty fabricating these structures in solution-processed OSCs has led to the use of heterojunctions or metal–semiconductor junctions (Schottky junctions) in diodes and transistors. In particular, bulk heterojunctions between an unintentionally p-type-doped OSC and an unintentionally n-type-doped OSC dominate the field of organic photovoltaics.[284,285] Heterojunctions can allow for stable p–n junctions if both the IE and EA of the n-type layer are larger than the p-type layer. This is because a dopant will face an energetic barrier equal to the difference in IE (p-type) or EA (n-type) energy between the materials when attempting to diffuse into the other material. These barriers are typically at least 0.3 eV in OPVs; thus, at room temperature dopants should remain confined to one material, even if they are free to diffuse.

In a homojunction, dopant diffusion results in compensation and degradation of device performance. Therefore, fabrication of stable doping gradients in a single material is a difficult task and requires good control of dopant diffusion rates. Nonetheless, the ability to fabricate sharp doping gradients both vertically and laterally in a single material would allow for significant reduction in the size of OSC devices and improved device performance at reduced cost. In this section, we will discuss methods for creating doping gradients and laterally patterning dopants in OSC films.

7.1. Vertical Doping Gradients

In small-molecule OSCs, vertical doping gradients can be fabricated by co-deposition of the OSC and dopant by thermal evaporation. The first reports of OSC p–n homojunctions appeared shortly after the first molecular n-type dopants were developed.[286] Doped layers fabricated by thermal evaporation are often used as doped contact layers in OPV or OLED devices, described in previous reviews.[17,32]

Forming doped homojunctions in polymer OSCs is more difficult. Evaporation of dopants, such as F4TCNQ, into polymer films does not lead to the formation of a vertical doping gradient because dopant diffusion is fast on the length scale of typical film thicknesses (<100 nm).[34,37,87,160,287] However, this technique may prove successful with suitably engineered dopants with bulky 3D structures or side groups. Prospects for controlling diffusion of molecular dopants will be discussed in Section 9.

An alternative approach for creating doping gradients is lamination of doped and undoped films using polydimethylsiloxane (PDMS) stamps.[288,289] Shu et al. used PDMS stamps to stack identical layers of P3HT and F8BT. Using UPS and Kelvin probe force microscopy, they did not observe discontinuities at the interface between the layers, which was confirmed by I–V measurements which were indistinguishable from films with increased thickness.[289] Dai et al. extended this concept to doped films, studying P3HT films doped by Mo(tfd)$_3$ laminated to undoped P3HT films.[287] Using this technique they formed inverted OPV devices using 4 wt% Mo(tfd)$_3$ doped P3HT as the hole transport layer (HTL), obtaining similar PCEs to devices with a PEDOT:PSS hole transport layer.[287] PDMS stamping could also be used to form lateral doping gradients by transferring patterned films, but this has not yet been experimentally realized.

Doping often strongly reduces the solubility of conducting polymers, so it is also sometimes possible to simply spin coat an undoped film onto a doped film. Jacobs et al. prepared P3HT/F8BT bilayers by this approach, and observed that it was possible to chemically dedope the stacked film to form an undoped bilayer.[37] In principle, it should be possible to apply the same technique to form a doped/undoped homojunction bilayer; however, careful control of the diffusion rate and solubility of the dopant molecule are necessary to maintain a sharp interface.

The most successful vertical doping approach to date is sequential solution doping with large, bulky dopants. This results in a kinetically controlled process rather than the thermodynamically controlled process as described in Section 4.3. Kolesov et al. studied doping of P3HT by the polyoxometalate phosphomolybdic acid (PMA).[198] **Figure 12**a shows optical transmittance spectra of undoped P3HT and P3HT films immersed into solutions of PMA/nitromethane for 1–30 min. The decrease in transmittance around 800 nm is from polaron absorption, indicating an increasing doping level with time.[198] Depth-dependent XPS measurements suggested an exponential decay in doping level as a function of distance from the film's top surface. To confirm this, the authors performed VASE of the films shown in Figure 12a. Exponential fits to these data, shown in the inset, matched both the ellipsometry and the
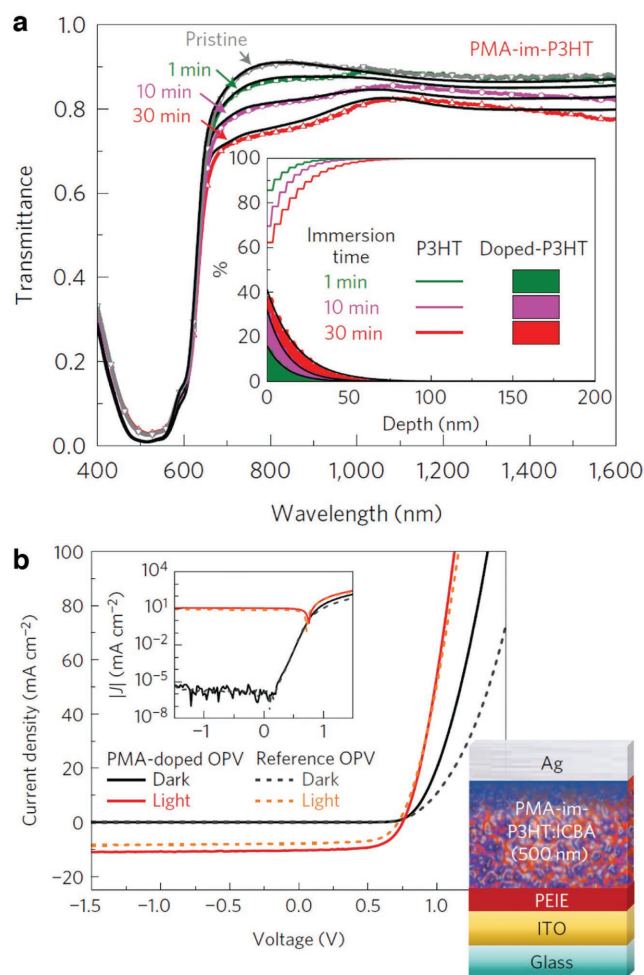
ADVANCED
SCIENCE NEWS
www.advancedsciencenews.com

ADVANCED
MATERIALS
www.advmat.de

Figure 12. a) Transmittance of 210 nm thick PMA-im-P3HT films with varying times of postimmersion in 50×10^{-6} M PMA nitromethane solution. The exponential profiles, calculated from variable angle spectroscopic ellipsometry (not shown), have decay constants of 12, 13, and 18 nm for 1, 10, and 30 min immersion times in 50×10^{-6} M PMA nitromethane solution are shown in the inset. b) J–V characteristics of PMA-doped and reference P3HT:ICBA (500 nm) OPV devices with structure: ITO/PMA-im-P3HT:ICBA/Ag and ITO/PEIE/P3HT:ICBA/MoO₃/Ag, respectively. The inset shows the J–V characteristics on a semilogarithimic scale. Reproduced with permission.[198] Copyright 2017, Nature Publishing Group.

absorption spectra. This confirms that vertical doping gradients can be controlled by varying the exposure time to the sequential doping solution.[198]

A thin doped layer capping an undoped film is desirable in device structures because it functions as a low-resistance hole selective contact. Figure 12 compares the J–V characteristics P3HT:1',1'',4',4''-tetrahydro-di[1,4]methanonaphtaleno[1,2:2',3',56,60:2'',3'']][5,6]fullerene-C₆₀ (ICBA) OPV devices fabricated with a conventional hole transport layer (MoO₃) and with a PMA-doped hole selective contact. The results are near identical, demonstrating that sequential doping of the surface of OPV device films eliminates the need for a separate hole transport layer. Similar results were demonstrated in poly-{4,4,9,9-tetrakis(4-hexylphenyl)-4,9-dihydro-s-indaceno[1,2-b:5,6-b']dithiophene-2,7-yl]-*alt*-{2,6-

bis([1,2,5]thiadiazolo[3,4-c]pyridine-4'-yl)-4,4-bis(2-ethylhexyl)-cyclopenta[2,1-b:3,4-b']dithiophene-7',7''-yl} (PIPCP):PC60BM and PffBT4T-2OD:PC70BM, yielding a PCE of 7.8% in the latter device.[198]

Previously, Kang et al. demonstrated that similar, self-assembled electron-selective contacts could be formed by the addition of poly(ethyleneimine) (PEIE), an electron donating polymer commonly used in modifying interface dipoles to create electron selective contacts,[290] to spin coating solutions.[291] These electron-selective contacts are formed by spontaneous vertical segregation of the PEIE to the OSC–substrate interface.[291] By using these two techniques together, Kolesov et al. demonstrated efficient single-layered OPV devices for the first time.[198] These results illustrate the usefulness of doping gradients and highlight the importance of controlling dopant diffusion.

7.2. Lateral Doping Gradients

The ability to precisely define doped regions with nanoscale resolution using photolithography has driven the computing revolution defined by Moore's law. We would like to apply the same photolithography techniques to organic semiconductors, however, due to mutual solubility most photoresists are incompatible with OSCs.[292–295] Fluorinated photoresists, which are coated and stripped using fluorinated solvents, have been developed for this purpose. However they are probably not compatible with highly fluorinated dopant molecules such as F4TCNQ and Mo(tfd)₃.[292–295] Supercritical CO_2 has also been proposed as a photoresist but thus far has not achieved high resolution.[296,297] Here, we will discuss two non-photolithographic methods based on doping-induced solubility control (DISC) for patterning dopants in polymer OSCs.

The simplest method is to define the doped regions by evaporating the dopants into the OSC through a shadow mask.[37] A schematic of this process is shown in the first two panels of **Figure 13**a. The left-most images in Figure 13b show laser scanning confocal microscope (LSCM) images of a P3HT film patterned by thermal evaporation of F4TCNQ through a shadow mask. The lower image, showing the film reflectance, has little contrast, but the upper image, showing film fluorescence, clearly matches the mask pattern (shown in the lower right). Dark regions are indicative of high doping levels and bright regions are indicative of low doping levels due to fluorescence quenching by free charge carriers.[37,130] This method can also be used to topographically pattern the OSC film, as will be discussed in Section 8.[37]

The optical dedoping reaction shown in Figure 11 can also be used to form lateral doping gradients.[36] Using this method, a doped OSC film is immersed in a poor solvent, such as AN, and exposed to focused laser light resonant with the absorption band of the neutral state of the dopant.[36,272] As discussed in Section 6.4, most p-type molecular dopants are unstable against reaction with weakly electrophilic solvent molecules in their excited state. The combination of optical excitation and the presence of a weak electrophile will lead to a dedoping reaction similar to the one shown in Figure 11a.

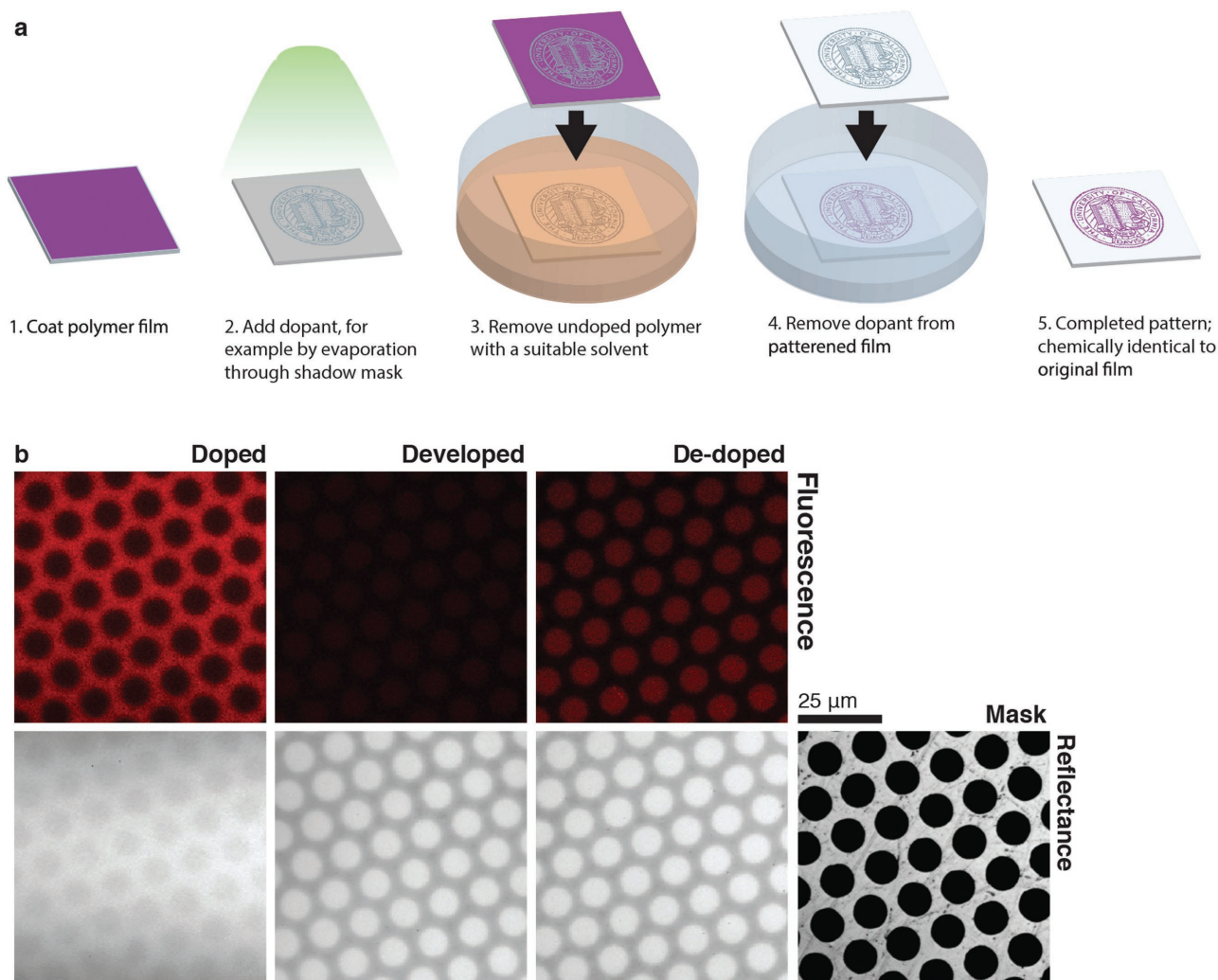Jacobs et al. used focused 405 nm light from an LSCM to simultaneously pattern and image P3HT:F4TCNQ films.[36]

ADVANCED
SCIENCE NEWS
www.advancedsciencenews.com

ADVANCED
MATERIALS
www.advmat.de

Figure 13. Additive DISC patterning. a) Schematic of the additive DISC patterning process. b) Laser scanning confocal micrographs showing reflectance (bottom) and photoluminescence (top) after doping, developing, and dedoping steps. Doped areas appear dark in the photoluminescence images, while undoped regions appear bright. Photoluminescence images are false-colored. A reflectance image of the mask is shown lower right, along with a 25 µm scale bar. Reproduced with permission.[37] Copyright 2015, American Chemical Society.

Figure 11b shows an LSCM fluorescence image (top) of a 2D grating formed by raster scanning a 405 nm laser over a P3HT:F4TCNQ film immersed in AN. The fluorescence intensity is normalized to an undoped P3HT film. Estimated doping level maps were obtained from the fluorescence intensity, indicating doping levels of 1.5 mol% in unexposed regions and ≈800 ppm in the exposed areas. However, the authors noted that the doping level in the exposed regions is an overestimate, because the width of the patterned features was smaller than the diffraction limit of the imaging laser. As a result, the observed fluorescence is emitted from a smaller volume than the excitation volume, reducing the intensity relative to a bulk film at the same doping level.[36]

To measure the resolution limit of this process, a new scanning probe technique called photoinduced force microscopy (PiFM) was used. PiFM allows for measurement of hyperspectral infrared images with spatial resolution of <20 nm.[298] PiFM allows for doping-level contrast imaging because doping results

in several changes to the OSC infrared absorption spectrum.[299] Figure 11c shows a doping level map of part the grating shown in Figure 11b, obtained by fitting the PiFM hyperspectral image to a linear combination of doped and undoped reference PiFM spectra (shown with orange and purple lines). PiFM spectra of the doped and undoped regions (blue and green lines) match the reference spectra. Quantitative measurement of doping level was not possible to environmental exposure to air before and during imaging. However, this measurement does show that sharp lateral doping gradients, with edges less 100 nm wide, can be formed using this method.[36]

It is interesting to consider how this process is able to achieve such high resolution when vertical dopant diffusion through 100 nm thick films is rapid.[34,37] One plausible explanation is that the solvent used during patterning, AN, dissolves most of the dopant present in the amorphous domains, leaving dopants primarily in the crystalline domains. Dopants in the crystalline domains may be considerably less mobile, allowing

**ADVANCED
SCIENCE NEWS**
www.advancedsciencenews.com

**ADVANCED
MATERIALS**
www.advmat.de

for the doping gradients to remain stable on this length scale for days. A discussion of dopant diffusion models will be given in Section 9.

7.3. Summary

Doping gradients rarely feature in solution-processed OSC devices largely because they are difficult to fabricate. Instead, researchers have focused on preparation of separate layers of high IE OSCs commonly known as HTLs and low EA OSCs known as electron transport layers (ETLs).[17,32] With the very recent advent of poorly soluble dopants that can be added to one specific layer interface, it is now possible to fabricate doping gradients that replace the need for HTLs and ETLs.[198] In addition, two DISC-based techniques were presented, including evaporation through a mask and laser patterning, that allow lateral control of the doping density with high resolution.[36,37] These new fabrication techniques and dopant materials enable the fabrication of OSC devices with submicrometer doped and intrinsic domains.

8. Doping-Induced Solubility Control

Many polymer OSCs, including P3HT and PBTTT, show strongly reduced solubility when p-type doped.[22,27,37,77] In particular, P3HT films are rendered completely insoluble in a wide range of solvents, including chlorobenzene, dichlorobenzene, chloroform, and THF, upon doping with only 2–4 mol% F4TCNQ.[27,37] In many situations, such as when coating films from mixed polymer:dopant solutions, this doping-induced insolubility effect is problematic because the polymer will precipitate out of solution. However, doping-induced insolubility also represents an opportunity. The difficulty of patterning or layering OSCs could be solved if it were possible to reversibly switch OSC solubility off and on at will.

Currently, the only method for controlling polymer solubility is cross-linking, which is irreversible and sometimes results in degraded material properties.[300–302] However, as discussed in Sections 4 and 6, it is possible to add dopants to undoped films or remove dopants from doped films. By spatially controlling doping level using the methods described in Section 7.2, we are also spatially controlling solubility. Therefore, by laterally patterning dopants in the film and then washing out the undoped soluble regions, it is possible to topographically pattern films. This method is called doping-induced solubility control (DISC). Two methods to laterally pattern OSC films using DISC are described below.

8.1. Additive DISC patterning

Additive DISC patterning is shown schematically in Figure 13.[37] Beginning from an undoped polymer film, dopants are added through a mask to locally switch off film solubility. Afterward, the film is immersed in a good solvent such as chlorobenzene to remove the soluble (undoped) regions, leaving a patterned doped film behind. The patterned

film can then be immersed in an amine-based dedoping solution (as described in Section 6.3) to quantitatively remove the dopants,[36] leaving an undoped patterned film.[37]

Figure 13b shows LSCM images of P3HT films undergoing additive DISC patterning by thermal evaporation of F4TCNQ through a shadow mask.[37] After evaporation of F4TCNQ, the fluorescence image (top left) shows strong quenching in the areas exposed by the mask, indicating efficient doping by F4TCNQ. The unquenched fluorescence surrounding the doped regions indicates that the F4TCNQ does not diffuse laterally further than a few hundred nanometers through the film. The reflectance image (bottom left) has very little contrast because the film thickness is uniform. After immersion in o-dichlorobenzene, the fluorescence image shows almost no signal because the undoped, fluorescent regions have been removed. However, the corresponding reflectance image now shows good contrast due to topographic patterning. Finally, dedoping using an amine solution results in recovery of fluorescence, but leaves the reflectance image unchanged. AFM imaging (not shown) after the second and third steps confirms that the dedoping step does not affect the sharpness of the patterned features.[37] Almost no residual polymer remains on the substrate between the patterned regions. The patterned features have smooth, flat surfaces with uniform thickness determined by the initial film spin coating.

This process is interesting for several reasons. First, it allows for patterning of polymers on the micrometer length scale using thermal evaporation, which so far has only been possible for oligomers or small molecules. Second, it could provide an easy way to generate flat patterned features using inkjet printing, by using dopant inks on precoated polymer films. Any excess dopant deposited has no further effect and can be washed out in the dedoping step, eliminating commonly observed thickness variations due "coffee stain effect."[199]

8.2. Subtractive DISC Patterning

In subtractive DISC patterning,[36,37] dopants are selectively removed from fully doped films using the photochemical dedoping reaction discussed in Section 6.4. **Figure 14**a–d shows the processing steps schematically. The implementation described here uses a 405 nm laser in an LSCM to drive a photochemical reaction between F4TCNQ and THF. As the laser is scanned over doped film, the irradiated areas dedope and regain their solubility, dissolving into the THF above. Once patterning is complete, the film can be chemically dedoped in a second sequential processing step, if desired, to recover intrinsic material properties.[244] This process could also be performed using standard photolithography equipment.

Subtractive DISC achieves remarkably high resolution. An AFM image of a 60 nm thick patterned P3HT:F4TCNQ film is shown in Figure 14e. Higher resolution images of the "s" feature taken before and after chemical dedoping are shown in Figure 14f and Figure 14g, respectively; vertical cross sections through these images are shown in Figure 14h,i. These cross sections reveal that subtractive DISC patterning is capable of generating positive features with widths on the order of 100 nm at half maximum and 280 nm at their base. This resolution
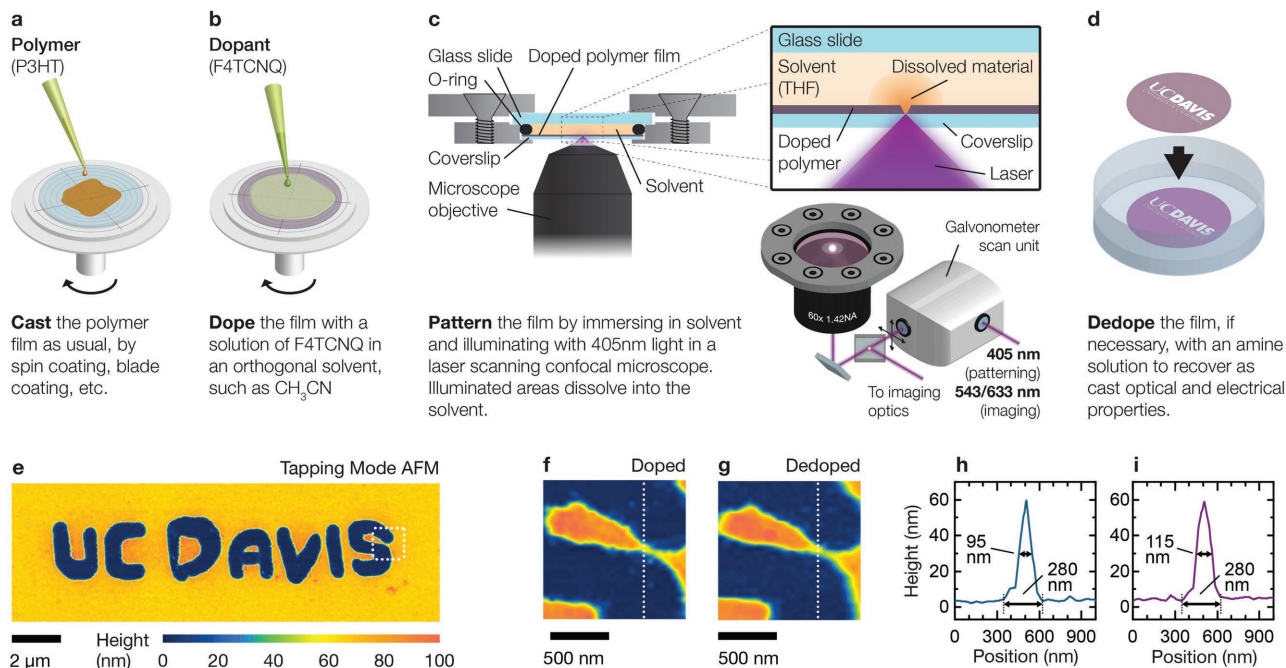
**ADVANCED
SCIENCE NEWS**

www.advancedsciencenews.com

**ADVANCED
MATERIALS**

www.advmat.de

Figure 14. DISC patterning process. a) A thin P3HT film is cast and b) sequentially doped with F4TCNQ in AN, rendering the film insoluble. c) The film is then loaded into a sealed sample holder filled with THF. A laser scanning confocal microscope (LSCM) is used to image and pattern the polymer layer. Regions of the film exposed to 405 nm light dissolve into the THF (see detail), while unexposed areas, or areas exposed to red or green light, remain insoluble. Focus and sample imaging is achieved using 543 nm excitation. d) Once patterning is complete, the film can be chemically dedoped to recover intrinsic (undoped) material properties. e) AFM reveals sub-micrometer patterning resolution. Enlargements of the "s" in part (e), indicated by white dashed lines, are shown f) before and g) after dedoping, respectively. h,i) Slices indicated by dotted lines in parts (f) and (g) are plotted, revealing positive features with widths of 280 nm at the base of the feature, and half-maximum widths of 95 nm (before dedoping) and 115 nm (after dedoping). Reproduced with permission.[36] Copyright 2017, Wiley.

capability is surprising because the diffraction limit for 405 nm light in the optical system used was 350 nm. Detailed characterization of line widths patterned at various exposure times and laser powers confirmed that this process breaks the diffraction limit as a result of a nonlinear relation with laser power and time. However, the authors were unable to determine the mechanism of this nonlinear behavior or the functional form of the rate law.[36]

8.3. DISC Mechanism

Both additive and subtractive DISC patterning are applicable to other polymer:dopant combinations, provided that doping strongly modifies the polymer solubility. A strong reduction in solubility upon doping has been observed in PBTTT[77] and, to a lesser extent, in MEH-PPV.[37,195] The mechanism for the change in solubility with doping is not well understood. Several explanations have been proposed, including a shift in the polymer dielectric[197] and strong interchain interactions mediated by CTCs.[303,304] However, neither of these mechanisms are a satisfactory explanation of the insolubility of P3HT/F4TCNQ. P3HT/F4TCNQ films swell in low-dielectric solvents such as CB and remain insoluble in more polar solvents, suggesting that the dielectric constant of doped polymer films is still low. Also, P3HT/F4TCNQ dopes by IP formation, indicating that CTCs cannot explain the solubility effect described here.

The most plausible hypothesis is that doping-induced insolubility results from stabilization of holes in solvochromic polymers.[27,35,180] When dissolved, the absorption bands of both P3HT and PBTTT show a strong hypsochromic shift, indicating an increase in band gap.[305] Assuming this shift is symmetric about the center of the gap, a hole on a dissolved polymer is at higher energy than a hole in that same polymer after aggregation. This energy difference could induce aggregation assuming that the stabilization overcomes both the Coulombic repulsion between holes and the polymer solvation energy. The same solubility argument should apply for n-type doping. We are not aware of any studies that have addressed solubility changes in OSCs with n-type doping, despite the fact that doping-induced insolubility has been known of since at least the 1990s.

8.4. Summary

DISC patterning is a new fabrication toolkit for OSCs that can yield unprecedented patterning resolution and is compatible with roll-to-roll solution coating. Unlike cross-linking reactions, DISC does not require synthesis, alter the OSC bond structure, or introduce heterogeneities to the OSC structure. The use of dopants for the purpose of patterning and advanced fabrication is a virtually unexplored research direction.

In both of these processes and those described in the preceding section, fortuitously low dopant diffusion rates have

**ADVANCED
SCIENCE NEWS**

www.advancedsciencenews.com

**ADVANCED
MATERIALS**

www.advmat.de

played a significant factor in the high resolutions achieved. These low diffusion rates are not a general feature of molecular dopants, but rather should be considered as an important synthetic goal. It will be interesting to see if similar or perhaps even better results can be achieved in other polymer:dopant systems, particularly those engineered for slower diffusion.

9. Molecular Dopant Diffusion

9.1. Vertical Diffusion Studies

Dopants in inorganic semiconductors are typically introduced at the surface and diffuse into the matrix at elevated temperatures. Once the semiconductor is cooled to room temperature, the dopant atoms have a very large activation energy to diffuse within the semiconductor because they occupy lattice sites in the crystal. In contrast, molecular dopants are not covalently bound into a crystal, so the dopant is held in place with a combination of van der Waals forces and the Coulombic attraction between the charged dopant and free or bound charge carriers. These are comparatively weak forces; therefore, the activation energy barrier to diffusion is much lower. Further, OSCs undergo glass transitions at device-relevant temperatures ($T_g \approx 0$–200 °C), which lower this activation barrier. Early experiments with molecular dopants such as I_2 or AsF_5 showed excellent conductivities[306,307] but poor thermal stability due to sublimation of the dopants at room temperature.[3] With the introduction of the larger molecular dopant molecules shown in Figure 6, volatility is less problematic, but the question still remains whether the dopants molecules diffuse within a layer or between layers, and at which temperature this becomes an issue.

Measurements of dopant diffusion are particularly challenging because molecular dopants are present in trace quantities, and composed of the same light elements (C, H, O, N, and S) as the host OSC. Most studies of dopant diffusion so far have focused on diffusion between two layers in a vertical layer stack. The question from the device perspective is whether the dopant remains in the layer of origin/intent or whether it diffuses to the adjacent layer and changes the electronic performance of the device.

One study from Qi et al. used Rutherford Back Scattering (RBS) to detect the Mo in Mo(tfd)$_3$ in a matrix of the amorphous small molecule hole conductor N,N′-bis(naphthalen-1-yl)-N,N′-bis(phenyl)benzidine (α-NPD).[152] **Figure 15** shows the RBS spectrum for a sample consisting of 55 nm of 2 mol% doped α-NPD with 100 nm of undoped α-NPD on top of the doped layer, prepared using thermal evaporation. The green curve is the simulation corresponding to the Mo peak assuming
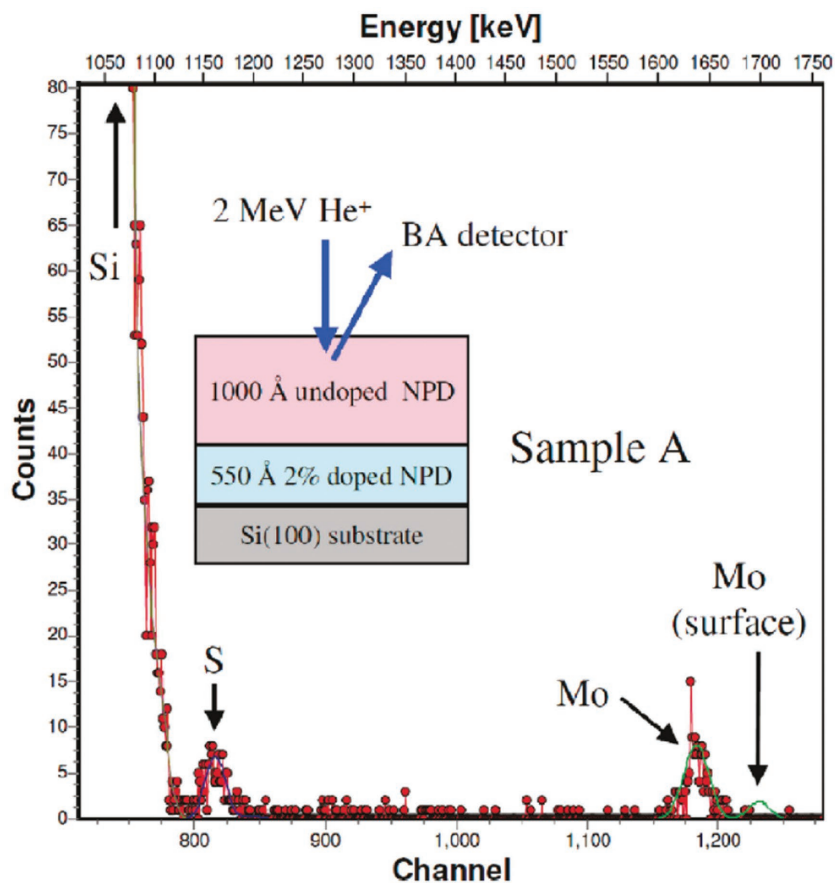

Figure 15. Extended part of experimental Rutherford Back Scattering (RBS) spectrum showing the Si, S, and Mo features and corresponding simulation (see the text) for the sample depicted in the inset. The spectrum is taken with a typical ion beam analysis detector. Reproduced with permission.[152] Copyright 2010, American Chemical Society.

no diffusion. The fact that there is no peak at 1230 nm indicates that no Mo has diffused to the surface of the film at room temperature. After heating the sample for 15 min at 110 °C no change was observed.[152] This test provides a relatively simple determination that the dopant molecules did not diffuse in the particular sample prepared.

In a similar experiment, Li et al. studied the diffusion of the dopants F4TCNQ and $C_{60}F_{36}$ through the small-molecule hole conductor N,N,N′,N′-tetrakis(4-methoxyphenyl)benzidine (MeO–TPD).[87] Again thermal evaporation was used to fabricate the bilayer structure. Because no heavy atom was present in the dopants, they instead used carbon K-edge near edge X-ray absorption fine structure (NEXAFS) spectroscopy to measure the surface composition of the films. **Figure 16** shows the change in the carbon K-edge NEXAFS spectrum as a function of heating temperature for a bilayer of MeO–TPD on $C_{60}F_{36}$. The ratio of the surface composition was determined by fitting the spectra to a linear combination of reference spectra consisting of neat samples of MeO–TPD and $C_{60}F_{36}$.

Figure 16c shows the change in surface composition as a function of temperature. Surprisingly, even for this quite large and insoluble dopant, it was not possible to fabricate a perfect bilayer, implying that significant diffusion occurred during
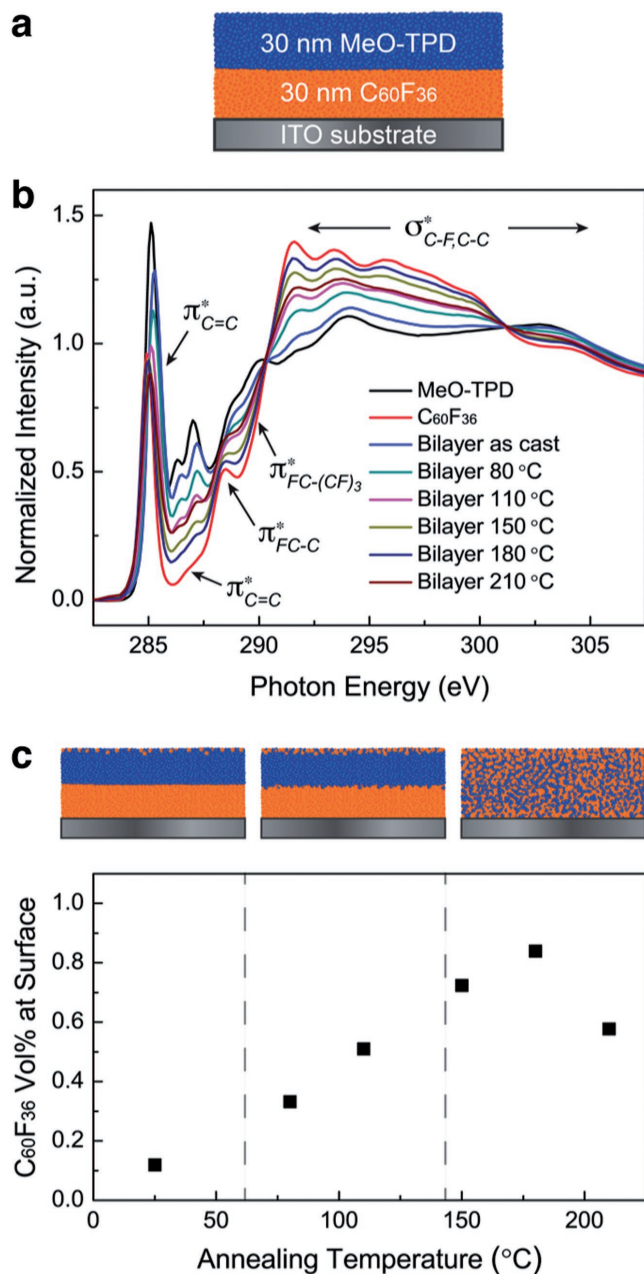
**ADVANCED
SCIENCE NEWS**

www.advancedsciencenews.com

**ADVANCED
MATERIALS**

www.advmat.de

Figure 16. a,b) Carbon K-edge NEXAFS spectra of bilayers of 30 nm MeO–TPD (blue) evaporated onto 30 nm of $C_{60}F_{36}$ (orange). The bilayers were measured as deposited (blue) and thermally annealed at 80 °C (cyan), 110 °C (magenta), 150 °C (dark yellow), 180 °C (navy), and 210 °C (wine). The peak assignments of $C_{60}F_{36}$ is shown in part (b). The NEXAFS spectra of bilayers were fit using the neat MeO–TPD and dopant spectra. c) This plot represents a fitting of the volume fraction of dopant material within the escape depth of the backscattered electron (≈4 nm). Reproduced with permission.[87] Copyright 2016, American Chemical Society.

deposition or storage at room temperature. For the F4TCNQ samples (not shown), the samples were well mixed even without heating.[87] The F4TCNQ is not believed to have come from the vacuum chamber walls, as was previously reported,[157] because a layer of Ag was deposited with the sample shutter

closed after the F4TCNQ deposition, to trap any F4TCNQ that might poison the sample.

SIMS is by far the most commonly used technique for bilayer diffusion studies due to its high spatial resolution and ability to differentiate between molecules. Treat et al. studied the vertical diffusion of deuterium labeled D-PCBM in P3HT in a bilayer geometry.[308] They found that a contact laminated bilayer would interdiffuse starting at 50 °C, but that complete mixing did not occur until heating to 150 °C. The low barrier for diffusion of PCBM into P3HT result surprised many in the OPV community. Another recent study showed that SIMS can be utilized to observe the diffusion of F4TCNQ in the hole transport layer of OLEDs.[309] The SIMS signal from fluorine atoms acts as a unique isotopic label.

More recently, SIMS was used to study the diffusion of the soluble p-type dopant Mo(tfd–CO_2Me)$_3$ into P3HT and P3HT/PCBM blend bilayer films using the Mo label.[287] In this case, the films were prepared on separate substrates and then stacked using soft-contact transfer lamination. **Figure 17** shows the SIMS profiles as a function of etch depth from the surface for a bilayer of P3HT doped with 3.8 wt% Mo(tfd-CO_2Me)$_3$ with a 80 nm layer of pure P3HT on top. Even for the room temperature (unannealed) sample (black), the Mo concentration is calculated to be 1.8 wt% in the top layer, indicating that the dopant diffused into the undoped P3HT layer before the SIMS measurement could be made. Heating to 100 °C (green) does not change the vertical concentration profile of the dopant, indicating that the room temperature diffusion was spontaneous and rapid. Again, this is a surprising result considering the large size of the dopant.[287]

In contrast, Mo(tfd–CO_2Me)$_3$ did not diffuse into the P3HT/PCBM film.[287] The most likely explanation for the increased thermal stability of the dopant is that the PCBM occupies all of the free volume in the mixed amorphous P3HT/fullerene phase[310,311] and thus blocks free diffusion of Mo(tfd–CO_2Me)$_3$ in the mixed film. This result strongly suggests that the PCBM
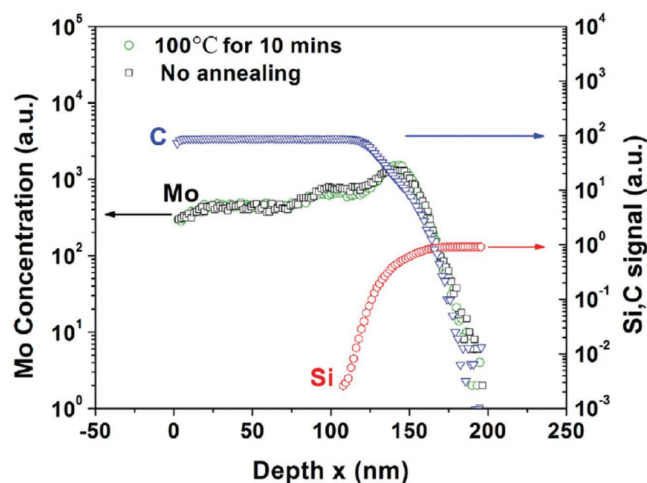

Figure 17. SIMS profiles of C, Si signal and Mo concentration versus depth for a 3.8 wt% Mo(tfd–CO_2Me)$_3$ doped P3HT/P3HT bilayer film on Si.[287] This sample was prepared by soft-contact transfer lamination of the separately prepared undoped and doped layers with details published here.[288] Reproduced with permission.[287] Copyright 2015, Elsevier.

**ADVANCED
SCIENCE NEWS**

www.advancedsciencenews.com

**ADVANCED
MATERIALS**

www.advmat.de

and dopant diffusion rates depend on the OSC morphology, the amorphous volume, and the mobility of polymer chains in the amorphous volume in ways that are not really understood.

Other dopant diffusion studies used measurement techniques such as XPS, UPS, neutron/X-ray/visible light scattering, and photoluminescence to measure the diffusion of dopants in layered samples.[151,198,273,312–314] Most of the these studies report that dopants did or did not diffuse beyond their original layer and at which temperature threshold, but do not quantify the dopant density as a function of distance from the layer interface. Finally, a series of articles have observed diffusion of dopants or lack thereof by creating bi- or trilayers of material and then measuring changes in the electronic properties of the layer stack.[153,157,275,278] For these electronic measurements, the movement of dopants is inferred but the change in concentration cannot be quantified.

Finally, two studies have observed that alteration of the polymer structure can affect the diffusion of dopants. Both studies observed that thiophenes with PEO side chains seem to bind F4TCNQ more effectively than polymers with alkane side chains. Li et al. showed that in a bilayer film, F4TCNQ diffuses out of P3HT and into SP-3-MEET, a self-doped polythiophene with PEO side chains.[273] Thermal measurements seem to indicate interaction between the charged dopant and the PEO side chains. Kroon et al. showed that the conductivity of P3HT doped with F4TCNQ drops sharply after heating to 100 °C due to sublimation of the F4TCNQ, but conductivity in p(g$_4$2T-T), a thiophene with PEO side chains, remains high to nearly 180 °C. These two results combined indicate that a polymer side chain engineering may be a promising approach to controlling dopant diffusion.[163]

We are aware of only one study to date that was able to measure diffusion as a function of distance and time. Fischer et al. were able to quantify the temperature dependence of the diffusion coefficient of C$_{60}$ in a cross-linked polyfluorene polymer layer in a vertical geometry using a time-resolved optical technique.[315] We note however that C$_{60}$ is not a dopant, and this study was only performed for one particular polymer.

It can be inferred from these studies that large dopant molecules are less likely to diffuse than small dopant molecules, and that amorphous materials with high T_gs are less likely to allow dopants to diffuse through them. However, it is not yet clear whether the different energetics or molecular-scale structures of CTCs versus IPs affect diffusion rates. Essentially all extant DFT doping studies focus on the optimal OSC/dopant geometry. However, in order to diffuse, the dopant would need to leave the ideal position and then move to another location. Given these difficulties, it is not surprising that there are no molecular modeling papers on diffusion of dopants in OSCs. Such a work could help answer questions such as whether the dopant remains fully charged during movement, changes its partial charge in nonideal geometries, or whether the dopant becomes completely neutral and then redopes at a new position.

How a chemical potential gradient of dopants affects the electrical potential gradient of the host OSC is also an open question. Because the Fermi energy of the doped OSC changes with doping level, there exists a static electric field within the OSC caused by a doping gradient. There is nothing published about how this static field might affect dopant diffusion or drift across a layer interface.

9.2. Lateral Diffusion Studies

Comparatively few studies have investigated the lateral diffusion of molecular dopants in OSC films, most likely because of the difficulty of creating initial doping geometries with known concentration. A second reason might be that it did not occur to the thin-film organic device community that lateral diffusion of dopants was important, because we are usually focused on the performance of single devices, not the interaction of multiple laterally spaced devices. Here, we will highlight two studies which demonstrate that a lateral geometry allows for better measurement of dopant concentration as a function of position and time, and that this quantification yields unique mechanistic insight. The discussion of dopant and polymer patterning using dopants in Sections 7.2 and 8 is a practical justification of the need for mechanistic studies of lateral dopant motion in OSC films.

The first study of these studies was conducted by Treat et al. on D-PCBM diffusing into P3HT. The sample was a contact-laminated bilayer of P3HT on patterned D-PCBM, and the D-PCBM concentration versus position was measured near the lateral edge of the D-PCBM layer using dynamic scanning SIMS imaging.[316] The measurement of dopant concentration as a function of distance from the interface and time yielded quantification of a 1D diffusion coefficient using Fick's second law:

$$\frac{\partial \varphi(x,t)}{\partial t} = D \frac{\partial^2 \varphi(x,t)}{\partial x^2} \tag{3}$$

where $\varphi(x, t)$ is the concentration of dopants, t is the time, D is the diffusion coefficient, and x is the distance from the $t = 0$ interface between the D-PCBM film and the P3HT film.[316] The determination of the diffusion rate was performed assuming that the D-PCBM layer represents an infinite well of dopants that cannot be depleted. The authors also determined the diffusion coefficient as a function of temperature and found that the equilibrium concentration of D-PCBM in P3HT is temperature dependent. The diffusion rate was also found to be weakly concentration dependent, with a higher diffusion rate measured for lower D-PCBM loading.[316] The last result is consistent with the reports by Dai et al. (discussed above) that Mo(tfd–CO$_2$Me)$_3$ diffuses readily through P3HT but not P3HT/PCBM mixtures.[287] These results together support the idea that the diffusion rate depends on the free volume in the amorphous phase of the polymer, at least in the case of P3HT.

The most significant result of the lateral diffusion study was the determination of the activation energy for diffusion using an Arrhenius analysis (**Figure 18**).[316] The activation energy (determined from the slope) of 65.5 kJ mol^{-1} for diffusion of D-PCBM in P3HT is consistent with previous measurements of diffusion of small molecules in amorphous polymers.[317] More importantly, this measurement sets the first quantifiable benchmark for the energy required to promote diffusive motion of a small molecule in an OSC film. This benchmark enables the use of a standard continuum diffusion model to predict the diffusive motion of D-PCBM in P3HT in other initial geometries.

The second lateral geometry study was conducted by Li et al. on F4TCNQ and F4MCTCNQ (**Figure 19**e,f) diffusing
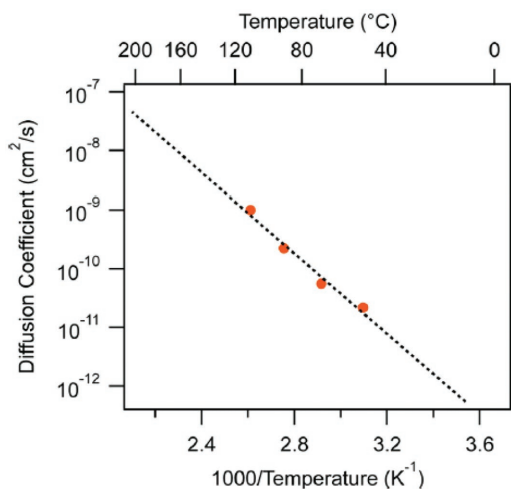
**ADVANCED
SCIENCE NEWS**
www.advancedsciencenews.com

**ADVANCED
MATERIALS**
www.advmat.de

Figure 18. Concentration-dependent diffusion coefficient, D ($\phi = 0.01$), of disordered D-PCBM in P3HT versus inverse temperature, where ϕ is the volume fraction of D-PCBM. The slope provides the activation energy of 65.5 kJ mol^{-1} (15.6 kcal mol^{-1}) for the diffusion of disordered D-PCBM through a P3HT:PCBM BHJ. Reproduced with permission.[316] Copyright 2013, American Chemical Society.

in P3HT films.[160] The samples were prepared by evaporating the dopants through a square grid (a transmission electron microscopy grid) shadow mask into a P3HT film, identical

to the geometry shown in Figure 13. After evaporation of the dopant, the sample was encapsulated with sequentially evaporated layers of MoO$_3$ and Ag, and subsequently sealed with epoxy and a glass coverslip to avoid any exposure to O$_2$ or sublimation of the F4TCNQ during heating steps. The dopant concentration in the P3HT was determined using laser scanning confocal fluorescence microscopy referenced to a calibration curve.

Figure 19a (cross section) and Figure 19c (2D image) shows the maps of the concentration of F4TCNQ in P3HT as a function of position and time obtained from fluorescence microscopy images. After the initial image, the sample was heated on a hot plate for 50 min at 348 K and then reimaged. It is clear that the F4TCNQ diffused from the high concentration (red) to the low concentration (blue) domains. Figure 19b,d shows corresponding images for P3HT samples doped with F4MCTCNQ, with the difference that the heating step was 11.2 times longer (560 min).

The authors took similar data at different annealing temperatures and times for each dopant and then attempted to fit the data to a 2D diffusion model (reasonable given that the films were thin relative to the diffusion lengths).[160] Figure 19a shows a cross section of the F4TCNQ concentration before and after thermal annealing and a fit to the data assuming simple Fickian diffusion (2D with one species) according to Equation (3). As can be seen, the fit is very poor and indicates
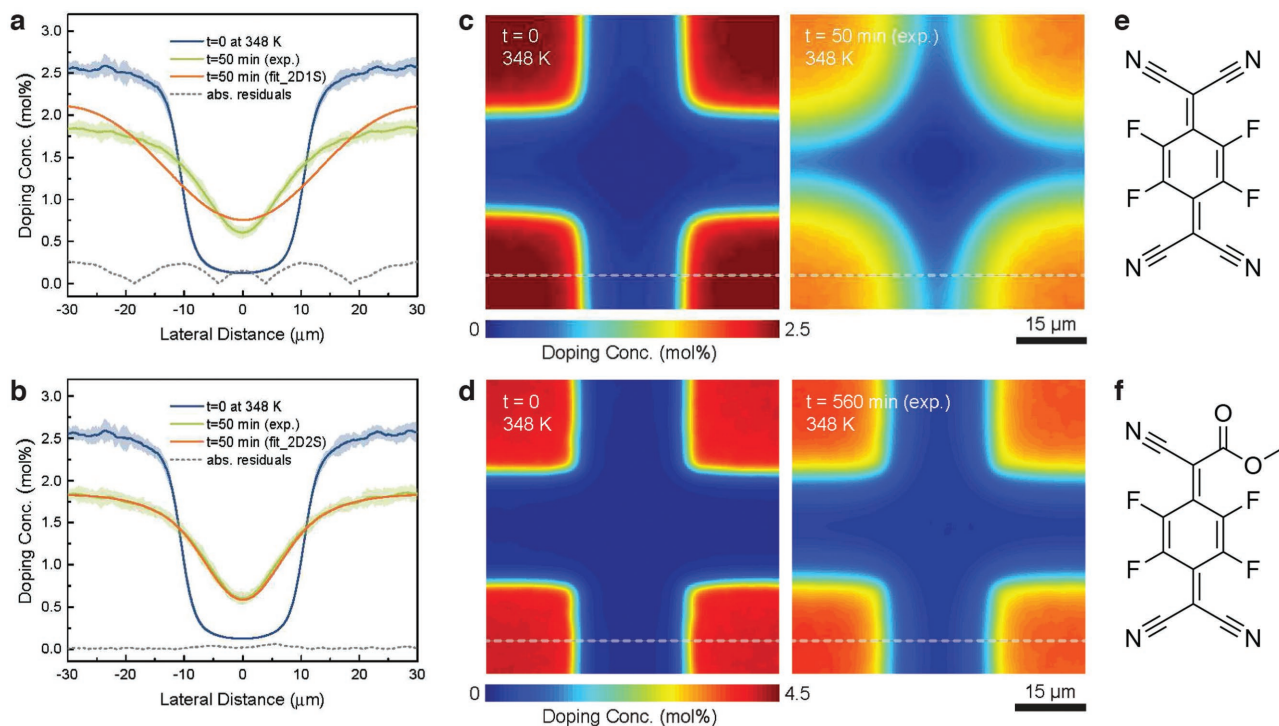

Figure 19. a,b) Measurement of lateral diffusion of F4TCNQ in P3HT:F4TCNQ films prepared using additive DISC patterning. The blue and green lines indicate cross sections of the experimental dopant concentration profiles before and after heating (c), indicated by the dashed lines in the 2D doping concentration maps. The 2D one-species (2D1S) model in part (a) yields a poor fit, while the 2D two-species (2D2S) fit in part (b) accurately matches the experimental data. c) 2D doping concentration maps obtained experimentally from LSCM at $t = 0$ (left) and $t = 50$ min (right); the dashed line indicates the cross sections shown in parts (a) and (b). d) 2D doping concentration maps showing diffusion of F4MCTCNQ through P3HT at 348 K, taken at $t = 0$ (left) and $t = 560$ min (right). Note that the heating time in part (d) was over ten times longer than in part (c). e) Structure of F4TCNQ. f) Structure of F4MCTCNQ. Reproduced with permission.[160] Copyright 2017, American Chemical Society.

that a simple diffusion model is not appropriate, even though the same model works well for PCBM in P3HT.[316]

Figure 19b shows the results of fitting the same data to an improved 2D Fickian model, which assumes two diffusing species are present (F4TCNQ and F4TCNQ$^{\bullet-}$) and are in fast equilibrium at each position following the Langmuir isotherm model (see Section 4.3).[27] In the blue regions >99.9% of the F4TCNQ is ionized, while in the red regions as much as 2% of the F4TCNQ is neutral. The diffusion coefficient and ratio of each species were tracked for temperatures from 298 to 398 K, allowing for determination of the diffusion activation energies (E_A).

Interestingly, the $E_{A, \text{neutral}}$ for neutral F4TCNQ was 74.2 kJ mol^{-1}, while the $E_{A, \text{ionized}}$ for ionized F4TCNQ was 55.5 kJ mol^{-1}. The $E_{A, \text{neutral}}$ is higher because this activation energy includes both the energy barrier for back electron transfer and the activation energy for thermal motion of the neutral molecule. However, in spite of the higher E_A (with correspondingly lower the jump attempt rate) and the lower concentration of neutral F4TCNQ, the macroscopic diffusion of the dopant was dominated by neutral F4TCNQ because the neutral dopant had a much longer jump distance than F4TCNQ$^{\bullet-}$. The neutral dopant must diffuse until it finds a vacant site on the OSC where it can re-dope. As a result the neutral dopant jump lengths are longer in highly doped regions, and shorter in less doped regions, giving the distinctive "V"-shaped concentration profile seen in Figure 19a,b. The F4TCNQ$^{\bullet-}$ moved more frequently, presumably along a P3HT chain, but only in very short hops and so was not the main driver of macroscopic motion.

Finally, comparing the two dopants, it is clear that the F4MCTCNQ diffuses much slower than the F4TCNQ. The images in Figure 19d before and after thermal annealing at 348 K for 560 min (11.2× longer than in the F4TCNQ images in Figure 19c) clearly show the F4MCTCNQ dopants have moved a shorter distance. The authors again found that a two-species diffusion model was most appropriate. The calculated activation energies for diffusion were $E_{A, \text{neutral}}$ = 53.8 kJ mol^{-1} and $E_{A, \text{ionized}}$ = 55.9 kJ mol^{-1}, similar to the value for F4TCNQ$^{\bullet-}$. The smaller $E_{A, \text{neutral}}$ for F4MCTCNQ can be attributed to its shallower LUMO level. F4MCTCNQ diffuses more slowly because its average jump distance is much shorter than that of F4TCNQ.[160] The fundamental reason for this observation has not yet been determined.

9.3. Summary

It is well known that dopant molecules can diffuse; however, very few studies have quantified the diffusion rate of dopants. It assumed that the onset of diffusion occurs as a result of heating to above the T_g of either the dopant or host OSC. However, one study showed that F4TCNQ diffuses at room temperature in P3HT[273] and another showed that PCBM diffuses into P3HT at 50 °C, which is below the T_g of P3HT.[308] Dopant diffusion is more complex than diffusion of neutral molecules such as PCBM due to the different diffusion rates of the neutral and ionized species, and the equilibrium between the two. It is not yet clear whether these results can be generalized to describe diffusion of a generic dopant in a generic OSC.

To our knowledge, there are no molecular level studies that look into the origin of the dopant diffusion activation barrier, or investigate how properties of the host material affect the onset of dopant diffusion. These studies are critical for the development of devices based on doped OSCs. Furthermore, we have not mentioned the drift of molecular dopants due to application of an electric field because we could not find any study that has measured or focused on this effect. It goes without saying the electric fields are common in electronic devices and that understanding dopant drift is therefore critical for fabrication of micro- and nanodevices with OSCs.

10. Conclusions and Outlook

The use of molecular dopants in organic electronic devices is becoming increasingly common and advantageous to the performance of a variety of devices.[17,32,318] A molecular dopant is defined as a neutral small molecule that can either donate or accept an electron from an OSC without undergoing any covalent bond breaking reaction. Thus, the only chemical interaction between a molecular dopant and an OSC is electron transfer, which is reversible. Although molecular dopants are only one method to dope organic semiconductors, they represent a particularly attractive approach because no modifications to the OSC chemical structure are required, and also because the approach is largely analogous to doping in inorganic semiconductors, which is well understood.

Recent advances in the theory of molecular doping have enabled better prediction of material properties and facilitated the use of molecular dopants in organic electronic devices. Molecular dopants can either form ionized pairs of charges in the OSC or charge-transfer complexes. Whether the molecular dopant forms an IP or a CTC with the OSC seems to depend more on the identity of the OSC than the dopant, though both IPs and CTCs can form in polymers and small-molecule OSCs. In fact, we cannot find any example of an OSC that forms both IP and CTC states even with dopants that have significantly different EAs. The degree of dopant loading does not seem to affect whether the OSC forms IPs or CTCs.

A recent model explains the energetic differences between IP and CTC states in the context that CTC states need to be thermally ionized even after formation to create free charge carriers in the OSC.[29] Due to the strong local interactions between charges in low dielectric materials, there is evidence that even completely ionized charges can be Coulombically bound, particularly at low doping levels.[23,24] All of these interactions between charges mean that doping in OSCs is local and that doping efficiency is considerably below unity.

Future work on the theory of molecular doping needs to focus on relating how the presence of the dopant affects the OSC structure to the disorder at the molecular scale. A related topic is to understand how the dopant shape, size, and orientation affect charge delocalization and disorder. While continuum level theory exists to explain the electronic function of a doped film, there is no way to predict how a new dopant structure will interact with an OSC or how efficiently the dopant will generate free charges.

These challenges require that electronic modeling, using DFT and other tools, is able to extend to larger volumes and

longer time scales. Instead of performing gas-phase simulations of molecular dimers in a particular configuration, it will be increasingly necessary to include surrounding molecules such as multiple repeat units of the OSC, to consider multiple configurations in order to determine the energetic landscape, and to consider dynamic motions and their effect on the dopant and OSC. To reach these goals, considerable development of new DFT functionals and methods that are more computationally efficient for charged and delocalized systems will be needed. Also, combined DFT and molecular dynamics approaches must be developed to capture longer length and time scales to model effects like aggregation, diffusion, and drift.

At present, very few high EA molecular dopant structures exist. Effective design of p-type molecular dopants places emphasis on maximizing the EA so that it is higher than the IE of most OSCs in order to efficiently accept electrons. There is a clear need for synthetic research to develop a range of new stable p-type dopants with EA in the range of 5.2–6.0 eV and n-type dopants with IE in the range of 2.8–3.6 eV. An increased variety of dopant structural families would help considerably to answer some of the theoretical questions outlined above.

Most molecular dopants are poorly soluble or insoluble. Only recently have some of the structures been altered with the additional design criteria of solubility or miscibility, and even for these structures systematic structural changes in the dopant's solubilizing side groups have not been carried out. Future work in the design and synthesis of molecular dopants needs to focus on increasing the dopant strength, designing for solubility/miscibility, and development of air-stable dopants. There is a particular unmet need in the area of dopant synthesis that is limiting the organic electronics community at this time.

This review has focused on the many ways in which processing or fabrication conditions can be used to affect the structure property relationships between the dopant and OSC. Since the OSC becomes charged by the dopant, the presence of the dopant has a large effect on the morphological development of mixed films, such that it is often not possible to meaningfully compare the doped and undoped samples. Solution-based codeposition often drastically modifies doped film morphology. Sequential deposition methods have recently been developed which allow for more control of the dopant position in the film, and allow the OSC morphology to be optimized before doping. This has resulted in drastic improvements in material properties, illustrating the importance of optimizing doped film morphology. These studies have also revealed that sequential doping densities are controlled by thermodynamic equilibrium with the available site density in the polymer, which has proved to be an important concept in understanding dopant diffusion.

Much of the literature exploring the use of molecular dopants has sought to improve the electronic properties of OSCs by using dopants to reduce the depth and density of trap sites in the OSC. This work is vitally important to both improving our understanding of the fundamental physics of OSCs, and better understanding how to engineer their optoelectronic properties. However, these studies are often complicated by difficulties in understanding the nature of dilute defects and impurities in OSCs, and the interaction nature of dopant molecules or additives with these sites. In most cases, the identity of OSC defects are poorly understood due to their low concentration. We stress the need for further multidisciplinary studies on defect and trap sites and the development of new experimental techniques which can unambiguously characterize dilute defects and impurities in OSCs. Here also, the synthesis of new dopants with unique metal centers could help in the unambiguous detection of the dopant location. More research is needed to determine the structural origin of traps and to develop methods to target the trap site structure with the trap filling dopant.

Molecular dopants are often highly mobile via diffusion and drift within the OSC film. Although we highlighted a number of dopant diffusion studies, it is clear that the diffusion rate, activation energy, and mechanism for diffusion are poorly understood. In particular, it is not known how the formation of IPs versus CTCs affects dopant diffusion. Nearly all DFT studies of dopant-OSC interactions have focused on optimized geometries, but during diffusion the dopant must leave its optimal geometry to move to another location. This brings to question whether the dopant remains fully charged during movement, changes its partial charge in nonideal geometries, or neutralizes and re-dopes at a new location. Another unanswered question is how the chemical potential gradient of dopants affects the host OSC's electrical potential gradient, or how the static field this induces might affect dopant diffusion or drift across a layer interface.

It is clear from this summary that significant research is needed to systematically measure and model dopant drift and diffusion within various OSCs as functions of temperature and applied field. The resulting models are needed not just at the continuum scale, but also to inform DFT and MD models. While understanding diffusion is one particular challenge, it is also necessary to understand how to control the position of the dopant under an applied field or thermal stress to improve device longevity. Here, synthetic research into anchoring groups for dopants and the interaction between the anchor group with the OSC is also needed.

Finally, we presented a suite of new solution-based techniques to create doping gradients and pattern OSCs that are loosely titled doping-induced solubility control (DISC). The idea is based on the (photo)reactivity of dopant molecules and the observation that the solubility of some polymeric OSCs is strongly affected by doping. The doping level in the film can be controlled using sequential deposition of dopants and postdeposition chemical and photochemical reactions with the dopants to destroy them. We showed that p-type dopants can, in general, be chemically deactivated by a reaction with stronger nucleophiles than the OSC, and removed using a selective solvent. Photochemical reactions with dopants can be induced with a variety of solvents upon excitation with a focused laser. While in principle these reactions are expected to be commonplace, they have not been studied in other dopants.

Both sequential deposition and selective removal of dopants using a photochemical reaction have been used to create doping gradients with sub-300 nm feature sizes. This process opens a wide range of new possibilities for the fabrication of OSC devices with combined doped and intrinsic domains and therefore directionally controlled charge transport and collection.

A further use of DISC is in patterning the OSC itself. Because creation of doping gradients also generates solubility gradients, the doped OSC functions as its own photoresist.

**ADVANCED
SCIENCE NEWS**

www.advancedsciencenews.com

**ADVANCED
MATERIALS**

www.advmat.de

These approaches—in particular optical DISC patterning using a focused laser to photochemically deactivate dopants—can achieve incredibly high resolution, exceeding the diffraction limit for the 405 nm write laser used.

While in many ways molecular doping in OSCs is essentially analogous to atomic doping in inorganic semiconductors, the application of molecular dopants to modify physical properties of OSCs, such as solubility or crystallinity, clearly does not fit this mold. In this sense, the applications of molecular doping go well beyond those directly derived from inorganic semiconductors. The natural flexibility of molecular doping processes, owing to their inherently reversible charge-transfer interactions, their (photo)reactivity, and most importantly, their strong and often complex interactions with OSC morphology, points toward an almost entirely unexplored line of research in which dopants are integral to not only the function but also the manufacture of electronic devices. We envision that these new processing pathways could yield not only new device architectures, but also help to address fundamental questions about the physics of diffusion, drift, and electronic states in OSCs.

Conflict of Interest

The authors declare no conflict of interest.

[1] R. E. Hummel, *Electronic Properties of Materials*, 4th ed., Springer, New York, **2011**.

[2] S. O. Kesap, *Principles of Electronic Materials and Devices*, 3rd ed., McGraw Hill, New York, **2006**.

[3] A. J. Heeger, N. S. Sariciftci, E. B. Namdas, *Semiconducting and Metallic Polymers*, Oxford Graduate Texts. Oxford University Press, Oxford, UK **2010**.

[4] B. R. Hsieh, Y. Wei, *Semiconducting Polymers: Applications, Properties and Synthesis*, ACS Symposium Series, Vol. *735*, American Chemical Society, Washington, D.C., USA **1999**.

[5] G. Hadziioannou, P. F. van Hutten, *Semiconducting Polymers: Chemistry, Physics and Engineering*, Wiley-VCH, New York, USA **2000**.

[6] T. A. Skotheim, J. R. Reynolds, *Conjugated Polymers: Theory, Synthesis, Properties, and Characterization, Handbook or Conducting Polymers*, 3rd ed., CRC Press, Boca Raton, FL, USA, **2007**.

[7] J. Maiti, S. Dolui, *Polythiophene Based Conjugated Polymer for Optoelectronic Application: Development of Soluble Pi Conjugated Polymers and Evaluation of Their Electroluminescence Properties*, VDM Verlag, Saarbruecken, Germany, **2010**.

[8] G. E. Zaikov, A. P. Iordanskii, V. S. Markin, *Diffusion of Electrolytes in Polymers (New Concepts in Polymer Science)*, VSP, Utrecht, The Netherlands **1988**.

[9] A. Elschner, S. Kirchmeyer, W. Lovenich, U. Merker, K. Reuter, *PEDOT: Principles and Applications of an Intrinsically Conductive Polymer*, CRC Press, New York, **2011**.

[10] M. S. Freund, B. Deore, *Self-Doped Conducting Polymers*, John Wiley and Sons, Chichester, UK, **2007**.

[11] I. Kulszewicz-Bajer, A. Proń, J. Abramowicz, C. Jeandey, J.-L. Oddou, J. W. Sobczak, *Chem. Mater.* **1999**, *11*, 552.

[12] J. Endo, T. Matsumoto, J. Kido, *Jpn. J. Appl. Phys.* **2002**, *41*, L358.

[13] P. Zalar, M. Kuik, Z. B. Henson, C. Woellner, Y. Zhang, A. Sharenko, G. C Bazan, T.-Q. Nguyen, *Adv. Mater.* **2014**, *26*, 724.

[14] E. Poverenov, N. Zamoshchik, A. Patra, Y. Ridelman, M. Bendikov, *J. Am. Chem. Soc.* **2014**, *136*, 5138.

[15] Y. Han, G. Barnes, Y.-H. Lin, J. Martin, Md. Al-Hashimi, S. Y. AlQaradawi, T. D. Anthopoulos, M. Heeney, *Chem. Mater.* **2016**, *28*, 8016.

[16] P. Pingel, M. Arvind, L. Kölln, R. Steyrleuthner, F. Kraffert, J. Behrends, S. Janietz, D. Neher, *Adv. Electron. Mater.* **2016**, *2*, 1600204.

[17] B. Lüssem, C.-M. Keum, D. Kasemann, B. Naab, Z. Bao, K. Leo, *Chem. Rev.* **2016**, *116*, 13714.

[18] J. L. Bredas, G. B. Street, *Acc. Chem. Res.* **1985**, *18*, 309.

[19] J. Blockwitz, T. Fritz, M. Pfeiffer, K. Leo, D. M. Alloway, P. A. Lee, N. R. Armstrong, *Org. Electron.* **2001**, *2*, 97.

[20] H. Ishii, K. Sugiyama, E. Ito, K. Seki, *Adv. Mater.* **1999**, *11*, 605.

[21] P. Pingel, D. Neher, *Phys. Rev. B* **2013**, *87*, 115209.

[22] D. T. Duong, C. Wang, E. Antono, M. F. Toney, A. Salleo, *Org. Electron.* **2013**, *14*, 1330.

[23] V. I. Arkhipov, E. V. Emelianova, P. Heremans, H. Bässler, *Phys. Rev. B* **2005**, *72*, 235202.

[24] V. I. Arkhipov, P. Heremans, E. V. Emelianova, H. Bässler, *Phys. Rev. B* **2005**, *71*, 045214.

[25] R. Noriega, J. Rivnay, K. Vandewal, F. P. V. Koch, N. Stingelin, P. Smith, M. F. Toney, A. Salleo, *Nat. Mater.* **2013**, *12*, 1037.

[26] P. Pingel, R. Schwarzl, D. Neher, *Appl. Phys. Lett.* **2012**, *100*, 143303.

[27] I. E. Jacobs, J. Li, E. W. Aasen, J. Lopez, T. Fonseca, G. Zhang, P. Stroeve, M. P. Augustine, M. Mascal, A. J. Moulë, *J. Mater. Chem. C* **2016**, *4*, 3454.

[28] B. Maennig, M. Pfeiffer, A. Nollau, X. Zhou, K. Leo, P. Simon, *Phys. Rev. B* **2001**, *64*, 195208.

[29] I. Salzmann, G. Heimel, M. Oehzelt, S. Winkler, N. Koch, *Acc. Chem. Res.* **2016**, *49*, 370.

[30] I. Salzmann, G. Heimel, *J. Electron Spectrosc. Relat. Phenom.* **2015**, *204*, 208.

[31] D. Jerome, *Chem. Rev.* **2004**, *104*, 5565.

[32] K. Walzer, B. Maennig, M. Pfeiffer, K. Leo, *Chem. Rev.* **2007**, *107*, 1233.

[33] X. Zhao, X. Zhan, *Chem. Soc. Rev.* **2011**, *40*, 3728.

[34] K. Kang, S. Watanabe, K. Broch, A. Sepe, A. Brown, I. Nasrallah, M. Nikolka, Z. Fei, M. Heeney, D. Matsumoto, K. Marumoto, H. Tanaka, S. Kuroda, H. Sirringhaus, *Nat. Mater.* **2016**, *15*, 896.

[35] J. Gao, E. T. Niles, J. K. Grey, *J. Phys. Chem. Lett.* **2013**, *4*, 2953.

[36] I. E. Jacobs, E. W. Aasen, D. Nowak, J. Li, W. Morrison, J. D. Roehling, M. P. Augustine, A. J. Moulë, *Adv. Mater.* **2017**, *29*, 1603221.

[37] I. E. Jacobs, J. Li, S. L. Berg, D. J. Bilsky, B. T. Rotondo, M. P. Augustine, P. Stroeve, A. J. Moulë, *ACS Nano* **2015**, *9*, 1905.

[38] A. Pron, P. Rannou, *Prog. Polym. Sci.* **2002**, *27*, 135.

**ADVANCED
SCIENCE NEWS**

www.advancedsciencenews.com

**ADVANCED
MATERIALS**

www.advmat.de

[39] B. Russ, A. Glaudell, J. J. Urban, M. L. Chabinyc, R. A. Segalman, *Nat. Rev. Mater.* **2016**, *1*, 16050.

[40] M. Pfeiffer, T. Fritz, J. Blochwitz, A. Nollau, B. Plönnigs, A. Beyer, K. Leo, *Controlled Doping of Molecular Organic Layers: Physics and Device Prospects*, Springer, Braunschweig, Germany, **1999**.

[41] H. Klauk, *Organic Electronics: Materials, Manufacturing, and Applications*, John Wiley & Sons, Weinheim, Germany, **2006**.

[42] S. H. Kim, K. Hong, W. Xie, K. H. Lee, S. Zhang, T. P Lodge, C. D. Frisbie, *Adv. Mater.* **2013**, *25*, 1822.

[43] K. Harada, M. Riede, K. Leo, O. R. Hild, C. M. Elliott, *Phys. Rev. B* **2008**, *77*, 195212.

[44] H. Mendez, G. Heimel, S. Winkler, J. Frisch, A. Opitz, K. Sauer, B. Wegner, M. Oehzelt, C. Rothel, S. Duhm, D. Tobbens, N. Koch, I. Salzmann, *Nat. Commun.* **2015**, *6*, 8560.

[45] J. B. Torrance, *Acc. Chem. Res.* **1979**, *12*, 79.

[46] J. B. Torrance, B. A. Scott, F. B. Kaufman, *Solid State Commun.* **1975**, *17*, 1369.

[47] J. B. Torrance, J. E. Vazquez, J. J. Mayerle, V. Y. Lee, *Phys. Rev. Lett.* **1981**, *46*, 253.

[48] H. Akamatu, H. Inokuchi, Y. Matsunaga, *Nature* **1954**, *173*, 168.

[49] M. J. Cohen, L. B. Coleman, A. F. Garito, A. J. Heeger, *Phys. Rev. B* **1974**, *10*, 1298.

[50] K. Vandewal, A. Gadisa, W. D. Oosterbaan, S. Bertho, F. Banishoeib, I. Van Severen, L. Lutsen, T. J. Cleij, D. Vanderzande, J. V. Manca, *Adv. Funct. Mater.* **2008**, *18*, 2064.

[51] K. Vandewal, K. Tvingstedt, A. Gadisa, O. Inganas, J. V. Manca, *Nat. Mater.* **2009**, *8*, 904.

[52] J. L. Bredas, J. E. Norton, J. Cornil, V. Coropceanu, *Acc. Chem. Res.* **2009**, *42*, 1691.

[53] K. Vandewal, S. Albrecht, E. T. Hoke, K. R. Graham, J. Widmer, J. D. Douglas, M. Schubert, W. R. Mateker, J. T. Bloking, G. F. Burkhard, A. Sellinger, J. M. J. Fréchet, A. Amassian, M. K. Riede, M. D. McGehee, D. Neher, A. Salleo, *Nat. Mater.* **2014**, *13*, 63.

[54] A. Panda, K. Ding, X. Liu, S. R. Forrest, *Phys. Rev. B* **2016**, *94*, 125429.

[55] E. E. Aziz, A. Vollmer, S. Eisebitt, W. Eberhardt, P. Pingel, D. Neher, N. Koch, *Adv. Mater.* **2007**, *19*, 3257.

[56] H. Mendez, G. Heimel, A. Opitz, K. Sauer, P. Barkowski, M. Oehzelt, J. Soeda, T. Okamoto, J. Takeya, J.-B. Arlin, J.-Y. Balandier, Y. Geerts, N. Koch, I. Salzmann, *Angew. Chem., Int. Ed.* **2013**, *52*, 7751.

[57] I. Salzmann, G. Heimel, S. Duhm, M. Oehzelt, P. Pingel, B. M. George, A. Schnegg, K. Lips, R. P. Blum, A. Vollmer, N. Koch, *Phys. Rev. Lett.* **2012**, *108*, 035502.

[58] P. Pahner, H. Kleemann, L. Burtone, M. L. Tietze, J. Fischer, K. Leo, B. Lussem, *Phys. Rev. B* **2013**, *88*, 195205.

[59] M. Lögdlund, R. Lazzaroni, S. Stafström, W. R. Salaneck, J.-L. Brédas, *Phys. Rev. Lett.* **1989**, *63*, 1841.

[60] H. Sirringhaus, P. J. Brown, R. H. Friend, M. M. Nielsen, K. Bechgaard, B. M. W. Langeveld-Voss, A. J. H. Spiering, R. A. J. Janssen, E. W. Meijer, P. Herwig, *Nature* **1999**, *401*, 685.

[61] R. Österbacka, C. P. An, X. M. Jiang, Z. V. Vardeny, *Science* **2000**, *287*, 839.

[62] C. C. Wang, D. T. Duong, K. Vandewal, J. Rivnay, A. Salleo, *Phys. Rev. B* **2015**, *91*, 085205.

[63] P. J. Brown, H. Sirringhaus, M. Harrison, M. Shkunov, R. H. Friend, *Phys. Rev. B* **2001**, *63*, 125204.

[64] E. Kampar, O. Neilands, *Russ. Chem. Rev.* **1986**, *55*, 334.

[65] L. Zhu, E.-G. Kim, Y. Yi, J.-L. Brédas, *Chem. Mater.* **2011**, *23*, 5149.

[66] F. Ghani, A. Opitz, P. Pingel, G. Heimel, I. Salzmann, J. Frisch, D. Neher, A. Tsami, U. Scherf, N. Koch, *J. Polym. Sci., Part B: Polym. Phys.* **2015**, *53*, 58.

[67] R.-Q. Png, M. C. Y. Ang, M.-H. Teo, K.-K. Choo, C. G. Tang, D. Belaineh, L.-L. Chua, P. K. H. Ho, *Nat. Commun.* **2016**, *7*, 11948.

[68] J. Hubbard, *Proc. R. Soc. London* **1963**, *276*, 238.

[69] R. Schwedhelm, L. Kipp, A. Dallmeyer, M. Skibowski, *Phys. Rev. B* **1998**, *58*, 13176.

[70] P.-J. Chia, S. Sivaramakrishnan, M. Zhou, R.-Q. Png, L.-L. Chua, R. H. Friend, P. K. H. Ho, *Phys. Rev. Lett.* **2009**, *102*, 096602.

[71] S. Winkler, P. Amsalem, J. Frisch, M. Oehzelt, G. Heimel, N. Koch, *Mater. Horiz.* **2015**, *2*, 427.

[72] G. Heimel, *ACS Cent. Sci.* **2016**, *2*, 309.

[73] B. J. Tropham, Z. G. Soos, *Phys. Rev. B* **2001**, *84*, 165405.

[74] S. D. Ha, Y. Qi, A. Kahn, *Chem. Phys. Lett.* **2010**, *495*, 212.

[75] J. Li, G. D'Avino, A. Pershin, D. Jacquemin, I. Duchemin, D. Beljonne, X. Blase, *Phys. Rev. Mater.* **2017**, *1*, 025602.

[76] D. Di Nuzzo, C. Fontanesi, R. Jones, S. Allard, I. Dumsch, U. Scherf, E. Von Hauff, S. Schumacher, E. Da Como, *Nat. Commun.* **2015**, *6*, 6460.

[77] J. E. Cochran, M. J. N. Junk, A. M. Glaudell, P. Levi Miller, J. S. Cowart, M. F. Toney, C. J. Hawker, B. F. Chmelka, M. L. Chabinyc, *Macromolecules* **2014**, *47*, 6836.

[78] M. L Tietze, P. Pahner, K. Schmidt, K. Leo, B. Lüssem, *Adv. Funct. Mater.* **2015**, *25*, 2701.

[79] S. Hamwi, J. Meyer, T. Winkler, T. Riedl, W. Kowalsky, *Appl. Phys. Lett.* **2009**, *94*, 174.

[80] A. Mityashin, Y. Olivier, T. Van Regemorter, C. Rolin, S. Verlaak, N. G. Martinelli, D. Beljonne, J. Cornil, J. Genoe, P. Heremans, *Adv. Mater.* **2012**, *24*, 1535.

[81] M. L. Tietze, K. Leo, B. Lussem, *Org. Electron.* **2013**, *14*, 2348.

[82] S. Olthof, S. Mehraeen, S. K Mohapatra, S. Barlow, V. Coropceanu, J.-L. Brédas, S. R. Marder, A. Kahn, *Phys. Rev. Lett.* **2012**, *109*, 176601.

[83] B. A. Gregg, S.-G. Chen, R. A. Cormier, *Chem. Mater.* **2004**, *16*, 4586.

[84] S. Wang, M. Ha, M. Manno, C. D. Frisbie, C. Leighton, *Nat. Commun.* **2012**, *3*, 1210.

[85] S. Olthof, W. Tress, R. Meerheim, B. Lüssem, K. Leo, *J. Appl. Phys.* **2009**, *106*, 103711.

[86] K.-H. Yim, G. L. Whiting, C. E. Murphy, J. J. M. Halls, J. H. Burroughes, R. H. Friend, J.-S. Kim, *Adv. Mater.* **2008**, *20*, 3319.

[87] J. Li, C. W. Rochester, I. E. Jacobs, S. Friedrich, P. Stroeve, M. Riede, A. J. Moulë, *ACS Appl. Mater. Interfaces* **2015**, *7*, 28420.

[88] J. Gao, B. W. Stein, A. K. Thomas, J. A. Garcia, J. Yang, M. L. Kirk, J. K. Grey, *J. Phys. Chem. C* **2015**, *119*, 16396.

[89] L. Müller, D. Nanova, T. Glaser, S. Beck, A. Pucci, A. K. Kast, R. R. Schröder, E. Mankel, P. Pingel, D. Neher, W. Kowalsky, R. Lovrincic, *Chem. Mater.* **2016**, *28*, 4432.

[90] R. J. Kline, M. D. McGehee, *Polym. Rev.* **2006**, *46*, 27.

[91] H. Shirakawa, E. J. Louis, A. G. MacDiarmid, C. K. Chiang, A. J. Heeger, *J. Chem. Soc., Chem. Commun.* **1977**, *16*, 578.

[92] Y. Yamamoto, K. Yoshino, Y. Inuishi, *J. Phys. Soc. Jpn.* **1979**, *47*, 1887.

[93] R. C. Haddon, A. F. Hebard, *Nature* **1991**, *350*, 320.

[94] L. Chang, H. A. W. Lademann, J. B. Bonekamp, K. Meerholz, A. J. Moulë, *Adv. Funct. Mater.* **2011**, *21*, 1779.

[95] G. Parthasarathy, C. Shen, A. Kahn, S. R. Forrest, *J. Appl. Phys.* **2001**, *89*, 4986.

[96] Md. S. A. Abdou, F. P. Orfino, Y. Son, S. Holdcroft, *J. Am. Chem. Soc.* **1997**, *119*, 4518.

[97] M. L Chabinyc, R. A. Street, J. E. Northrup, *Appl. Phys. Lett.* **2007**, *90*, 123508.

[98] C.-K. Lu, H.-F. Meng, *Phys. Rev. B* **2007**, *75*, 235206.

[99] N. Ljungqvist, T. Hjertberg, *Macromolecules* **1995**, *28*, 5993.

[100] T. Caronna, M. Forte, M. Catellani, S. V. Meille, *Chem. Mater.* **1997**, *9*, 991.

[101] E. J. Meijer, C. Detcheverry, P. J. Baesjou, E. Van Veenendaal, D. M. De Leeuw, T. M. Klapwijk, *J. Appl. Phys.* **2003**, *93*, 4831.

**ADVANCED
SCIENCE NEWS**

www.advancedsciencenews.com

**ADVANCED
MATERIALS**

www.advmat.de

[102] S. Ogawa, T. Naijo, Y. Kimura, H. Ishii, M. Niwano, *Jpn. J. Appl. Phys.* **2006**, *45*, 530.

[103] C. Krellner, S. Haas, C. Goldmann, K. P. Pernstich, D. J. Gundlach, B. Batlogg, *Phys. Rev. B* **2007**, *75*, 245115.

[104] W. L. Kalb, K. Mattenberger, B. Batlogg, *Phys. Rev. B* **2008**, *78*, 035334.

[105] M. Bjerring, J. S. Nielsen, A. Siu, N. C. Nielsen, F. C. Krebs, *Sol. Energy Mater. Sol. Cells* **2008**, *92*, 772.

[106] H.-H. Liao, C.-M. Yang, C.-C. Liu, S.-F. Horng, H.-F. Meng, J.-T. Shy, *J. Appl. Phys.* **2008**, *103*, 104506.

[107] M. Manceau, A. Rivaton, J.-L. Gardette, S. Guillerez, N. Lemaître, *Polym. Degrad. Stab.* **2009**, *94*, 898.

[108] M. Manceau, S. Chambon, A. Rivaton, J.-L. Gardette, S. Guillerez, N. Lemaître, *Sol. Energy Mater. Sol. Cells* **2010**, *94*, 1572.

[109] M. Manceau, M. Helgesen, F. C. Krebs, *Polym. Degrad. Stab.* **2010**, *95*, 2666.

[110] J. Schafferhans, A. Baumann, A. Wagenpfahl, C. Deibel, V. Dyakonov, *Org. Electron.* **2010**, *11*, 1693.

[111] H. Hintz, H.-J. Egelhaaf, L. Lüer, J. Hauch, H. Peisert, T. Chassé, *Chem. Mater.* **2010**, *23*, 145.

[112] A. Rivaton, S. Chambon, M. Manceau, J.-L. Gardette, N. Lemaître, S. Guillerez, *Polym. Degrad. Stab.* **2010**, *95*, 278.

[113] H. Hintz, H. J. Egelhaaf, H. Peisert, T. Chassé, *Polym. Degrad. Stab.* **2010**, *95*, 818.

[114] H. Hintz, H. Peisert, H.-J. Egelhaaf, T. Chasse, *J. Phys. Chem. C* **2011**, *115*, 13373.

[115] A. Sperlich, H. Kraus, C. Deibel, H. Blok, J. Schmidt, V. Dyakonov, *J. Phys. Chem. B* **2011**, *115*, 13513.

[116] A. Seemann, T. Sauermann, C. Lungenschmied, O. Armbruster, S. Bauer, H.-J. Egelhaaf, J. Hauch, *Sol. Energy* **2011**, *85*, 1238.

[117] E. López-Elvira, E. Escasaín, A. Baró, J. Colchero, E. Palacios-Lidón, *Polym. Degrad. Stab.* **2011**, *96*, 1279.

[118] A. Guerrero, P. P. Boix, L. F Marchesi, T. Ripolles-Sanchis, E. C. Pereira, G. Garcia-Belmonte, *Sol. Energy Mater. Sol. Cells* **2012**, *100*, 185.

[119] U. B. Cappel, T. Daeneke, U. Bach, *Nano Lett.* **2012**, *12*, 4925.

[120] A. Armin, G. Juska, B. W. Philippa, P. L. Burn, P. Meredith, R. D. White, A. Pivrikas, *Adv. Energy Mater.* **2013**, *3*, 321.

[121] Y. Aoyama, T. Yamanari, N. Koumura, H. Tachikawa, M. Nagai, Y. Yoshida, *Polym. Degrad. Stab.* **2013**, *98*, 899.

[122] Y. Aoyama, T. Yamanari, T. N. Murakami, T. Nagamori, K. Marumoto, H. Tachikawa, J. Mizukado, H. Suda, Y. Yoshida, *Polym. J.* **2015**, *47*, 26.

[123] A. Nollau, M. Pfeiffer, T. Fritz, K. Leo, *J. Appl. Phys.* **2000**, *87*, 4340.

[124] F. Li, M. Pfeiffer, A. Werner, K. Harada, K. Leo, N. Hayashi, K. Seki, X. Liu, X.-D. Dang, *J. Appl. Phys.* **2006**, *100*, 023716.

[125] A. G. Werner, F. Li, K. Harada, M. Pfeiffer, T. Fritz, K. Leo, *Appl. Phys. Lett.* **2003**, *82*, 4495.

[126] A. Werner, F. Li, K. Harada, M. Pfeiffer, T. Fritz, K. Leo, S. Machill, *Adv. Funct. Mater.* **2004**, *14*, 255.

[127] C. J. Bloom, C. M. Elliott, P. G. Schroeder, C. B. France, B. A. Parkinson, *J. Phys. Chem. B* **2003**, *107*, 2933.

[128] T. Menke, D. Ray, J. Meiss, K. Leo, M. Riede, *Appl. Phys. Lett.* **2012**, *100*, 60.

[129] B. A. Gregg, R. A. Cormier, *J. Am. Chem. Soc.* **2001**, *123*, 7959.

[130] Z. Q. Liang, B. A. Gregg, *Adv. Mater.* **2012**, *24*, 3258.

[131] C. K. Chan, W. Zhao, S. Barlow, S. Marder, A. Kahn, *Org. Electron.* **2008**, *9*, 575.

[132] Y. Zhang, B. de Boer, P. W. M. Blom, *Phys. Rev. B* **2010**, *81*, 085201.

[133] S. Guo, S. K Mohapatra, A. Romanov, T. V. Timofeeva, K. I. Hardcastle, K. Yesudas, C. Risko, J. Brédas, S. R. Marder, S. Barlow, *Chemistry – Eur. J.* **2012**, *18*, 14760.

[134] Y. Qi, S. K. Mohapatra, S. B. Kim, S. Barlow, S. R. Marder, A. Kahn, *Appl. Phys. Lett.* **2012**, *100*, 083305.

[135] P. Wei, J. H. Oh, G. Dong, Z. Bao, *J. Am. Chem. Soc.* **2010**, *132*, 8852.

[136] S. K. Mohapatra, A. Fonari, C. Risko, K. Yesudas, K. Moudgil, J. H. Delcamp, T. V. Timofeeva, J. Brédas, S. R. Marder, S. Barlow, *Chemistry – Eur. J.* **2014**, *20*, 15385.

[137] Y. Karpov, T. Erdmann, I. Raguzin, M. Al-Hussein, M. Binner, U. Lappan, M. Stamm, K. L. Gerasimov, V. Beryozkina, V. Bakulev, D. V. Anokhin, D. A. Ivanov, F. Gunther, S. Gemming, G. Seifert, B. Voit, R. Di Pietro, A. Kiriy, *Adv. Mater.* **2016**, *28*, 6003.

[138] D. S. Acker, R. J. Harder, W. R. Hertler, W. Mahler, L. R. Melby, R. E. Benson, W. E. Mochel, *J. Am. Chem. Soc.* **1960**, *82*, 6408.

[139] R. G. Kepler, P. E. Bierstedt, R. E. Merrifield, *Phys. Rev. Lett.* **1960**, *5*, 503.

[140] D. S. Acker, W. R. Hertler, *J. Am. Chem. Soc.* **1962**, *84*, 3370.

[141] L. R. Melby, R. J. Harder, W. R. Hertler, W. Mahler, R. E. Benson, W. E. Mochel, *J. Am. Chem. Soc.* **1962**, *84*, 3374.

[142] J. W. Chen, Y. Cao, *Acc. Chem. Res.* **2009**, *42*, 1709.

[143] M. F. Falzon, M. M. Wienk, R. A. J. Janssen, *J. Phys. Chem. C* **2011**, *115*, 3178.

[144] Y. Wang, T. Michinobu, *J. Mater. Chem. C* **2016**, *4*, 6200.

[145] P.-O. Morin, T. Bura, M. Leclerc, *Mater. Horiz.* **2016**, *3*, 11.

[146] T. Lei, J.-Y. Wang, J. Pei, *Acc. Chem. Res.* **2014**, *47*, 1117.

[147] P. Bujak, I. Kulszewicz-Bajer, M. Zagorska, V. Maurel, I. Wielgus, A. Pron, *Chem. Soc. Rev.* **2013**, *42*, 8895.

[148] J. E. Coughlin, Z. B. Henson, G. C. Welch, G. C. Bazan, *Acc. Chem. Res.* **2014**, *47*, 257.

[149] J. E. Anthony, *Chem. Rev.* **2006**, *106*, 5028.

[150] J. E. Anthony, *Angew. Chem., Int. Ed.* **2008**, *47*, 452.

[151] W. Gao, A. Kahn, *J. Appl. Phys.* **2003**, *94*, 359.

[152] Y. Qi, T. Sajoto, M. Kröger, A. M. Kandabarow, W. Park, S. Barlow, E.-G. Kim, L. Wielunski, L. C. Feldman, R. A. Bartynski, J.-L. Brédas, S. R. Marder, A. Kahn, *Chem. Mater.* **2010**, *22*, 524.

[153] W. Gao, A. Kahn, *Appl. Phys. Lett.* **2001**, *79*, 4040.

[154] G. M. Rangger, O. T. Hofmann, B. Broker, E. Zojer, *Synth. Met.* **2010**, *160*, 1456.

[155] P. K. Koech, A. B. Padmaperuma, L. Wang, J. S. Swensen, E. Polikarpov, J. T. Darsell, J. E. Rainbolt, D. J. Gaspar, *Chem. Mater.* **2010**, *22*, 3926.

[156] R. Meerheim, B. Lussem, K. Leo, *Proc. IEEE* **2009**, *97*, 1606.

[157] R. Meerheim, S. Olthof, M. Hermenau, S. Scholz, A. Petrich, N. Tessler, O. Solomeshch, B. Lüssem, M. Riede, K. Leo, *J. Appl. Phys.* **2011**, *109*, 103102.

[158] J. E. Rainbolt, P. K. Koech, E. Polikarpov, J. S. Swensen, L. Cosimbescu, A. Von Ruden, L. Wang, L. S. Sapochak, A. B. Padmaperuma, D. J. Gaspar, *J. Mater. Chem. C* **2013**, *1*, 1876.

[159] J. Li, G. Zhang, D. M. Holm, I. E. Jacobs, B. Yin, P. Stroeve, M. Mascal, A. J. Moulé, *Chem. Mater.* **2015**, *27*, 5765.

[160] J. Li, C. Koshnick, S. O. Diallo, S. Ackling, D. M. Huang, I. E. Jacobs, T. F. Harrelson, K. Hong, G. Zhang, J. Beckett, M. Mascal, A. J. Moulé, *Macromolecules* **2017**, *50*, 5476.

[161] P. R. Hammond, *J. Chem. Soc.* **1963**, *0*, 3113.

[162] K. M. Al-Ahmary, M. M. El-Kholy, I. A. Al-Solmy, M. M. Habeeb, *Spectrochim. Acta, Part A* **2013**, *110*, 343.

[163] R. Kroon, D. Kiefer, D. Stegerer, L. Yu, M. Sommer, C. Müller, *Adv. Mater.* **2017**, *29*, 1700930.

[164] J. Niederhausen, P. Amsalem, J. Frisch, A. Wilke, A. Vollmer, R. Rieger, K. Müllen, J. P. Rabe, N. Koch, *Phys. Rev. B* **2011**, *84*, 165302.

[165] T. Fukunaga, *J. Am. Chem. Soc.* **1976**, *98*, 610.

[166] T. Fukunaga, *J. Am. Chem. Soc.* **1976**, *98*, 611.

[167] Y. Karpov, T. Erdmann, M. Stamm, U. Lappan, O. Guskova, M. Malanin, I. Raguzin, T. Beryozkina, V. Bakulev, F. Günther, S. Gemming, G. Seifert, M. Hambsch, S. Mannsfeld, B. Voit, A. Kiriy, *Macromolecules* **2017**, *50*, 914.

[168] O. Solomeshch, Y. J. Yu, A. A. Goryunkov, L. N. Sidorov, R. F. Tuktarov, D. H. Choi, J.-I. Jin, N. Tessler, *Adv. Mater.* **2009**, *21*, 4456.

[169] A. Tadich, M. T. Edmonds, L. Ley, F. Fromm, Y. Smets, Z. Mazej, J. Riley, C. I. Pakes, T. Seyller, M. Wanke, *Appl. Phys. Lett.* **2013**, *102*, 241601.

[170] N. C. Cates, R. Gysel, Z. Beiley, C. E. Miller, M. F. Toney, M. Heeney, I. McCulloch, M. D. McGehee, *Nano Lett.* **2009**, *9*, 4153.

[171] A. C. Mayer, M. F. Toney, S. R. Scully, J. Rivnay, C. J. Brabec, M. Scharber, M. Koppe, M. Heeney, I. McCulloch, M. D. McGehee, *Adv. Funct. Mater.* **2009**, *19*, 1173.

[172] Y. Qi, T. Sajoto, S. Barlow, E.-G. Kim, J.-L. Brédas, S. R. Marder, A. Kahn, *J. Am. Chem. Soc.* **2009**, *131*, 12530.

[173] S. A. Paniagua, J. Baltazar, H. Sojoudi, S. K. Mohapatra, S. Zhang, C. L. Henderson, S. Graham, S. Barlowa, S. R. Marder, *Mater. Horiz.* **2014**, *1*, 111.

[174] C. Y. Kao, B. Lee, L. S. Wielunski, M. Heeney, I. McCulloch, E. Garfunkel, L. C. Feldman, V. Podzorov, *Adv. Funct. Mater.* **2009**, *19*, 1906.

[175] O. Khatib, B. Lee, J. Yuen, Z. Q. Li, M. Di Ventra, A. J. Heeger, V. Podzorov, D. N. Basov, *J. Appl. Phys.* **2010**, *107*, 123702.

[176] H. Huang, D. E. Gross, X. Yang, J. S. Moore, L. Zang, *ACS Appl. Mater. Interfaces* **2013**, *5*, 7704.

[177] H. Tanaka, M. Hirate, S. Watanabe, S.-i. Kuroda, *Adv. Mater.* **2014**, *26*, 2376.

[178] A. M. Glaudell, J. E. Cochran, S. N. Patel, M. L. Chabinyc, *Adv. Energy Mater.* **2015**, *5*, 1401072.

[179] S. N. Patel, A. M. Glaudell, D. Kiefer, M. L. Chabinyc, *ACS Macro Lett.* **2016**, *5*, 268.

[180] J. Gao, J. D. Roehling, Y. Li, H. Guo, A. J. Moulé, J. K. Grey, *J. Mater. Chem. C* **2013**, *1*, 5638.

[181] X. Lin, G. E. Purdum, Y. Zhang, S. Barlow, S. R. Marder, Y.-L. Loo, A. Kahn, *Chem. Mater.* **2016**, *28*, 2677.

[182] Z. Shang, T. Heumueller, R. Prasanna, G. F. Burkhard, B. D. Naab, Z. Bao, M. D. McGehee, A. Salleo, *Adv. Energy Mater.* **2016**, *6*, 1601149.

[183] C. Poelking, K. Daoulas, A. Troisi, D. Andrienko, *Adv. Polym. Sci.* **2014**, *265*, 139.

[184] P. Kordt, D. Andrienko, *J. Chem. Theory Comput.* **2016**, *12*, 36.

[185] C. Poelking, M. Tietze, C. Elschner, S. Olthof, D. Hertel, B. Baumeier, F. Wuerthner, K. Meerholz, K. Leo, D. Andrienko, *Nat. Mater.* **2015**, *14*, 434.

[186] R. P. Fornari, P. W. M. Blom, A. Troisi, *Phys. Rev. Lett.* **2017**, *118*, 086601.

[187] S. Illig, A. S. Eggeman, A. Troisi, L. Jiang, C. Warwick, M. Nikolka, G. Schweicher, S. G. Yeates, Y. H. Geerts, J. E. Anthony, H. Sirringhaus, *Nat. Commun.* **2016**, *7*, 10736.

[188] M. H. Lee, J. Arago, A. Troisi, *J. Phys. Chem. C* **2015**, *119*, 14989.

[189] T. F. Harrelson, A. J. Moulé, R. Faller, *Mol. Simul.* **2017**, *43*, 730.

[190] V. Coropceanu, J. Cornil, D. A. da Silva, Y. Olivier, R. Silbey, J. L. Brédas, *Chem. Rev.* **2007**, *107*, 2165.

[191] T. Korzdorfer, J. L. Bredas, *Acc. Chem. Res.* **2014**, *47*, 3284.

[192] C. Sutton, C. Risko, J. L. Bredas, *Chem. Mater.* **2016**, *28*, 3.

[193] K. Do, M. K. Ravva, T. H. Wang, J. L. Bredas, *Chem. Mater.* **2017**, *29*, 346.

[194] V. Coropceanu, H. Li, P. Winget, L. Y. Zhu, J. L. Bredas, *Annu. Rev. Mater. Res.* **2013**, *43*, 63.

[195] Y. Zhang, B. de Boer, P. W. M. Blom, *Adv. Funct. Mater.* **2009**, *19*, 1901.

[196] I. D. V. Ingram, D. J. Tate, A. V. S. Parry, R. Sebastian Sprick, M. L. Turner, *Appl. Phys. Lett.* **2014**, *104*, 153304.

[197] D. T. Scholes, S. A. Hawks, P. Y. Yee, H. Wu, J. R. Lindemuth, S. H. Tolbert, B. J. Schwartz, *J. Phys. Chem. Lett.* **2015**, *6*, 4786.

[198] V. A. Kolesov, C. Fuentes-Hernandez, W.-F. Chou, N. Aizawa, F. A. Larrain, M. Wang, A. Perrotta, S. Choi, S. Graham, G. C. Bazan, T.-Q. Nguyen, S. R. Marder, B. Kippelen, *Nat. Mater.* **2017**, *16*, 474.

[199] A. C. Arias, J. D. MacKenzie, I. McCulloch, J. Rivnay, A. Salleo, *Chem. Rev.* **2010**, *110*, 3.

[200] C. W. Rochester, S. A. Mauger, A. J. Moulé, *J. Phys. Chem. C* **2012**, *116*, 7287.

[201] J. C. Aguirre, S. A. Hawks, A. S. Ferreira, P. Yee, S. Subramaniyan, S. A. Jenekhe, S. H. Tolbert, B. J. Schwartz, *Adv. Energy Mater.* **2015**, *5*, 1402020.

[202] K. H. Lee, P. E. Schwenn, A. R. G. Smith, H. Cavaye, P. E. Shaw, M. James, K. B. Krueger, I. R. Gentle, P. Meredith, P. L. Burn, *Adv. Mater.* **2011**, *23*, 766.

[203] A. J. Ferguson, N. Kopidakis, S. E. Shaheen, G. Rumbles, *J. Phys. Chem. C* **2008**, *112*, 9865.

[204] B. Lüssem, M. Riede, K. Leo, *Phys. Status Solidi A* **2013**, *210*, 9.

[205] I. Langmuir, *J. Am. Chem. Soc.* **1918**, *40*, 1361.

[206] D. T. Duong, H. Phan, D. Hanifi, P. S. Jo, T. Nguyen, A. Salleo, *Adv. Mater.* **2014**, *26*, 6069.

[207] R. Dingle, H. L. Störmer, A. C. Gossard, W. Wiegmann, *Appl. Phys. Lett.* **1978**, *33*, 665.

[208] S. N. Patel, A. M. Glaudell, K. A. Peterson, E. M. Thomas, K. A. O'Hara, E. Lim, M. L. Chabinyc, *Sci. Adv.* **2017**, *3*, e1700434.

[209] L. W. Shacklette, R. R. Chance, D. M. Ivory, G. G. Miller, R. H. Baughman, *Synth. Met.* **1979**, *1*, 307.

[210] K. Seeger, W. D. Gill, T. C. Clarke, G. B. Street, *Solid State Commun.* **1978**, *28*, 873.

[211] S. D. Kang, G. J. Snyder, *Nat. Mater.* **2017**, *16*, 252.

[212] T. F. Harrelson, Y. Q. Cheng, J. Li, I. E. Jacobs, A. J. Ramirez-Cuesta, R. Faller, A. J. Moulé, *Macromolecules* **2017**, *50*, 2424.

[213] D. Venkateshvaran, M. Nikolka, A. Sadhanala, V. Lemaur, M. Zelazny, M. Kepa, M. Hurhangee, A. J. Kronemeijer, V. Pecunia, I. Nasrallah, I. Romanov, K. Broch, I. McCulloch, D. Emin, Y. Olivier, J. Cornil, D. Beljonne, H. Sirringhaus, *Nature* **2014**, *515*, 384.

[214] M. J. Panzer, C. D. Frisbie, *Adv. Funct. Mater.* **2006**, *16*, 1051.

[215] A. S. Dhoot, J. D. Yuen, M. Heeney, I. McCulloch, D. Moses, A. J. Heeger, *Proc. Natl. Acad. Sci. USA* **2006**, *103*, 11834.

[216] J. D. Yuen, A. S. Dhoot, E. B. Namdas, N. E. Coates, M. Heeney, I. McCulloch, D. Moses, A. J. Heeger, *J. Am. Chem. Soc.* **2007**, *129*, 14367.

[217] H. Tanaka, S. Nishio, H. Ito, S.-i. Kuroda, *Appl. Phys. Lett.* **2015**, *107*, 113.

[218] J. Rivnay, R. Noriega, J. E. Northrup, R. J. Kline, M. F. Toney, A. Salleo, *Phys. Rev. B* **2011**, *83*, 121306.

[219] H. Yang, T. J. Shin, Z. Bao, C. Y. Ryu, *J. Polym. Sci., Part B: Polym. Phys.* **2007**, *45*, 1303.

[220] C. P. Jarrett, R. H. Friend, A. R. Brown, D. M. De Leeuw, *J. Appl. Phys.* **1995**, *77*, 6289.

[221] S. C. Jain, W. Geens, A. Mehra, V. Kumar, T. Aernouts, J. Poortmans, R. Mertens, M. Willander, *J. Appl. Phys.* **2001**, *89*, 3804.

[222] G. Dicker, M. P. de Haas, J. M. Warman, D. M. de Leeuw, L. D. A. Siebbeles, *J. Phys. Chem. B* **2004**, *108*, 17818.

[223] B. A. Gregg, *Soft Matter* **2009**, *5*, 2985.

[224] W. L. Kalb, S. Haas, C. Krellner, T. Mathis, B. Batlogg, *Phys. Rev. B* **2010**, *81*, 155315.

[225] J. Dacuña, A. Salleo, *Phys. Rev. B* **2011**, *84*, 195209.

[226] H. T. Nicolai, M. Kuik, G. A. H. Wetzelaer, B. De Boer, C. Campbell, C. Risko, J. L. Brédas, P. W. M. Blom, *Nat. Mater.* **2012**, *11*, 882.

[227] A. Higgins, S. K Mohapatra, S. Barlow, S. R. Marder, A. Kahn, *Appl. Phys. Lett.* **2015**, *106*, 163301.

[228] Z. Q. Liang, A. Nardes, D. Wang, J. J. Berry, B. A. Gregg, *Chem. Mater.* **2009**, *21*, 4914.

**ADVANCED
SCIENCE NEWS**

www.advancedsciencenews.com

**ADVANCED
MATERIALS**

www.advmat.de

[229] M. Pope, C. E. Swenberg, *Electronic Processes in Organic Crystals and Polymers*, Oxford University Press, Oxford, UK **1999**.

[230] N. Bacalis, E. N. Economou, M. H. Cohen, *Phys. Rev. B* **1988**, *37*, 2714.

[231] O. Tal, Y. Rosenwaks, Y. Preezant, N. Tessler, C. K. Chan, A. Kahn, *Phys. Rev. Lett.* **2005**, *95*, 256405.

[232] W. L. Kalb, B. Batlogg, *Phys. Rev. B* **2010**, *81*, 035327.

[233] J. Puigdollers, A. Marsal, S. Cheylan, C. Voz, R. Alcubilla, *Org. Electron.* **2010**, *11*, 1333.

[234] F. Bussolotti, S. Kera, K. Kudo, A. Kahn, N. Ueno, *Phys. Rev. Lett.* **2013**, *110*, 267602.

[235] H. E. Katz, Z. Bao, S. L. Gilat, *Acc. Chem. Res.* **2001**, *34*, 359.

[236] D. B. A. Rep, A. F. Morpurgo, W. G. Sloof, T. M. Klapwijk, *J. Appl. Phys.* **2003**, *93*, 2082.

[237] O. D. Jurchescu, J. Baas, T. T. M. Palstra, *Appl. Phys. Lett.* **2004**, *84*, 3061.

[238] L.-L. Chua, J. Zaumseil, J.-F. Chang, E. C.-W. Ou, P. K.-H. Ho, H. Sirringhaus, R. H. Friend, *Nature* **2005**, *434*, 194.

[239] R. Zeis, C. Besnard, T. Siegrist, C. Schlockermann, X. Chi, C. Kloc, *Chem. Mater.* **2006**, *18*, 244.

[240] L. G. Kaake, P. F. Barbara, X.-Y. Zhu, *J. Phys. Chem. Lett.* **2010**, *1*, 628.

[241] P. A. Bobbert, A. Sharma, S. G. J. Mathijssen, M. Kemerink, D. M. de Leeuw, *Adv. Mater.* **2012**, *24*, 1146.

[242] M. Nikolka, I. Nasrallah, B. Rose, M. K. Ravva, K. Broch, A. Sadhanala, D. Harkin, J. Charmet, M. Hurhangee, A. Brown, S. Illig, P. Too, J. Jongman, I. McCulloch, J.-L. Bredas, H. Sirringhaus, *Nat. Mater.* **2017**, *16*, 356.

[243] D. Wang, N. Kopidakis, M. O. Reese, B. A. Gregg, *Chem. Mater.* **2008**, *20*, 6307.

[244] I. E. Jacobs, F. Wang, N. Hazefi, C. Medina-Plaze, T. F. Harrelson, J. Li, M. P. Augustine, M. Mascal, A. J. Moulé, *Chem. Mater.* **2017**, *29*, 832.

[245] R. Schmechel, *J. Appl. Phys.* **2003**, *93*, 4653.

[246] B. A. Gregg, *J. Phys. Chem. C* **2009**, *113*, 5899.

[247] A. Liu, S. Zhao, S. Rim, J. Wu, M. Könemann, P. Erk, P. Peumans, *Adv. Mater.* **2008**, *20*, 1065.

[248] F. Deschler, E. Da Como, T. Limmer, R. Tautz, T. Godde, M. Bayer, E. von Hauff, S. Yilmaz, S. Allard, U. Scherf, *Phys. Rev. Lett.* **2011**, *107*, 127402.

[249] S. Olthof, S. Singh, S. K. Mohapatra, S. Barlow, S. R. Marder, B. Kippelen, A. Kahn, *Appl. Phys. Lett.* **2012**, *101*, 253303.

[250] Y. Abe, T. Hasegawa, Y. Takahashi, T. Yamada, Y. Tokura, *Appl. Phys. Lett.* **2005**, *87*, 153506.

[251] E. Lim, B.-J. Jung, M. Chikamatsu, R. Azumi, Y. Yoshida, K. Yase, L.-M. Do, H.-K. Shim, *J. Mater. Chem.* **2007**, *17*, 1416.

[252] L. Ma, W. H. Lee, Y. D. Park, J. S. Kim, H. S. Lee, K. Cho, *Appl. Phys. Lett.* **2008**, *92*, 063310.

[253] F. Maddalena, E. J. Meijer, K. Asadi, D. M. de Leeuw, P. W. M. Blom, *Appl. Phys. Lett.* **2010**, *97*, 158.

[254] C.-T. Lee, H.-C. Chen, *Org. Electron.* **2011**, *12*, 1852.

[255] M. M. Mandoc, F. B. Kooistra, J. C. Hummelen, B. De Boer, P. W. M. Blom, *Appl. Phys. Lett.* **2007**, *91*, 263505.

[256] X. Lei, F. Zhang, T. Song, B. Sun, *Appl. Phys. Lett.* **2011**, *99*, 267.

[257] C. G. Shuttle, N. D. Treat, J. D. Douglas, J. M. J. Fréchet, M. L. Chabinyc, *Adv. Energy Mater.* **2012**, *2*, 111.

[258] X. Han, Z. Wu, B. Sun, *Org. Electron.* **2013**, *14*, 1116.

[259] B. Maennig, J. Drechsel, D. Gebeyehu, P. Simon, F. Kozlowski, A. Werner, F. Li, S. Grundmann, S. Sonntag, M. Koch, *Appl. Phys. A: Mater. Sci. Process.* **2004**, *79*, 1.

[260] S. W. Yu, J. Frisch, A. Opitz, E. Cohen, M. Bendikov, N. Koch, I. Salzmann, *Appl. Phys. Lett.* **2015**, *106*, 203301.

[261] H. Yan, J. G. Manion, M. Yuan, F. P. García de Arquer, G. R. McKeown, S. Beaupré, M. Leclerc, E. H. Sargent, D. S. Seferos, *Adv. Mater.* **2016**, *28*, 6491.

[262] Y. Zhang, H. Zhou, J. Seifter, L. Ying, A. Mikhailovsky, A. J. Heeger, G. C. Bazan, T.-Q. Nguyen, *Adv. Mater.* **2013**, *25*, 7038.

[263] R. A. Cruz, T. Catunda, W. M. Facchinatto, D. T. Balogh, R. M. Faria, *Synth. Met.* **2013**, *163*, 38.

[264] E. Busby, E. Carroll, E. Chinn, L. Chang, A. J. Moule, D. S. Larsen, *J. Phys. Chem. Lett.* **2011**, *2*, 2764.

[265] T. P. Martin, A. J. Wise, E. Busby, J. Gao, J. D. Roehling, M. J. Ford, D. S. Larsen, A. J. Moule, J. K. Grey, *J. Phys. Chem. B* **2013**, *117*, 4478.

[266] H. Liu, J. Kameoka, D. A. Czaplewski, H. G. Craighead, *Nano Lett.* **2004**, *4*, 671.

[267] D. T. McQuade, A. E. Pullen, T. M. Swager, *Chem. Rev.* **2000**, *100*, 2537.

[268] J. Janata, M. Josowicz, *Nat Mater.* **2003**, *2*, 19.

[269] A. Zen, J. Pflaum, S. Hirschmann, W. Zhuang, F. Jaiser, U. Asawapirom, J. P. Rabe, U. Scherf, D. Neher, *Adv. Funct. Mater.* **2004**, *14*, 757.

[270] A. J. Moulé, K. Meerholz, *Appl. Phys. B: Lasers Opt.* **2008**, *92*, 209.

[271] Z. Liang, M. O. Reese, B. A. Gregg, *ACS Appl. Mater. Interfaces* **2011**, *3*, 2042.

[272] J. Fuzell, I. E. Jacobs, A. Ackling, T. F. Harrelson, D. M. Huang, D. S. Larsen, A. J. Moulé, *J. Phys. Chem. Lett.* **2016**, *7*, 4297.

[273] J. Li, C. W. Rochester, I. E. Jacobs, E. W. Aasen, S. Friedrich, P. Stroeve, A. J. Moule, *Org. Electron.* **2016**, *33*, 23.

[274] J. Drechsel, M. Pfeiffer, X. Zhou, A. Nollau, K. Leo, *Synth. Met.* **2002**, *127*, 201.

[275] P. Wellmann, M. Hofmann, O. Zeika, A. Werner, J. Birnstock, R. Meerheim, G. He, K. Walzer, M. Pfeiffer, K. Leo, *J. Soc. Inf. Disp.* **2005**, *13*, 393.

[276] C.-C. Chang, M.-T. Hsieh, J.-F. Chen, S.-W. Hwang, C. H. Chen, *Appl. Phys. Lett.* **2006**, *89*, 253504.

[277] I. Bruder, S. Watanabe, J. Qu, I. B. Müller, R. Kopecek, J. Hwang, J. Weis, N. Langer, *Org. Electron.* **2010**, *11*, 589.

[278] Z. Q. Gao, B. X. Mi, G. Z. Xu, Y. Q. Wan, M. L. Gong, K. W. Cheah, C. H. Chen, *Chem. Commun.* **2008**, 117.

[279] Y.-J. Yu, O. Solomeshch, H. Chechik, A. A. Goryunkov, R. F. Tuktarov, D. H. Choi, J.-I. Jin, Y. Eichen, N. Tessler, *J. Appl. Phys.* **2008**, *104*, 124505.

[280] Y. Smets, C. B. Stark, F. Schmitt, M. T. Edmonds, S. Lach, C. A. Wright, D. P. Langley, K. J. Rietwyk, A. Schenk, A. Tadich, M. Wanke, C. Ziegler, L. Ley, C. I. Pakes, *Org. Electron.* **2013**, *14*, 169.

[281] W. R. Hertler, H. D. Hartzler, D. S. Acker, R. E. Benson, *J. Am. Chem. Soc.* **1962**, *84*, 3387.

[282] O. A. El Seoud, F. P. Ribeiro, A. Martins, P. P. Brotero, *J. Org. Chem.* **1985**, *50*, 5099.

[283] D. de Caro, M. Souque, C. Faulmann, Y. Coppel, L. Valade, J. Fraxedas, O. Vendier, F. Courtade, *Langmuir* **2013**, *29*, 8983.

[284] G. Dennler, M. C. Scharber, C. J. Brabec, *Adv. Mater.* **2009**, *21*, 1323.

[285] C. J. Brabec, S. Gowrisanker, J. J. M. Halls, D. Laird, S. J. Jia, S. P. Williams, *Adv. Mater.* **2010**, *22*, 3839.

[286] K. Harada, A. G. Werner, M. Pfeiffer, C. J. Bloom, C. M. Elliott, K. Leo, *Phys. Rev. Lett.* **2005**, *94*, 036601.

[287] A. Dai, A. Wan, C. Magee, Y. Zhang, S. Barlow, S. R. Marder, A. Kahn, *Org. Electron.* **2015**, *23*, 151.

[288] A. Dai, Y. Zhou, A. L. Shu, S. K. Mohapatra, H. Wang, C. Fuentes-Hernandez, Y. Zhang, S. Barlow, Y.-L. Loo, S. R. Marder, B. Kippelen, A. Kahn, *Adv. Funct. Mater.* **2014**, *24*, 2197.

[289] A. L. Shu, A. Dai, H. Wang, Y.-L. Loo, A. Kahn, *Org. Electron.* **2013**, *14*, 149.

[290] Y. Zhou, C. Fuentes-Hernandez, J. Shim, J. Meyer, A. J. Giordano, H. Li, P. Winget, T. Papadopoulos, H. Cheun, J. Kim, M. Fenoll, A. Dindar, W. Haske, E. Najafabadi, T. M. Khan, H. Sojoudi,

S. Barlow, S. Graham, J.-L. Brédas, S. R. Marder, A. Kahn, B. Kippelen, *Science* **2012**, *336*, 327.

[291] H. Kang, S. Kee, K. Yu, J. Lee, G. Kim, J. Kim, J.-R. Kim, J. Kong, K. Lee, *Adv. Mater.* **2015**, *27*, 1408.

[292] B. M. Dhar, G. S. Kini, G. Xia, B. J. Jung, N. Markovic, H. E. Katz, *Proc. Natl. Acad. Sci. USA* **2010**, *107*, 3972.

[293] A. A. Zakhidov, J.-K. Lee, J. A. DeFranco, H. H. Fong, P. G. Taylor, M. Chatzichristidi, C. K. Ober, G. G. Malliaras, *Chem. Sci.* **2011**, *2*, 1178.

[294] C. Balocco, L. A. Majewski, A. M. Song, *Org. Electron.* **2006**, *7*, 500.

[295] J. A. DeFranco, B. S. Schmidt, M. Lipson, G. G. Malliaras, *Org. Electron.* **2006**, *7*, 22.

[296] H. S. Hwang, A. A. Zakhidov, J.-K. Lee, X. Andre, J. A. DeFranco, H. H. Fong, A. B. Holmes, G. G. Malliaras, C. K. Ober, *J. Mater. Chem.* **2008**, *18*, 3087.

[297] M. E. Bahlke, H. A. Mendoza, D. T. Ashall, A. S. Yin, M. A. Baldo, *Adv. Mater.* **2012**, *24*, 6136.

[298] D. Nowak, W. Morrison, H. K. Wickramasinghe, J. Jahng, E. Potma, L. Wan, R. Ruiz, T. R. Albrecht, K. Schmidt, J. Frommer, D. P. Sanders, S. Park, *Sci. Adv.* **2016**, *2*, e1501571.

[299] G. H. Lu, J. Blakesley, S. Himmelberger, P. Pingel, J. Frisch, I. Lieberwirth, I. Salzmann, M. Oehzelt, R. Di Pietro, A. Salleo, N. Koch, D. Neher, *Nat. Commun.* **2013**, *4*, 1588.

[300] C. D. Muller, A. Falcou, N. Reckefuss, M. Rojahn, V. Wiederhirn, P. Rudati, H. Frohne, O. Nuyken, H. Becker, K. Meerholz, *Nature* **2003**, *421*, 829.

[301] J. W. Rumer, I. McCulloch, *Mater. Today* **2015**, *18*, 425.

[302] R.-Q. Png, P.-J. Chia, J.-C. Tang, B. Liu, S. Sivaramakrishnan, M. Zhou, S.-H. Khong, H. S. O. Chan, J. H. Burroughes, L.-L. Chua, R. H. Friend, P. K. H. Ho, *Nat. Mater.* **2010**, *9*, 152.

[303] O. D. Parashchuk, T. V. Laptinskaya, D. Yu. Paraschuk, *Phys. Chem. Chem. Phys.* **2011**, *13*, 3775.

[304] O. D. Parashchuk, V. V. Bruevich, D. Y. Paraschuk, *Phys. Chem. Chem. Phys.* **2010**, *12*, 6021.

[305] M. M. Bouman, E. E. Havinga, R. A. J. Janssen, E. W. Meijer, *Mol. Cryst. Liq. Cryst. Sci. Technol., Sect. A* **1994**, *256*, 439.

[306] C. K. Chiang, C. R. Fincher Jr., Y. W. Park, A. J. Heeger, H. Shirakawa, E. J. Louis, S. C. Gau, A. G. MacDiarmid, *Phys. Rev. Lett.* **1977**, *39*, 1098.

[307] G. D. Sharma, S. G. Sangodkar, M. S. Roy, *Mater. Sci. Eng.* **1996**, *B41*, 222.

[308] N. D. Treat, M. A. Brady, G. Smith, M. F. Toney, E. J. Kramer, C. J. Hawker, M. L. Chabinyc, *Adv. Energy Mater.* **2011**, *1*, 82.

[309] P. Tyagi, M. K. Dalai, C. K. Suman, S. Tuli, R. Srivastava, *RSC Adv.* **2013**, *3*, 24553.

[310] W. Yin, M. Dadmun, *ACS Nano* **2011**, *5*, 4756.

[311] J. D. Roehling, K. J. Batenburg, F. B. Swain, A. J. Moulé, I. Arslan, *Adv. Funct. Mater.* **2013**, *23*, 2115.

[312] P. Tyagi, S. Tuli, R. Srivastava, *J. Chem. Phys.* **2015**, *142*, 054707.

[313] L. Zhang, F.-S. Zu, Y.-L. Deng, F. Igbari, Z.-K. Wang, L.-S. Liao, *ACS Appl. Mater. Interfaces* **2015**, *7*, 11965.

[314] M.-C. Jung, Y. Qi, *Org. Electron.* **2016**, *31*, 71.

[315] F. Fischer, T. Hahn, H. Bässler, I. Bauer, P. Strohriegl, A. Köhler, *Adv. Funct. Mater.* **2014**, *24*, 6172.

[316] N. D. Treat, T. E. Mates, C. J. Hawker, E. J. Kramer, M. L. Chabinyc, *Macromolecules* **2013**, *46*, 1002.

[317] P. Neogi, *Diffusion in Polymers*, CRC Press, New York, USA **1996**.

[318] M. Riede, T. Mueller, W. Tress, R. Schueppel, K. Leo, *Nanotechnology* **2008**, *19*, 424001.